Dynamics, Neutronics, and the Safeguarding of Molten Salt Reactors from Plutonium Diversion

A Dissertation Presented for the

Doctor of Philosophy

Degree

The University of Tennessee, Knoxville

Alexander McGuire Walker Wheeler

May 2025

© by Alexander McGuire Walker Wheeler, 2025
All Rights Reserved.

To my patient wife who is ready for me to graduate and my loving pups who could not care less

Acknowledgments

This work comes as the product of many years of study and effort, but this study would not be possible without the help of many collaborators and sponsors.

This work received support from US Department of Energy, US Nuclear Regulatory Commission, and Oak Ridge National Laboratory/UT-Battelle.

For collaborators, I would first like to thank Dr. Ondrej Chvala for introducing me to Molten Salt Reactors (MSRs). In fact, he also correctly pointed out that safeguards for MSRs were critically underexplored, and that's what I spent my first year studying in graduate school.

Next, I would like to thank Vikram Singh. The non-linear dynamic modeling methodology for MSRs was first developed by Vikram; I mainly focused on adding new capabilities like accounting for variable flow. He also showed me that passion can drive research forward, something I have been incredibly grateful for.

It was when both I and Vik were students working for Ondrej that a possible signature for plutonium removal was first discovered. We were nearing the end of a funding opportunity on MSR dynamics when Ondrej told us to see if there was any way to tie together international safeguards and reactor dynamics. I ran a simple burnup case in SCALE for an infinite lattice and noted the change in the delayed neutron fraction before and after removing the plutonium. Vik took these numbers and ran them in the breeder MSR model. Sure enough, there was a change in the frequency response. This result was presented in a poster to the University of Tennessee Department of Nuclear Engineering.

Research continued in earnest under Ondrej and Dr. Steven Skutnik (a leader in fuel cycle modeling) as part of a broader research project on MSR safeguards. It was at this

point, under their direction, that most of the presented work was completed. With their advice this research reached its current form.

When we received the grant from NEUP on MSRs, I also received help from my fellow grad students; Jarod Richardson and Dr. Nicholas Dunkle worked diligently on producing an open-source thermal MSR that I could use for the fuel cycle and diversion studies presented here.

Throughout all of this, the most important help I received was from my loving parents. They supported me through my years at college and held my family together while I was away.

Finally, I need to thank Zoë, who is not only a great editor, but the best wife I could ask for.

Abstract

Molten Salt Reactors (MSRs) face unique challenges and requirements for material accountancy and control. Current techniques such as item counting and serial numbers are suited for the current fleet of solid-fueled reactors. However, as the next generation of reactors enter the market, new means of material accountancy and safeguarding will need to be introduced. This research takes a novel approach to assessing the plutonium concentration in the liquid fuel medium found in MSRs.

When a reactor is subjected to a periodic reactivity transient, it can have drastically different responses depending on frequency of the transient. This frequency response is sensitive to parameters, such as the delayed neutron fraction, that are highly linked to what isotope is currently fissioning (e.g. U-235, Pu-239, etc.). Therefore, if plutonium is diverted, a characteristic change in neutronic parameters are observable in a reactor frequency response. Using this discrepancy, the frequency response can be very low latency, nondestructive measurement that does not disturb reactor operations.

This research examines the frequency response while plutonium is being diverted in fast and thermal spectrum MSRs. In doing so, the paper reveals how key neutronic parameters evolve with burnup and change when plutonium is diverted. The means to predicting the frequency response of an MSR is also detailed. Finally, the frequency response is quantified for both normal burnup conditions as well as when a significant quantity of plutonium has been diverted.

The final results show that for a small modular reactor sized thermal MSR, a diversion of plutonium is very noticeable in the frequency response. However, for the large fast spectrum MSRs, there is little to no change in the parameters. Therefore, the frequency response signature is not recommended for large MSRs.

All custom tools created to perform this study have been uploaded on a public repository. They can be quickly adapted for evaluation of any liquid fuel reactor design. While this study used these specific tools, the method is not married to any tool (i.e. either burnup code or dynamic model) can be replicated using the steps presented here.

Table of Contents

1 Introduction **1**

1.1 Molten Salt Reactors . . . 3

1.2 Safeguards and Molten Salt Reactors . . . 4

1.3 Scope . . . 5

2 Safeguards for Molten Salt Reactor Like Systems **7**

2.1 General Safeguards Approaches . . . 7

2.2 Safeguards for Aqueous Reprocessing Facilities . . . 10

2.3 Safeguards for Pyroprocessing Facilities . . . 12

2.4 Additional Consideration for Molten Salt Reactor Safeguards . . . 13

3 Use of Reactor Dynamic Response for Safeguards **16**

3.1 Reactor Dynamic Modeling Method . . . 17

3.2 Kinetic Parameters, Burnup, and Diversion Scenarios . . . 19

3.3 Results . . . 23

3.4 Discussion . . . 27

3.5 Conclusion . . . 31

4 Molten Salt Reactor Fuel Cycle and Plutonium Diversion Modeling **32**

4.1 MSR Fuel Cycle Modeling Considerations . . . 33

4.2 Neutronic Modeling Methodology . . . 34

4.2.1 Thermal Spectrum Molten Salt Reactor Neutronic Modeling Methodology . . . 36

4.2.2 Fast Spectrum Molten Salt Reactor modeling . . . 45
4.3 Parameter Evolution over Burnup . . . 49
4.3.1 Neutronic Parameters . . . 52
4.3.2 Temperature Feedback Coefficients . . . 54
4.3.3 Fission Product Poisons . . . 59
4.3.4 Decay Heat . . . 62
4.4 Plutonium Diversion . . . 65
4.4.1 Plutonium Grade during Burnup . . . 65
4.4.2 Plutonium Diversion Effect on Parameters . . . 67
4.5 Conclusions . . . 72

5 Dynamic Models for Thermal and Fast Molten Salt Reactors 74
5.1 Background on Frequency Response and MSR Dynamic Modeling . . . 75
5.2 Governing Theories in Nodal Dynamic Modeling . . . 77
5.2.1 Modified Point Kinetics Equations and Power Production . . . 77
5.2.2 Nodal Representation Theory and Heat Transfer . . . 80
5.3 General MSR Nodalized Model Representation . . . 84
5.3.1 Core and Coolant Representation . . . 84
5.3.2 Once-Though Steam Generator . . . 87
5.3.3 Decay Heat Production . . . 87
5.3.4 Reactivity Feedback Mechanisms . . . 92
5.4 Physical Parameters used in MSR Modeling . . . 94
5.5 Discussion . . . 95

6 Frequency Response during Burnup and Plutonium Diversion 96
6.1 Thermal MSR Frequency Response . . . 96
6.1.1 The Effect of Burnup on the Thermal MSR Frequency Response . . . 96
6.1.2 Plutonium Diversion's Effect on the Thermal MSR Frequency Response 100
6.2 FSMSR Frequency Response . . . 102
6.2.1 The Effect of Burnup on the FSMSR Frequency Response . . . 102
6.2.2 The Effect of Plutonium Diversion on the FSMSR Frequency Response 104

7 Conclusions **109**

7.1 Future Work and Considerations . . . 110

7.1.1 Detector Systems . . . 110

7.1.2 Different Fuel Cycles . . . 110

7.1.3 Tailored Diversion Scenarios . . . 111

7.1.4 Effectiveness in Solid Fuel Reactors . . . 112

7.1.5 Neutron Noise . . . 112

7.1.6 Transient Modeling . . . 113

Bibliography **114**

Appendices **124**

A Plutonium Diversion Neutronic Parameters . . . 125

A.1 Thermal MSR with Only Pure Pu Diversion . . . 125

A.2 Thermal MSR with Pure Pu Diversion and Refuel Uranium to Make Up Reactivity . . . 130

A.3 Fast Spectrum MSR with Increasing Amounts of Plutonium Diverted (2.67 GWd/MTHM - 366 full power days) . . . 133

B Parameters Used in Dynamic models . . . 138

Vita **141**

List of Tables

2.1 IAEA timeliness goals and significant quantities for direct use material [2] . . 8

3.1 Kinetic parameters for plutonium diversion scenarios after one full powered year 22

4.1 Delayed neutron fraction for various isotopes. 35
4.2 Physical dimensions of the thermal MSR. 40
4.3 Weight percentages of the materials in the thermal MSR Serpent model. . . 42
4.4 Chemical reprocessing groups for the Thermal MSR burnup calculation. . . . 44
4.5 Chemical reprocessing groups for the FSMSR burnup calculation. 48
4.6 The amount of plutonium needed to be diverted to form an SQ of plutonium for several levels of burnup. 68

5.1 Percent change in β_{circ} when 1% of the β_{total} drop occurs in just one delayed neutron precursor groups (longer half life to shorter half life). 81

A1 Change in reactor parameters when a SQ of plutonium is removed from a thermal MSR after a burnup of 0.316 GWd/MTHM (23.2 full power days). . 125
A2 Change in the six group effective delayed neutron fraction parameters when a SQ of plutonium is removed from a thermal MSR after a burnup of 0.316 GWd/MTHM (23.2 full power days). 125
A3 Change in reactor parameters when a SQ of plutonium is removed from a thermal MSR after a burnup of 0.8867 GWd/MTHM (65 full power days). . 126

A4 Change in the six group effective delayed neutron fraction parameters when a SQ of plutonium is removed from a thermal MSR after a burnup of 0.8867 GWd/MTHM (65 full power days). 126
A5 Change in reactor parameters when a SQ of plutonium is removed from a thermal MSR after a burnup of 1.5527 GWd/MTHM (114 full power days). . 127
A6 Change in the six group effective delayed neutron fraction parameters when a SQ of plutonium is removed from a thermal MSR after a burnup of 1.5527 GWd/MTHM (114 full power days). 127
A7 Change in reactor parameters when a SQ of plutonium is removed from a thermal MSR after a burnup of 4.9777 GWd/MTHM (366 full power days). . 128
A8 Change in the six group effective delayed neutron fraction parameters when a SQ of plutonium is removed from a thermal MSR after a burnup of 4.9777 GWd/MTHM (366 full power days). 128
A9 Change in reactor parameters when a SQ of plutonium is removed from a thermal MSR after a burnup of 32.1878 GWd/MTHM (2368 full power days). 129
A10 Change in the six group effective delayed neutron fraction parameters when a SQ of plutonium is removed from a thermal MSR after a burnup of 32.1878 GWd/MTHM (2368 full power days). 129
A11 Change in reactor parameters when a SQ of plutonium is removed and makeup uranium is added to a thermal MSR after a burnup of 0.316 GWd/MTHM (23.2 full power days). 130
A12 Change in the six group effective delayed neutron fraction parameters when a SQ of plutonium is removed and makeup uranium is added to a thermal MSR after a burnup of 0.316 GWd/MTHM (23.2 full power days). 130
A13 Change in reactor parameters when a SQ of plutonium is removed and makeup uranium is added to a thermal MSR after a burnup of 0.8867 GWd/MTHM (65 full power days). 131
A14 Change in the six group effective delayed neutron fraction parameters when a SQ of plutonium is removed and makeup uranium is added to a thermal MSR after a burnup of 0.8867 GWd/MTHM (65 full power days). 131

A15 Change in reactor parameters when a SQ of plutonium is removed and makeup uranium is added to a thermal MSR after a burnup of 1.5527 GWd/MTHM (114 full power days). 132
A16 Change in the six group effective delayed neutron fraction parameters when a SQ of plutonium is removed and makeup uranium is added to a thermal MSR after a burnup of 1.5527 GWd/MTHM (114 full power days). 132
A17 Change in reactor parameters when 0.5% of plutonium (4.8 kg) is removed from an FSMSR after a burnup of 2.67 GWd/MTHM (366 full power days). 133
A18 Change in the eight group effective delayed neutron fraction parameters when 0.5% of plutonium (4.8 kg) is removed from an FSMSR after a burnup of 2.67 GWd/MTHM (366 full power days). 133
A19 Change in reactor parameters when 1% of plutonium (9.6 kg) is removed from an FSMSR after a burnup of 2.67 GWd/MTHM (366 full power days). . . . 134
A20 Change in the eight group effective delayed neutron fraction parameters when 1% of plutonium (9.6 kg) is removed from an FSMSR after a burnup of 2.67 GWd/MTHM (366 full power days). 134
A21 Change in reactor parameters when 5% of plutonium (48.2 kg) is removed from an FSMSR after a burnup of 2.67 GWd/MTHM (366 full power days). 135
A22 Change in the eight group effective delayed neutron fraction parameters when 5% of plutonium (48.2 kg) is removed from an FSMSR after a burnup of 2.67 GWd/MTHM (366 full power days). 135
A23 Change in reactor parameters when 10% of plutonium (96.4 kg) is removed from an FSMSR after a burnup of 2.67 GWd/MTHM (366 full power days). 136
A24 Change in the eight group effective delayed neutron fraction parameters when 10% of plutonium (96.4 kg) is removed from an FSMSR after a burnup of 2.67 GWd/MTHM (366 full power days). 136
A25 Change in reactor parameters when 25% of plutonium (241.0 kg) is removed from an FSMSR after a burnup of 2.67 GWd/MTHM (366 full power days). 137

A26 Change in the eight group effective delayed neutron fraction parameters when 25% of plutonium (241.0 kg) is removed from an FSMSR after a burnup of 2.67 GWd/MTHM (366 full power days). 137
B1 Power production related parameters. 138
B2 Specific heat capacities for materials and heat transfer areas in Simulink model. 138
B3 Initial temperatures for Simulink model 139
B4 Mass and mass flow rates in the primary core system. 139
B5 Parameters used in the once through stem generator. 140

List of Figures

3.1 The representative change in mean neutron generation time (top) and total static delayed neutron fraction plotted on top of the summation of delayed neutron group fits (bottom). 21
3.2 The power response of an MSR to a +50 pcm step insertion of reactivity. . . 24
3.3 Frequency response for a clean fuel salt and the same fuel salt after one full power year. 24
3.4 The ratio of the gain of the frequency response over the fresh fuel salt as a function of burnup. 25
3.5 Change in frequency (degrees) response phase shift over the fresh fuel salt as a function of burnup. 26
3.6 Frequency response for an MSR with one year burnup and various amounts of plutonium diverted. 26
3.7 Difference in frequency response between normal operation and various amounts of plutonium removed. 28
3.8 The frequency response of the fresh fuel salt and diversion of all plutonium case. 28
3.9 The frequency response of the fresh fuel salt and diversion of all plutonium case. 29

4.1 The cross section of the thermal MSR [29] 37
4.2 The hexagonal lattice of the thermal MSR [29]. 39
4.3 The relative neutron spectrum of the thermal and fast spectrum MSRs. . . . 50
4.4 The multiplication factor over burnup in the thermal MSR. 51

4.5 The multiplication factor over burnup in the FSMSR. 51
4.6 The fission fraction for each major actinide in the thermal MSR (top) and fast MSR (bottom) 53
4.7 The evolution of the mean neutron generation time with burnup for a thermal (top) and fast (bottom) MSR. 55
4.8 The six group delayed neutron precursor calculation for the thermal (top) and fast (bottom) MSR. 56
4.9 The temperature feedback coefficients for the thermal MSR over burnup. . . 58
4.10 The temperature feedback coefficients for the fast spectrum MSR over burnup. 58
4.11 Fission yields for fission product poisons in the thermal MSR. 60
4.12 Fission yields for fission product poisons in the FSMSR. 60
4.13 The operational reactivity absorbed by Xe-135 in the thermal MSR. 61
4.14 The operational reactivity absorbed by Sm-149 in the thermal MSR. 61
4.15 The operational reactivity absorbed by Sm-149 in the FSMSR. 63
4.16 Decay heat relative to the operational power of the thermal MSR, sorted by what remains in the fuel salt and the isotopes that do not. 63
4.17 Fraction of power in the thermal MSR resulting from fission product decay. . 64
4.18 Fraction of power in the FSMSR resulting from fission product decay. 64
4.19 Total mass plutonium in the thermal spectrum MSR. 66
4.20 Total mass plutonium in the fast spectrum MSR. 66
4.21 The percentage that an SQ (8kg) of plutonium represents of the total plutonium in the thermal MSR fuel salt. 68
4.22 The percentage that an SQ (8kg) of plutonium represents of the total plutonium in the fast spectrum MSR fuel salt. 69

5.1 Diagram of heat transfer between liquid and solid nodes. 83
5.2 Nodalization of the reactor dynamic models [29]. 86
5.3 Example of how the introduction of a steam generator can change the frequency response from a previous study [75]. 88
5.4 A diagram of how the OTSG is nodalized [75]. 88

5.5 Example of four group decay heat precursors fitting Serpent calculated decay heat in terms of operational power with time zero when fission stops. 90
5.6 How the inclusion of different methods for accounting for decay heat changes the frequency response of a reactor for both Gain (top) and phase shift (bottom) relative to not including decay heating. 91

6.1 Gain in the reactor response over burnup of the thermal MSR. 98
6.2 Percentage change in frequency response gain over burnup of the thermal MSR. 98
6.3 The shift in phase of reactor frequency response over burnup of the thermal MSR. 99
6.4 The absolute change in the phase shift over burnup of the thermal MSR. . . 99
6.5 The frequency response of the thermal MSR at 0.32 MWd/MTUi for nominal operation and during plutonium diversion both with and without makeup uranium to account for criticality drop. 101
6.6 The change that plutonium diversion causes in frequency response from nominal operation at 0.32 MWd/MTUi. 101
6.7 Change in the thermal MSR frequency response at different levels of burnup during plutonium diversion. 103
6.8 Gain in the reactor response over burnup for the FSMSR. 105
6.9 Percentage change in frequency response gain over burnup for the FSMSR. . 105
6.10 Phase shift in frequency response of the FSMSR over burnup. 106
6.11 Degree change in phase shift of the FSMSR during burnup. 106
6.12 The frequency response of a FSMSR with different levels of plutonium removed. 107
6.13 The relative change in the frequency response of a FSMSR due to plutonium diversion of increasing amounts. 107

Chapter 1

Introduction

Leaps in human civilization are often correlated to the energy availability. From the development of agriculture to the harnessing of steam power, each step has opened new possibilities for humankind. In the early twentieth century, a new and extremely dense form of energy came onto the stage of human development; the 1940s marked the first time that humans were able to draw energy from the fissioning of heavy nuclei. Our current ability to harness nuclear energy benefits our society in many ways. Nuclear technology provides clean and safe energy in an era marked by heavy reliance on fossil fuels. Additionally, nuclear technology also allows the usage of many advanced medicine techniques, such as medical imaging and cancer treatment, along with agriculture, radio-tracing, food sterilization, and so on. However, the immense power of nuclear technology also resides in the history of nuclear weapons.

The first major human undertaking harnessing nuclear power was for the creation of weapons during the Manhattan Project. This culminated in the bombs dropped on Hiroshima and Nagasaki. For the majority of people in the world, these bombings were the first introduction to nuclear technology. The Cold War would eventually accelerate the development of nuclear weapons around the world. In the early 1950s, efforts were made to push for the peaceful use of nuclear technology rather than military use. Oppenheimer, who had previously worked on the Manhattan Project, became a vocal advocate for disarmament. He and other luminaries urged the United States to move away from nuclear weapons production and towards the peaceful use of atomic energy. This philosophy was later

vocalized by Eisenhower in his historic 1953 speech "Atoms for Peace." In the speech, Eisenhower advocated for the peaceful use of nuclear technology.

Despite the large growth in usage of peaceful atomic energy, there was also a large growth in the development and production of nuclear weaponry. In the mid-1960s, world leaders began to recognize the need to address nuclear proliferation. In 1968, leaders sought to address this need by signing the Treaty of the Non-Proliferation of Nuclear Weapons, also known as the Non-Proliferation Treaty (NPT). The NPT stands on three pillars: non-proliferation, disarmament, and the right to peacefully use nuclear technology. This treaty created two groups: the countries that are considered nuclear weapon states, and those that are considered non-nuclear weapon states. Nuclear weapon states are countries that posses nuclear weapons in accordance with international law, and in the NPT, they promise to work towards disarmament. Non-nuclear weapon states have access to peaceful nuclear technology. However, they are required to provide adequate assurance that their nuclear technology and materials are not being used for non-peaceful purposes.

The measures set in place to detect nuclear material diversion from peaceful use are known as safeguards, and these safeguards are managed by the International Atomic Energy Agency (IAEA). Exactly what safeguard measures get put into place is the result of an agreement between the host country and the IAEA. Though, the IAEA has a base requirement of detecting whether a minimum amount of material is diverted or unaccounted for in a timely manner. Given the information from a safeguarding regime, the IAEA can inform its member states whether a facility is using all its nuclear material for peaceful use or whether that assertion cannot be verified.

The use of safeguards is well established in current Light Water Reactors (LWRs). There are still several fields of research that can be studied to improve safeguarding regimes for LWRs, but given current methods, we can be reasonably sure that the safeguards in place can detect a malicious diversion of nuclear material. However, this may not be the case for new advanced reactors. Generation IV reactors have widely different types of fuel, coolant, and topology. Every unique feature a next generation design incorporates creates another difficulty in incorporating current safeguarding techniques. One design in particular that has many unconventional features is the Molten Salt Reactor (MSR).

1.1 Molten Salt Reactors

As the name implies, MSRs are reactors that incorporate molten salt into their design. The molten salt can be used as either a coolant or as a coolant-fuel mixture. A few designs use molten salt as a coolant for pebble bed fuel, but these designs are not explored in this study [15, 7]. The majority of MSR designs melt actinides into the salt to use it for both a coolant and fuel.

MSRs have a rich history; the first proposed liquid-fueled MSR dates back to the 1950s. At the time, the United States Air Force was looking to make a nuclear-powered aircraft. It was thought that a liquid-fueled MSR would be the most viable design since it operated at ambient pressure, thus reducing the need for a heavy pressure vessel [11]. During this research project at Oak Ridge National Laboratory (ORNL), The Aircraft Reactor Experiment (ARE), the first-ever MSR, was built and operated for seven days before shutting down. It was later realized that the weight of the shielding for any reactor would make nuclear flight impractical, and the program ended.

MSR research would continue during the Molten Salt Research Program (MSRP) at ORNL during the 1960s and 1970s [53]. The goal of this research project was to create a reactor that is based on the thorium fuel cycle. In the mid-century, known uranium reserves were limited, and with the expected expansion of nuclear reactors and atomic weaponry, other means of obtaining fissile material were needed. As a result, there was a race to produce a working breeding fuel cycle. As time went on, though, more uranium reserves were found, and the MSRP and the impending need for a thorium cycle ended. Research into breeding programs were consolidated into the fast U/Pu cycle, fast spectrum research. Nevertheless, the only power-operated MSR, known as the Molten-Salt Reactor Experiment (MSRE), was constructed and operated [34]. The experiments on MSRE provides researchers to this day invaluable data on the operation of MSRs.

In recent times, MSR research has seen a resurgence. Now, the future of peaceful nuclear power is not dependent on the successful deployment of a breeder reactor, but instead on being cost-effective in a competitive energy market. LWRs can be quickly and cost effectively built [45]. However, LWRs are often in the news for construction delays and cost overruns

in the US [30]. It is possible that if new reactor designs have enough passive safety features, these new reactors would be cost-competitive with other forms of electric generation. This is where many hope MSRs could come into play. Since MSRs have liquid fuel and operate at low pressure, there is great potential for making a safer design.

As a result, there are many different entities pursuing MSR technology, and there are as many, if not more, proposed molten salt design iterations. These MSRs span a wide design space from thermal neutron spectrum [20, 44] to fast spectrum [92, 87], from spent fuel [37] to thorium cycle [76, 25, 41, 65], as well as many more designs that challenge conventional thinking on reactors [56, 68]. With so many possible designs, it becomes difficult to determine which ones will be brought into the market. However, there is still research that can help the development of every design that utilizes liquid fuel. One of the big research areas that is prime for development is establishing a creditable safeguards regime for MSRs.

1.2 Safeguards and Molten Salt Reactors

MSRs possess unique features that make implementation of safeguards different from LWRs. Most notably, the fuel in MSRs is liquid rather than solid like in LWRs. MSRs also have online refueling by mixing fresh fuel with actively burning fuel, and the liquid fuel also opens up the possibility of online reprocessing of the fuel. Given the fuel circulation, the fuel salt would be considered well-mixed as well. Current reactor safeguarding methods rely heavily on item counting [31]. The homogeneous nature of molten salt fuel makes safeguarding an MSR more akin to safeguarding a bulk handling facility, at least from the reactor core side. However, being an actively fissioning reactor, MSRs are also very different from currently operating bulk handling facilities. MSRs span this gap in safeguard understanding that has not been fully explored, but many promoters of MSRs are aiming for the global deployment of these reactors. Establishing a reliable safeguards and material accountancy systems is a prerequisite for when they can reach the global market.

The lack of an agreed-upon safeguarding regime for MSRs is not a crisis as much as it is an opportunity. MSRs are still in the design phase of development. This allows researchers and engineers to develop along the approach of safeguards-by-design [14]. By incorporating

safeguards early in the design phase, new reactor designs can have more efficient safeguards. Additionally, the safeguards-by-design approach can also be advantageous to the designer, as a more intimate connection between safeguards and the facility could result in less intrusion to operation. Perhaps, the safeguards could also provide data relevant to the reactor operation. It is during this time that researchers get the exciting opportunity to create new and useful safeguarding methods, and it is at this point in time which this dissertation is written.

This research does not attempt to create a full safeguards regime, but rather it looks at existing safeguarding methods for both reactors and bulk handling facilities that could be applied to MSRs. In addition, this dissertation will explore a novel method of determining relative plutonium concentration by analyzing the frequency response. The frequency response is a reactor's dynamic behavior when a periodic reactivity transient is introduced to the core, and the frequency response is highly dependent on the type and quantity of fissile material present. This research will use this type of analysis to answer the question: Is it possible to detect the withdrawal of a Significant Quantity (SQ) of plutonium from MSR fuel salt? In the process, this research will explore the changes in operating state variables over burnup and during the diversion of plutonium. The cases are for thermal spectrum MSR and a fast spectrum MSR, both of which produce a significant amount of plutonium during operation. By exploring the answers to the question above, the hope is to provide valuable signature that could be used for safeguarding MSRs.

1.3 Scope

This study is organized into several chapters. The next chapter provides background on the relatively underexplored field of safeguards for MSRs. The intention of this chapter is to indicate where, in the MSR safeguard research space, this study would find itself. Chapter 3 is a reprint of the first peer-reviewed article exploring frequency response for use in material accountancy. It presents more accessible frequency analysis by examining only the two most important nuclear parameters: effective delayed neutron fraction and mean neutron generation time. These parameters are calculated in an infinite lattice model, then

applied to a generic MSR with a layout similar to that of the MSRE. Chapter 4 provides a much more detailed fuel cycle model for both a generic thermal and a fast spectrum MSR. In this chapter, all parameters relevant to the frequency response of a reactor are modeled for both nominal operation and plutonium diversion scenarios. In Chapter 5, a new streamlined model is introduced with a focus on frequency response for both thermal and fast MSRs. This model has an order of magnitude, lower runtime, and higher stability, resulting in fewer crashed runs. Chapter 6 combines the model and parameters to demonstrate the frequency response of each reactor type and how plutonium diversion changes reactor behavior. Finally, Chapter 7 details the study's conclusions and introduces the most relevant possible future work.

Chapter 2

Safeguards for Molten Salt Reactor Like Systems

2.1 General Safeguards Approaches

The NPT, along with the Tlatelolco and Rarotonga Treaties, set out the lofty goal of nuclear disarmament. Critical to this goal is maintaining confidence in the peaceful use of the atom. Nuclear facility operators will report on the inventory and location of special nuclear material, but the IAEA verifies these claims through technical means known as safeguards [2]. The host country and IAEA will form a comprehensive safeguards agreement detailing what and how the IAEA will implement safeguards and inspections. The exact measures put in place will vary depending on the comprehensive safeguarding agreement. However, safeguards are designed to detect if there has been a diversion of a significant quantity of nuclear material from peaceful use in a timely manner [1]. A significant quantity was defined by the amount of special nuclear material presumably needed to make a nuclear weapon. Significant quantities of nuclear material are indicated in Table 2.1. This amount forms a legal basis for which all reactors must comply.

Table 2.1: IAEA timeliness goals and significant quantities for direct use material [2]

Material Type	**Significant Quantities**	**Timeliness Goals**
Plutonium	8 kg (all isotopes; <80% Pu-238)	1 month 3 months (irradiated)
Uranium-233	8 kg	1 month 3 months (irradiated)
Highly Enriched Uranium	25 kg	1 month
Low-Enriched Uranium	75 kg	12 months

The IAEA determines appropriate safeguarding measures based on the design specifics of a given facility. The IAEA can use the design to determine what possible diversion pathways exist to safeguard them adequately. Typically, this can put a facility into one of two major categories: item facilities and bulk handling facilities. LWR core falls under the term of item facility and relies heavily on item counting and containment and surveillance (C/S) [2]. All significant quantities will be contained in the solid fuel structures. Inspectors can count the assemblies that go in and are removed from the core. Serial numbers placed on the assemblies can verify the history of the fuel and thus the amount of irradiated special nuclear material present. When not in a core, the fuel is kept under a regularly checked seal to ensure proper use. In doing so, these safeguards set up material balance areas that an inspector can verify material as it moves from one material balance area to another. It should be noted that a loss of surveillance is possible, and it is considered a potential safeguarding concern that requires reverification. This process can be long and costly, so an ideal safeguarding regime would have redundancy or other means of reverification.

For current reactors, there is a fixed unit of material (such as a fuel pellet) that changes in the actinide makeup during operation. That material makeup is verified using a combination of signatures and computational modeling to estimate makeup. These solid units (whether they be pellets, rods or assemblies) thus lend themselves well to item accountancy.

The item accountancy approach poses a problem for MSRs. Given the liquid nature of the fuel, serial numbers cannot be used to verify irradiation history. Item accountancy and reverification face similar problems, since the fuel is one mass that material can be removed or added to. Pebble Bed Reactors (PBRs) face similar challenges to safeguards as MSRs since pebble fuel faces challenges when it comes to serial numbers [31]. Thus, the safeguards for the HTR-10 (a PBR in China) rely heavily on material balance areas. However, it has been noted that reverification should be addressed for large-scale deployment [10]. It is likely that if an MSR were to be built today, it would follow a similar approach. However, PBRs can still somewhat utilize item counting. In contrast, MSR fuel properties are more similar to batch material found in bulk handling facilities. As a result, MSRs may be able to use some safeguarding techniques used in bulk handling facilities.

Bulk handling facilities, such as reprocessing plants, have strikingly similar requirements and challenges as MSR fuel would have. The special nuclear material is in bulk form rather than item form, direct access to the material is based on the amount of radiation emitted, and there can be uncertainty in the input of material into the facility [5]. While MSRs may have higher certainty in what is put in the core since that is usually fresh fuel, there is higher uncertainty in the fuel salt's outflow, while the other demands carry over to MSRs.

Safeguards in such reprocessing and other bulk handling facilities rely first on process monitoring and maintaining a continuity of knowledge, as well as other measurements [5]. If inspectors have accurate information on the process, they can determine if the declared is operating in the declared, peaceful way. Continuity of knowledge refers to maintaining surveillance to assure that this information gathered is accurate. Given the stochastic nature of radiation measurements, there is always a certain level of uncertainty in the results. However, to meet the MC&A regulations, this error is often kept low, at about 1%-2%. Samples used for destructive analysis are periodically taken to reinforce the result from the non-destructive measurements. Given the similarities, there is value in exploring safeguards for closely related facilities like aqueous reprocessing and pyroprocessing.

2.2 Safeguards for Aqueous Reprocessing Facilities

The primary form of aqueous reprocessing is Plutonium and Uranium Recovery by Extraction (PUREX). PUREX dates back to the Cold War and is used for both weapons manufacturing and waste recycling [23]. As of now, all commercial-scale reprocessing uses aqueous reprocessing methods like PUREX [21]. PUREX is a continuous process that separates uranium, plutonium, and fission products from irradiated nuclear fuel.

Once used nuclear fuel (UNF) is removed from the core, it is placed in cooling ponds until the radioactivity and heat production have lowered enough for reprocessing. After the UNF has cooled, the spacer grids and end pieces are sheared off, and the UNF and cladding are dropped into nitric acid. There the UNF is dissolved and separated from the cladding (hulls). The resulting solvent contains uranium, plutonium and fission products is sent to into a liquid-liquid extraction column with an organic solvent (tributyl-n-phosphate) [40].

There, differences in dissolution coefficients will separate the fission products from the more useful plutonium and uranium to a degree. Many of these columns are placed in succession to achieve high separation factors. After the fission products are removed, the plutonium and uranium are separated from each other using the same method.

Given how much PUREX increases resource utilization and the long development history at scale, many nations pursue this technology. Given PUREX's ability it has to separate near pure plutonium, it is of serious safeguarding concern. Sites like Orano la Hague in France and the Rokkasho Reprocessing Plant in Japan provide a wealth of safeguarding experience [16, 43]. Since PUREX is a multistage process, measurements between each stage indicate whether the processing is operated as stated and that no material has been diverted. These measurements consist of both non-destructive and destructive methods.

The non-destructive measurement methods are $\gamma-$ and $\alpha-$spectrometry as well as Hybrid K-Edge Densitometry (HKED) [16]. $\gamma-$spectrometry uses the natural γ emission from the decay of uranium and plutonium isotopes to determine the isotopic makeup of a sample. $\alpha-$spectrometry used only for isotopic ratios of plutonium. HKED is a combination of k-edge densitometry and x-ray fluorescence [60]. K-edge densitometry is the measurement of the transmission differences around the binding energies of an element's k-shell electrons. By analyzing the attenuation of x-ray transmission, uranium density is revealed. The attenuation of the x-rays is caused by the absorption and subsequent emission of the k-shell electrons. Another higher-energy electron will fill the vacancy left by the expulsion of the k-shell electron. When that electron de-excites, it emits x-rays characteristic of the element. From these emissions, the ratio between uranium and plutonium is determined.

Some destructive analysis methods supplement the non-destructive means. The destructive analysis takes the form of Thermal Ionisation Mass Spectrometry (TIMS) and Isotope Dilution Mass Spectrometry (IDMS) [16]. TIMS determines the isotopic composition of uranium and plutonium. IDMS measures plutonium and uranium mass fractions. The expected error from these measurements is at or below 0.1%.

MSRs will likely use many analogs of the non-destructive and destructive methods used in PUREX with some key differences. In PUREX (and other aqueous reprocessing methods) uranium and plutonium are in oxide form while they are not in an MSR. There are additional

differences when looking at process monitoring. PUREX has multiple stages with varying product purity and attractiveness. MSRs instead consist mostly of single fuel salt mass, where nuclear material is both created and destroyed. However, safeguards and process monitoring for PUREX do provide a good basis for those in MSRs.

2.3 Safeguards for Pyroprocessing Facilities

When taking process monitoring into account, pyroprocessing may be a more similar environment to MSRs is pyroprocessing. Pyroprocessing was initially developed to be coupled with fast-spectrum, sodium-cooled fast breeder reactors [71]. These reactors were designed to burn plutonium and use excess neutrons for breeding more plutonium from U-238 in the core blanket. These reactors were planned to have on-site reprocessing facilities to extract the bred plutonium from the metal uranium blanket rods for fissile in new metal fuel rods [39]. Reprocessing metal fuel for a fast reactor had requirements that made aqueous reprocessing not ideal. The fuel rods are not left to cool as long as in aqueous reprocessing. Therefore, the process needs to be able to handle more heat and higher levels of radiation. Since pyroprocessing uses a eutectic molten salt mixture (usually LiCl-KCl), the dissolving medium would not suffer from radiation damage the way the organic solvent in aqueous reprocessing would. Once mixed into the molten salt, the actinides are separated from the fission products by taking advantage of Gibbs's free energy differences. A voltage potential is added to the molten salt mixture, causing the uranium and transuranic metals to plate out on the cathode.

The fast breeder reactors were never brought to a large-scale commercial release as planned. As a result, there are no full-scale pyroprocessing plants in use in the nuclear fuel cycle today. However, there has been some renewed interest in reprocessing uranium oxide pellets in a place like the Republic of Korea, and some have speculated that pyroprocessing may be more proliferation-resistant than the PUREX process [88]. Regardless, there is no example of a fully safeguarded facility that can be drawn from. Additionally, the environment and process differences make it uncertain whether some of the methods used

for aqueous reprocessing can be applied to pyroprocessing. For instance, PUREX is a multi-stage continuous process while pyroprocessing is a batch process [22]. This batch process is also not a perfect means of extracting the nuclear material, thus complicating material balance areas. The high temperatures and radiation fields make instrumentation difficult. Moreover, several issues need to be accounted for when it comes to sampling, such as high temperature and sample inhomogeneity.

Despite these difficulties, there have been many proposed methods of safeguarding a pyroprocessing facility. Coble et al. provides an overview of the proposed methods with detailed descriptions of the measurement techniques [22]. These measurement techniques are split into passive radiation signatures, active radiation signatures, and process monitoring. Passive radiation signatures include $\gamma-$ and $\alpha-$spectrometry but also other methods like microcalorimetry and neutron counting. These passive measurements produce results quickly but have higher uncertainty. The opposite case is true for active radiation signatures. Active interrogation methods would have a high level of accuracy with high latency. Such methods that fit here would be HKED, laser-induced breakdown spectroscopy, neutron interrogation, and much more. The final proposed safeguards means are monitoring control and process state variables. By checking things such as density, salt level, temperature, and so on, inspectors can determine whether the facility is operating for peaceful uses as intended. By combining several methods from these different categories, pyroprocessing facilities can have a robust safeguarding regime.

2.4 Additional Consideration for Molten Salt Reactor Safeguards

Ultimately, MSRs will likely use a combination of item accountancy methods found in current reactors and process monitoring like that in bulk handling facilities. The activity fission fuel salt in MSRs will need some sort of burnup prediction similar to what current reactors use. Though, online reprocessing and refueling require process monitoring not too dissimilar

from reprocessing plants. These methods would need to be evaluated for MSRs, as the environment is so alien to current facilities.

One of the major ways the MSR environment distinguishes itself from reprocessing the radiation field. The fuel salt is activity fission and therefore has zero cooling time for online monitoring and little cooling time for off-line monitoring. As a result, any instrumentation and detectors will have to deal with a very strong radiation field [90]. That is not to mention the high temperatures and corrosive nature of the fuel salt itself. Furthermore, the burnup taking place in the reactor will slowly change the composition of the fuel. This will result in various chemical species such as noble metals that can plate out throughout the reactor that could complicate detector placement. Detector placement would also have to consider the circulation of the fuel and how the passive signatures would change from the core region and through the exterior circulation loop.

Another possible issue with developing a safeguarding regime for MSRs is the large MSR design space. There is no guarantee that a particular method would be applicable to every design [91]. For instance, if a specific method is tuned to measuring plutonium, it would be of little use to a thorium cycle reactor. There are numerous other design choices, such as reprocessing, which would also determine the possible diversion pathways. Therefore, it is likely that the various designs will have different safeguarding measures to account for their unique features.

Although safeguarding an MSR may pose a significant yet attainable challenge. Although item facility methods may not work on the fuel salt, much of the bulk handling safeguards will likely be applicable to MSRs. MSRs also have the advantage that the circulation of the fuel makes obtaining a homogeneous sample representative of the entirety of the fuel easier. Additionally, the operation of the reactor is highly dependent on the presence of the special nuclear material in the core, and any attempt to remove special material from the core could alter operational parameters. There is significant work ongoing to develop methods and detectors for use in safeguarding MSRs [27]. Many detectors are being converted from their current working environments to environments that would have high temperatures and string radiation fields, like high dose neutron detectors. Other detectors like microcalorimeters being developed for use in pyroprocessing would have a good chance of working for MSRs.

Recent work showed that voltammetry can determine actinide concentration in molten salt fuel as well [93].

Despite these developments, there is no agreed upon safeguarding regime. All MSRs are currently in the design phase. As a result, designers should follow the safeguards-by-design criteria when planning their reactors. It is key that the MSR design community and safeguarding community collaborate to bring effective and non-intrusive safeguards.

Chapter 3

Use of Reactor Dynamic Response for Safeguards

In the past, it was common practice to measure a reactor's response to periodic reactivity insertions across a range of frequencies. This technique was often employed to determine various thermal properties of the reactor, including heat transfer characteristics. However, the approach had limitations—particularly in boiling water reactors, where phase changes introduced complexities that did not align well with the linearized models used on the analog computers of the time [63]. Over the years, improvements in the precision of thermophysical parameter measurements have reduced some of these uncertainties. All this led to the gradually declined in the use of frequency analysis on modern reactor applications. Despite this, the method remains a valid and powerful tool for characterizing reactor behavior. Discussion on frequency analysis in the context of dynamic modeling is in Chapter 5. In the context of safeguards, the primary uncertainties now lie in the neutronic parameters—specifically, the kinetic parameters, mean neutron generation time, and delayed neutron fraction—rather than thermal properties.

As the reactor undergoes burnup, higher actinides increase in density. As a result, an actinide's share of fission evolves with burnup, and, consequently, the reactor kinetic parameters evolve as well. It can be reasoned that the shift in kinetic parameters should create a corresponding shift in dynamic response (specifically for certain frequencies of periodic insertions) of the reactor. It could also be deduced that a diversion of fissile, such as

plutonium, would also result in a shift in dynamic response. These theories were put to the test in Reference [85], the body of which is reproduced here for this chapter. The study calculates the kinetic parameters for a infinite, 2-D, graphite-moderated lattice. The kinetic parameters for are also calculated for the case of plutonium diversion. Using these kinetic parameters in a dynamic model of an MSR shows that the frequency response of the reactor shifts with burnup, and the diversion of plutonium also causes a characteristic change in the frequency response.

The author of this dissertation served as the primary role in modeling methodology, data generation, data visualization, and writing. This work would not have been possible without the contribution of coauthors Dr. Ondřej Chvála and Dr. Steven Skutnik who provided supervision, funding, and editing/reviewing of the paper. The author would also like to acknowledge the contribution of Vikram Singh who contributed early discussion and investigation to preliminary results that this work draws from. The completion of the work would also not have been possible without the financial contribution from a grant sponsored by the U.S. Department of Energy, Office of Nuclear Energy, award number DE-NE0008793.

The work in this chapter is drown from:

Wheeler, A. M., Chvála, O., & Skutnik, S. (2021). Signatures of Plutonium Diversion in Molten Salt Reactor Dynamics. *Annals of Nuclear Energy*, 160, 108370.

3.1 Reactor Dynamic Modeling Method

To simulate reactor response to reactivity insertions, a previously developed nodal modified point kinetic modeling method was chosen [74, 73, 75]. This method is validated against data from the Molten-Salt reactor Experiment (MSRE) and accounts for the drift of delayed neutron precursors outside and back into the core, which is crucial for this work. It is also adaptable and light enough to be readily applied to many different designs and transients while requiring little computational resources. This is useful since many transients cases need to be run to determine corresponding sensitives. It has been theorized that similar modeling approaches could be used to inform MSR safeguard development [33]. This study

puts that theory to practice. All the model needs is parameters fed to it from a reactor analysis code. This study utilizes Serpent 2 [51].

Since the goal of this paper is to develop and analyze the method, no particular design is explored. Instead, a generic MSR system topology is adopted. This generic topology is near identical to the MSRE's topology, with only a few minor exceptions. First, the boundary condition of the model is not a radiator but a constant heat removal. This new boundary condition can be more easily scaled to different nominal power levels if need be. Second, the salt flow rate is increased so that the core transit time 5 seconds and the external loop transit time is 10 seconds. This affects the effective delayed neutron fraction due to precursor drag and resonance frequencies positions. Third and final is that the key kinetic parameters of mean neutron generation time and delayed neutron fraction are derived from burnup calculations rather than MSRE parameters, which is at the heart of this study. All other parameters such as power, heat transfer coefficients, mass flow rate, etc. are the same as the MSRE. Consequently, the model analyzed is very similar to the MSRE model presented in detail in Reference [74] but more streamlined to improve computational performance.

The most important feature of this model is the ability to insert reactivity into the core. What will be shown in Section 4 is that the reactor is only somewhat sensitive to plutonium concentration during a step reactivity insertions. However, the sensitivity varies for periodic (sinusoidal) insertions. When a wave of reactivity is inserted into the core, there are corresponding heat and delayed neutron precursor waves. These waves induce their own associated reactivity via thermal feedbacks, and thus either constructively or destructively interfere with the ongoing initiating wave as they circulate throughout the reactor system. As a result, the reactor power will have an accompanying power wave with a gain in amplitude and a shifted phase. Different frequencies of reactivity inputs will have different gains and phase shifts. Graphs of these frequency-dependent amplitude gains and phase shifts are known as Bode plots [80]. Performing this frequency analysis is an integral part of verifying a reactor's stability [46]. Frequency analysis is also done to verify dynamic models, as was done for the MSRE [9]. In this study, the application of frequency analysis is expanded to safeguards, and the effect plutonium has on the mean neutron generation time and delayed neutron fraction. There have been previous studies

that looked into the sensitivity of frequency analysis for various parameters [72], and this study combines parameters to replicate plutonium removal.

3.2 Kinetic Parameters, Burnup, and Diversion Scenarios

As a reactor that contains U-238 undergoes burnup, plutonium will accumulate in the fuel. Consequently, plutonium fissions take an increasing percentage of the fissions in the chain reaction. The introduction of plutonium is the main driver for the change in kinematic parameters and the resulting reactor dynamic change. To perform this analysis on any particular reactor, there needs to be a detailed burnup calculation that accounts for all the underlining physics. In solid fuel reactors, the fuel pellets will have to be removed due to thermal and radiation damage sustained after a certain level of burnup. MSRs, however, do not have these constraints. Fresh fuel can be continually added, and fission products can be removed online. As a result, there can be a significant deviation in long term isotopic makeup of MSR fuels compared to solid fuel reactors. Any reasonable estimate of plutonium concentration needs to account for this. This study uses Serpent 2 to determine fuel concentration since it can model continuous material feed and removal, and it also calculates kinetic parameters [51]. It should be noted that Serpent can also calculate some dynamic parameters, such as temperature coefficients of reactivity. However, the void reactivity coefficient is not expected to change dramatically. The Doppler coefficient will to a degree change, but it is an order of magnitude lower in size than the void coefficient. Therefore, the feedback coefficients were not taken into account for this study. Additionally, since serpent does not have an internal means of accounting for neutron precursor drift, the effects of precursor drift are ignored.

As mentioned before, no particular MSR design is being explored rather the methodology. Therefore, a single hexagonal channel with reflective boundaries geometry is used for burnup calculations. The fuel salt, which consists of $3.353\,\mathrm{g/cm^3}$ LiF-BeF_2-UF_4 (72-16-12 mole%, 99% Li-7, 1.3% U-235), fills a central channel with a radius of 2.7 cm and pitch of 14 cm.

The graphite moderator is $1.8\,\mathrm{g/cm^3}$ carbon with a 1 ppm boron impurity. To maintain criticality, the salt is refueled with a salt with the same molecular makeup as the starting fuel but with 10% enriched uranium. All gaseous fission products are removed at a rate of 1%/s. This removal rate is similar to that presented in Reference [64]. All other fission products remain in the fuel salt. For the purposes of preserving the density of the fuel salt, there is a removal rate for the homogeneous composition of the fuel overflow tank during operation. The overflow tank is simply a material card within Serpent that keeps the removed material separate and does not reintroduce it to the fuel salt.

This model is burned for five full-power years with a power density of $20\,\mathrm{W/g}$. This burnup simulation resulted in a representative fuel material evolution. From this estimated fuel salt material evolution, the accompanying kinetic parameters change is also calculated. Mean neutron generation time (Λ) and delayed neutron fractions (β_i, in this case six group) are two of the highest impacting kinetic parameters. These parameters were extracted and used in the dynamic model to represent respective levels of burnup. Figure 3.1 (top) depicts the mean neutron generation time over burnup. Since Serpent 2 is a Monte Carlo code, there is statistical noise associated with its calculated parameters. This noise can be reduced by running a higher number of neutron histories. However, since this study is a focused on exploring the method rather than providing a reactor-specific study, the less computationally expensive mean of fitting the resulting parameters is used for each of the delayed neutron fraction groups to establish a smooth parameter evolution with burnup. Furthermore, there would be no noise if a deterministic transport method was used, which will likely be the case for an analysis of a mature MSR design. The resulting total static delayed neutron fraction and trend line are shown in Figure 3.1 (bottom). The mean neutron generation time was not fit, since the noise was negligible. These trends are not meant to be perfectly representative of any specific MSR design, but it is instead meant to be a reasonably close enough approximation to demonstrate the capability of this approach. The mean neutron generation time drops with burnup due to fission product buildup, which increases absorption. The delayed neutron fraction decreases, on the other hand, due to the increase in Pu-239 fissions. The decrease is slowed before the plutonium concentration reaches maximum due to the change in its isotopic composition.

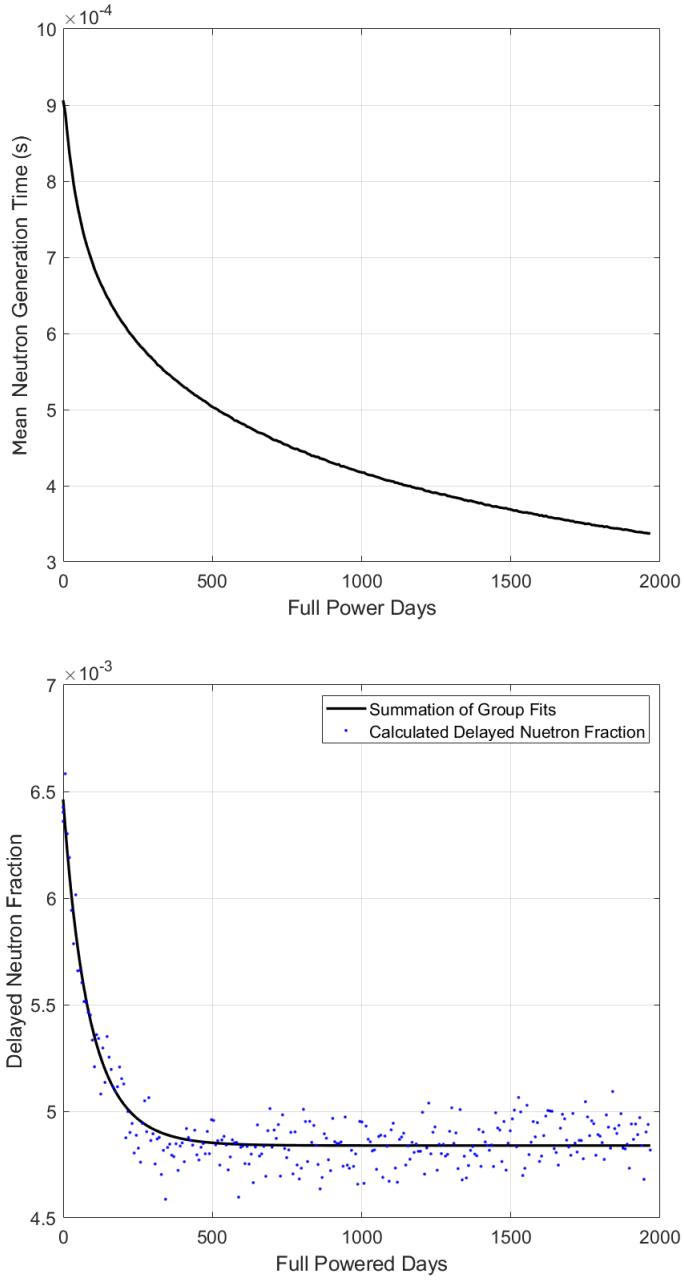

Figure 3.1: The representative change in mean neutron generation time (top) and total static delayed neutron fraction plotted on top of the summation of delayed neutron group fits (bottom).

These calculations form the expected behavior evolution of a reactor over burnup. However, this behavior will be disrupted if plutonium is removed. To examine what can be seen when some plutonium is removed, the mean neutron generation time and the six-group delayed neutron fractions are calculated for a plutonium diversion case. This study examines the case where a fraction of plutonium is removed all at once from an MSR after one year of operation. The kinetic parameters for one year burnup calculated earlier are used as the expected behavior for a reactor without material diversion (referred to as "nominal Pu"). To determine the kinetic parameters in the case of plutonium diversion, the plutonium concentrations in the material card is scaled down to represent the diversion of different percentages of plutonium. All other parameters remain the same. The kinetic parameters calculated for the different percentages of plutonium removal are shown in Table 3.1.

An additional case of when fissile uranium is added to the fuel salt to replace diverted plutonium is also examined. Since the removal of plutonium will act as a negative reactivity insertion, there will be a temperature drop, which could signal the diversion. This temperature drop could be masked by a control rod movement. However, if control rod position is well tracked, the only way to mask the diversion is the addition of more fissile material. Therefore, to determine how the reactor would respond during such a scenario, the material card for 50% plutonium removal had the enrichment increase to the original critical levels. The resulting delayed neutron fraction is 0.00571, mean neutron generation time is 6.2E-4 s.

Table 3.1: Kinetic parameters for plutonium diversion scenarios after one full powered year

Pu in fuel (% nominal)	Λ	β
100	5.4E-4	0.00483
90	5.7E-4	0.00490
75	6.0E-4	0.00509
50	6.8E-4	0.00512
25	7.8E-4	0.00584
0	9.4E-4	0.00658

3.3 Results

This section shows how the simulated response from the model detailed in Section 3.1 changes with the parameters calculated for various scenarios in Section 3.2. This section will focus on the frequency response of the reactor. A more intuitive transient would be a step reactivity insertion or a ramp insertion. This would be akin to a control rod movement from one position to another. One such transient is shown in Figure 3.2 where +50 pcm reactivity is inserted into the core. This figure shows the power response of the model MSR after one year of depletion, where the calculated amount of plutonium is present compared to where all the plutonium is removed. The only part of the transient that shows a significant, perhaps measurable, difference is the initial power peak. Even then, the difference is small and short lived. Additionally, these step insertions, unlike a small, ±1 pcm, sinusoidal insertion, leaves lasting temperature changes in the fuel salt, which may put strain on the reactor system. For these reasons, the step insertion transients are not explored as viable safeguards signatures.

This change is exemplified in Figure 3.3, which depicts the frequency response for the reactor to a ±1 pcm sinusoidal insertion at the beginning of the fuel cycle and after one full power year of depletion. There is significant difference in both the gain and the phase shift at certain ranges of frequencies, which are different for the phase and gain. Investigating this burnup dependency in more detail, a ratio of the frequency response to the fresh fuel baseline was formed. Figure 3.4 shows the ratio of gain as a function of burnup to the fresh salt gain. Figure 3.5 shows the same burnup dependency of the phase shift ratio. Clearly, the burnup evolution of frequency response shows a specific, smoothly evolving, pattern, which could be leveraged to verify that the reactor was operated as declared.

When a reactor operator claims a certain level of burnup, the frequency response should fit the established trend. If the frequency characteristics diverges from its expected shape, it indicates that some unreported alteration may have occurred. In the case that plutonium is removed, it is likely easily observed using this method. Using the parameters calculated in Section 3.2 for the various plutonium diversion cases, the frequency response shows where to find these signature patterns. Figure 3.6 shows the characteristics of a system after one

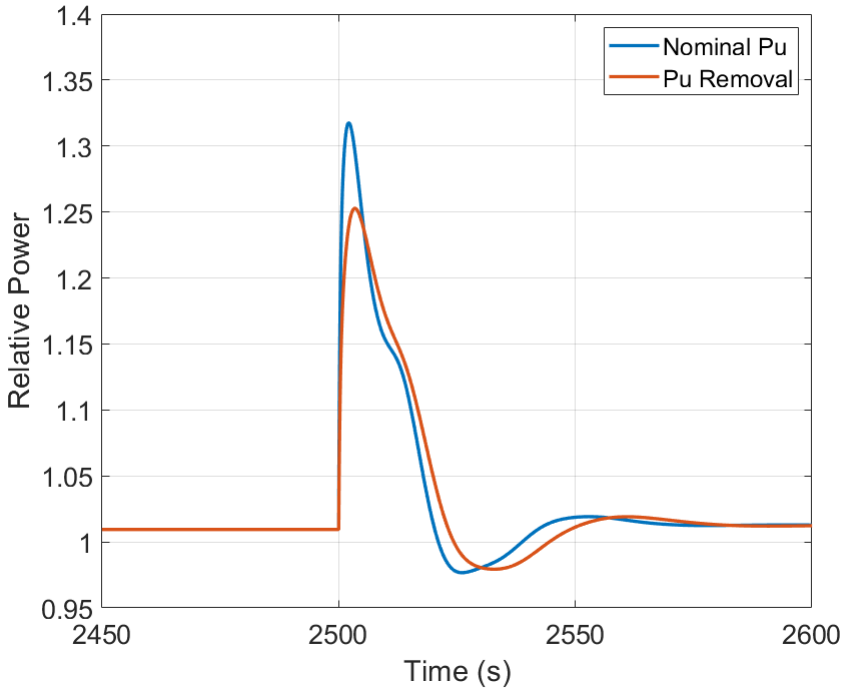

Figure 3.2: The power response of an MSR to a +50 pcm step insertion of reactivity.

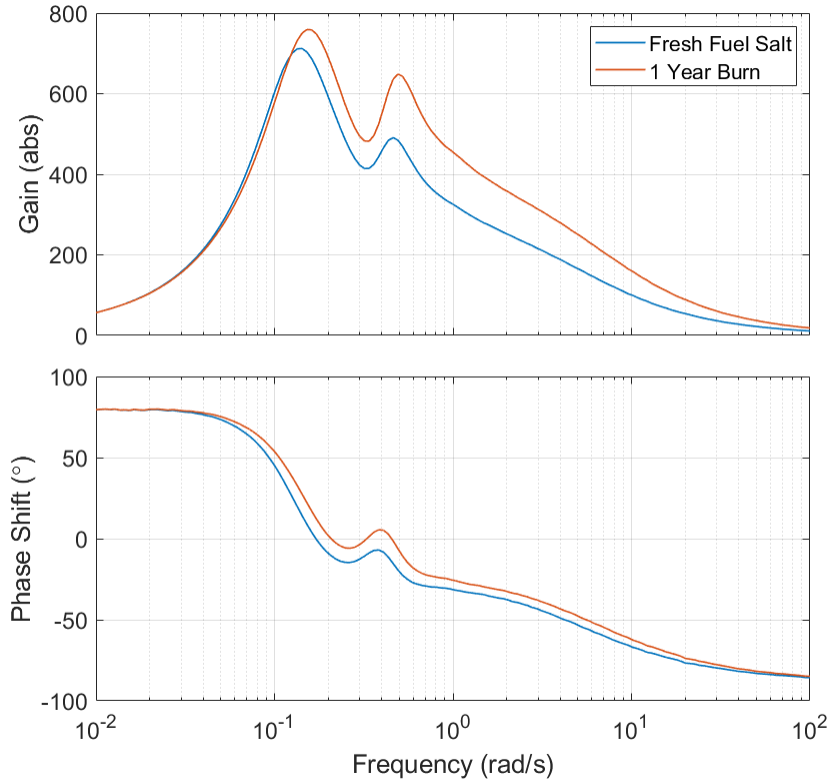

Figure 3.3: Frequency response for a clean fuel salt and the same fuel salt after one full power year.

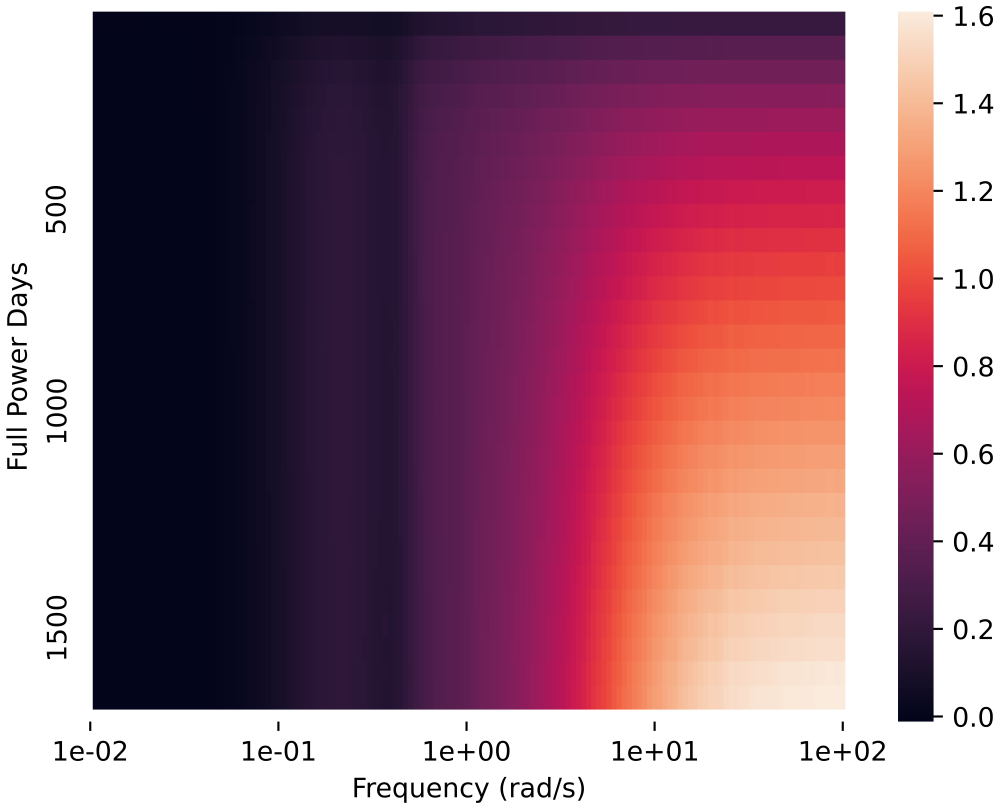

Figure 3.4: The ratio of the gain of the frequency response over the fresh fuel salt as a function of burnup.

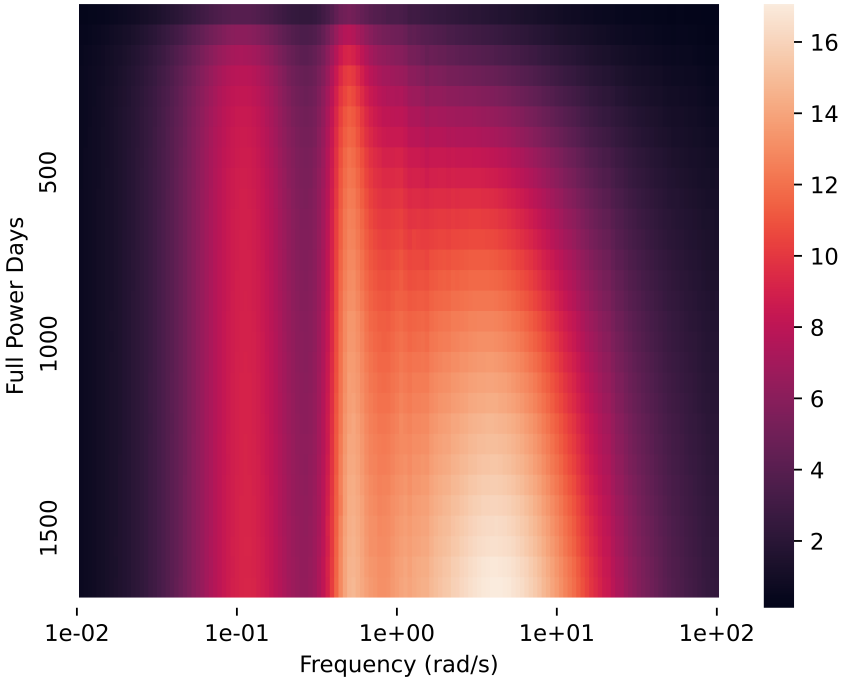

Figure 3.5: Change in frequency (degrees) response phase shift over the fresh fuel salt as a function of burnup.

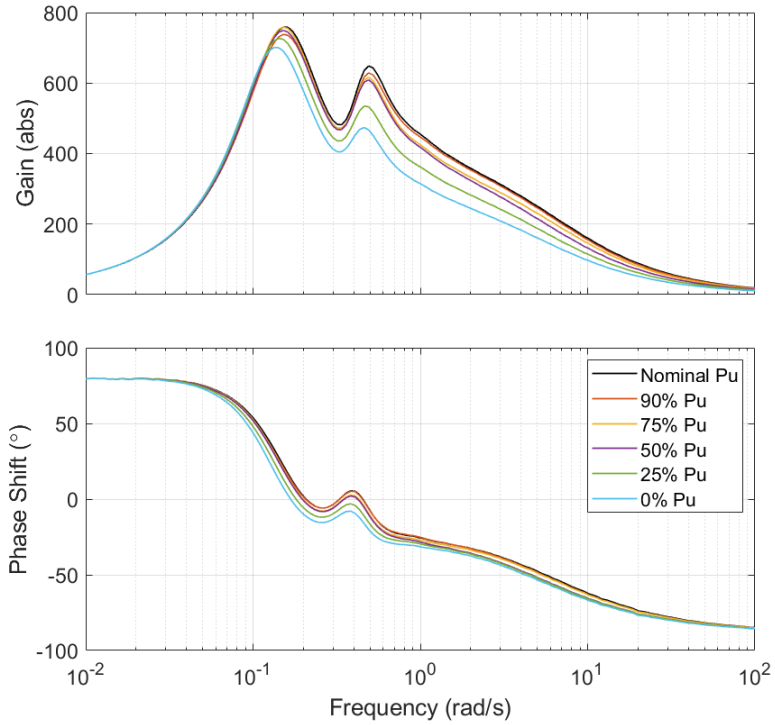

Figure 3.6: Frequency response for an MSR with one year burnup and various amounts of plutonium diverted.

full power year of depletion, for differing levels of plutonium left in the fuel salt. There are specific frequency ranges of difference in both gain and phase shift.

This is emphasized in Figure 3.7 where this difference in response for each case is shown explicitly as the difference in response for the diversion cases as a percentage of the expected nominal material composition. These results indicate that there is a significant divergence in the frequency response if there is removal of plutonium from the fuel salt. Take, as an example, a reactor system that contains 10.7 kg of plutonium in the fuel salt. Then a nefarious actor were to remove a significant quantity of plutonium (8 kg). As a result, there would only be about 25% of bred plutonium left in the core. The gain would be off by as much as 30% for higher frequencies, and the phase shift can be off by almost 10° for the medium frequencies.

There are more implications found when comparing the frequency response of the total diversion of plutonium to that of the fresh fuel salts shown in Figure 3.8. It can be seen that the frequency response is near identical, save a small discrepancy in the gain for some frequency. This suggests that all the change in response over burnup is the result of the plutonium build up.

The case for when uranium is added to counteract the criticality drop from plutonium diversion, shown in Figure 3.9. For a large range of frequencies, the addition of uranium fissile makes the diversion more noticeable. This means that in the case where plutonium is removed, there is a negative reactivity insertion that can be seen with either temperature, fuel salt level, or control rod placement in addition to the dynamic signatures. However, if cover uranium is added to the core at plutonium removal, the dynamic signatures (change in frequency response) remain while the other indicators (loss of reactivity, temperature changes) are gone.

3.4 Discussion

Ideally, material flow in and out of the core would be well tracked in a manner that can be independently verified. However, in the case that observation is lost or additional assurances are required, the presented method poses a viable option to add into a larger safeguarding

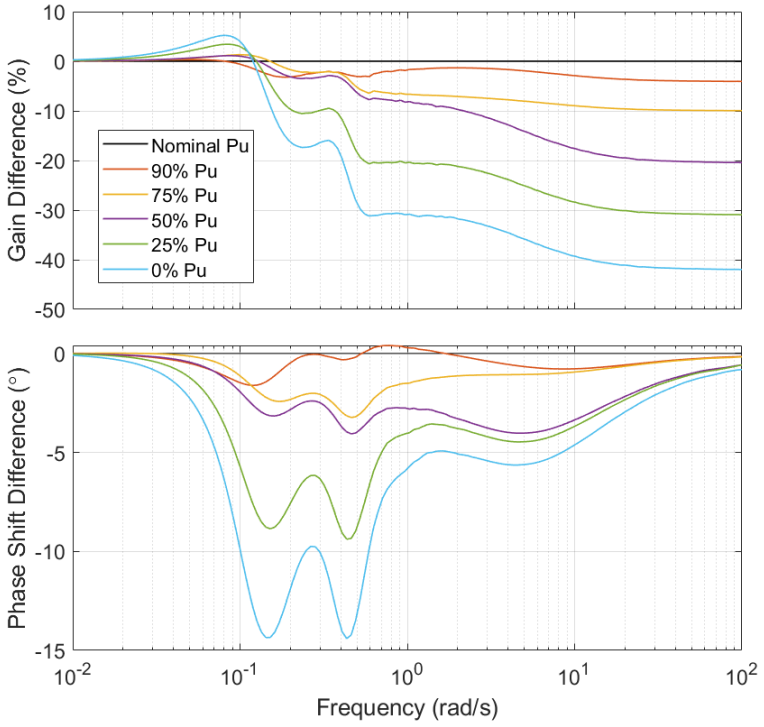

Figure 3.7: Difference in frequency response between normal operation and various amounts of plutonium removed.

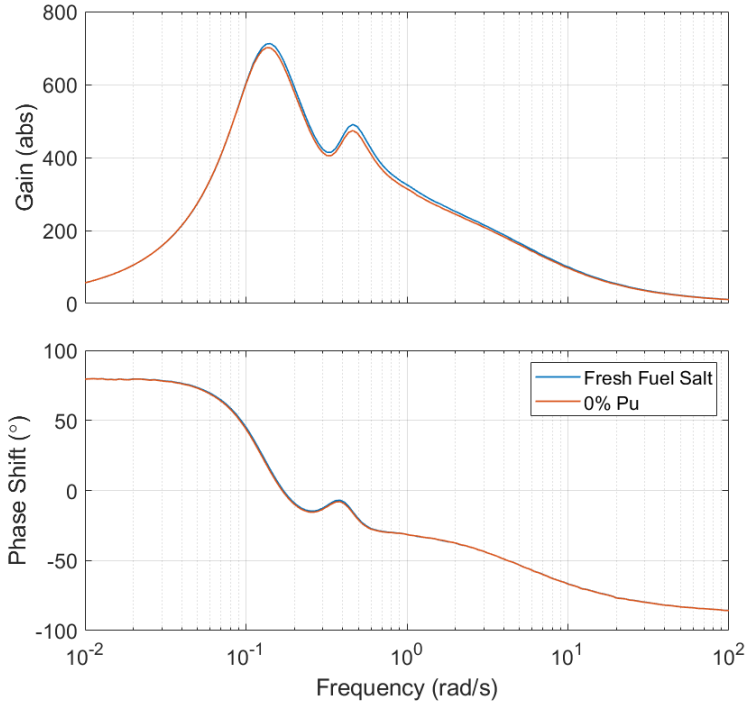

Figure 3.8: The frequency response of the fresh fuel salt and diversion of all plutonium case.

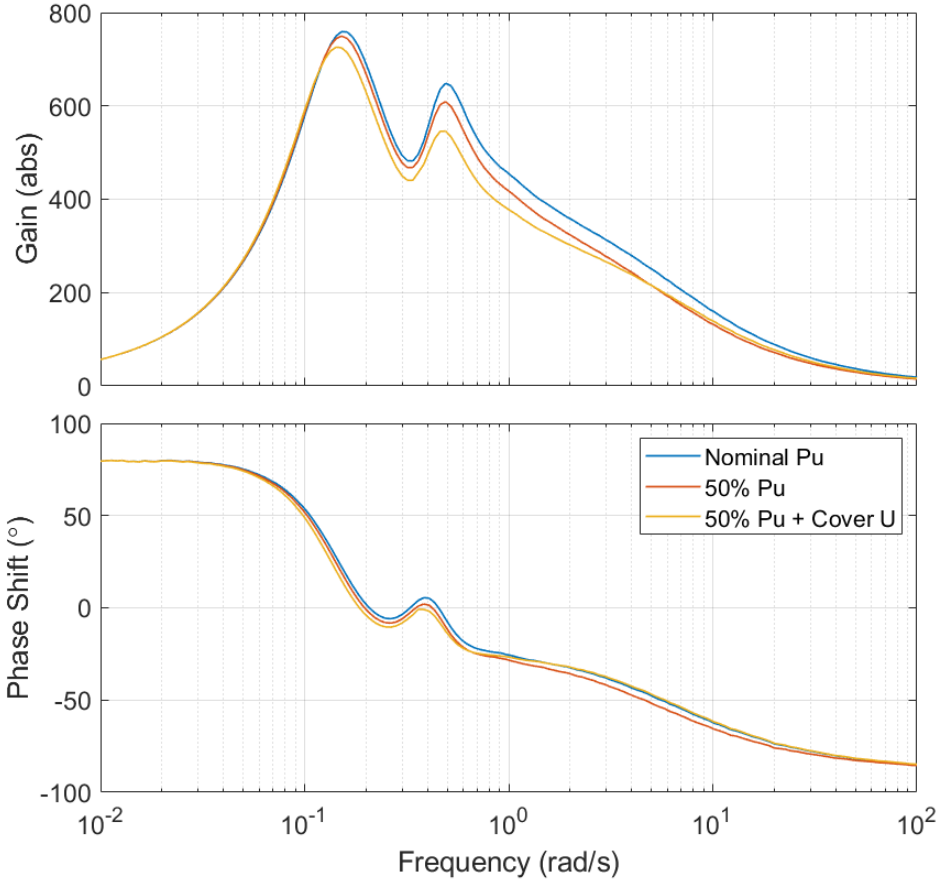

Figure 3.9: The frequency response of the fresh fuel salt and diversion of all plutonium case.

regime, along with tracking of salt volume, various means of physical protection, and possibly archiving salt samples.

Frequency analysis can be done quickly. Reference [80] goes over many methods that could be done in its time, including a reactivity insertion using a pseudo random binary sequence, which allows sampling of a wide range of frequencies at the same time. Such an insertion was used to form the MSRE's frequency analysis, and the measurement only took 15 minutes with no lasting changes to operating conditions [9]. Additionally, this method requires no shutdown of the reactor, and in fact requires the reactor to be operating.

The drawback of this method is its sensitivity to the relative concentration of fissile actinides. Consequently, the reactor's frequency response is less sensitive to a diversion of a set amount of material, such as the significant quantity, in a very large reactor containing a large total inventory of plutonium than in a smaller reactor. The concentration of plutonium at the time of diversion presented in this study is around 7.45E-3 $\mathrm{g/cm^3}$, which corresponds to approximately 1.07 $\mathrm{m^3}$ — about 4.2 standard bath tubs. It should also be noted that Pu-241 has a higher delayed neutron fraction when compared to Pu-239. As a result, this method will be more sensitive to diversion during the beginning of plant operation when the plutonium is mainly Pu-239, which is more attractive for diversion.

A physical system that could implement this detection method could be readily designed. As mentioned before, this type of insertion could be done with control rod movements. However, a less invasive alternative would be the addition of a rotating neutron reflector/absorber in the reflector region that could make a ± 1 pcm reactivity sine wave. This could be controlled independently of the reactor operators. A further benefit of a sine wave reactivity insertion is a generation of a heatwave circulating through the system, which could be utilized to reconstruct local flow speeds using only thermocouple readings correlated with power measurement. Exploring this possibility is outside of the scope of this paper.

While this method was developed for MSRs, it could be applied to any reactor system where fuel undergoes evolution of its actinide composition that has impacts in its kinetics parameters. It is proposed that the method could be applied to reactors with pebble bed fuel, both gas cooled and salt cooled, since the fuel pebbles also face material accountancy challenges [10].

3.5 Conclusion

The major hurdle that MSRs face when dealing with safeguards is the difficulty in assaying and tracking the core fuel actinide composition for material accountancy purposes. This issue applies more broadly to other advanced reactor concepts with fuel that cannot be easily item-counted, e.g., aqueous homogeneous reactors and high-temperature gas and salt cooled pebble bed reactors.

The groundbreaking methodology presented in this paper shows a path forward for developing safeguards for these reactors. It can be surmised from the data that given the increase in plutonium through burnup, the reactor's kinetic parameters shift enough to have a measurable effect on the dynamic response of a reactor, presenting a distinct pattern in both amplitude gain and phase shift of the frequency response. The method of using frequency analysis to determine whether plutonium has been diverted or not appears to be a viable possible component of a safeguarding regime. This method only relies on small reactivity insertion, whether periodic or pseudo-random binary, and a neutron counter. Therefore, it can be easily implemented with existing instrumentation, or, if desired due to the nature of international safeguards, with an additional dedicated but cheap and simple instrumentation. Performing this analysis for any particular future design could be quickly done and with minimal burden, given that accurate transient simulations are required for licensing to begin with. The major constraints for this method would be having a complete understanding of reactor burnup and operational history. As a result, this method would require a thorough burnup calculation to form expected reactor behavior and rigorous monitoring of the reactor's operational history. Given the promising results shown in this study, coupling the presented method with an in-depth reactor design study appears as a clear next step in developing this method further.

Chapter 4

Molten Salt Reactor Fuel Cycle and Plutonium Diversion Modeling

As established in the previous chapter, the presence and removal of plutonium in the fuel salt changes the neutronic parameters enough to alter the frequency response in an MSR. This phenomenon opens the possibility of utilizing the frequency response for monitoring burnup as well as detecting plutonium diversion. Therefore, it is imperative to investigate which parameters measurably evolve over burnup and how they link to the frequency response. Additionally, international safeguards have strict mass and timeliness requirements for detecting a diversion of a SQ of plutonium 2.1. Thus, the speed and accuracy at which a frequency response could indicate plutonium diversion are attractive from a safeguards and Material Control and Accounting (MC&A) perspective.

This chapter details the methodology used to establish the evolution of reactor parameters relevant to the frequency response during normal operation and plutonium diversion. This work models two different classes of reactor systems, which both produce an appreciable amount of plutonium in their fuel cycle. The first reactor investigated is a thermal spectrum, LEU-fueled MSR. The second reactor investigated is a fast spectrum, chloride salt MSR initially fueled with high-assay low-enriched uranium (HALEU). Even though both systems will breed plutonium, the rate and isotopic makeup of the plutonium will differ drastically between the two, and each reactor also has different design requirements which affect the frequency response. By examining both reactors, we can better understand the applicability

of using frequency response to assess plutonium concentration in a range of liquid-fueled reactors and thus apply this metric to MC&A programs.

4.1 MSR Fuel Cycle Modeling Considerations

The fuel cycles of MSRs and other liquid-fueled reactors differ significantly from solid-fueled reactors. In the most common type of solid fuel reactors, LWRs, fuel assemblies are placed in fixed positions in the core and only moved or replaced during refueling at somewhat fixed intervals. In most MSRs, the fuel is also the coolant and therefore is circulated and mixed. Refueling happens online, and certain elements will volatilize or plate out during operation, depending on the fuel salt chemistry. As a result, there are no specific units of fuel that have undergone a level of burnup different from others. Additionally, the concentration of common burnup indicators such as cesium (a daughter of the gaseous fission product xenon) will be affected by inherent chemical separation and/or active reprocessing. Therefore, MSRs requires fundamentally different approaches to understanding the fuel cycle and even further granularity within the MSR design space.

There has never been a power-operated MSR in the thermal spectrum that utilizes LEU as the primary fissile material. However, the early operation of the MSRE used uranium enriched to 33 wt. %, and could have had a similar fuel cycle management scheme as some proposed reactors. More importantly, the use of a moderator and U-235 as the primary fissile isotope means the neutronic behavior will be similar. Despite the lack of a dedicated experiment, there have been several studies that explore the open cycle, LEU fueled MSR concept [13, 94, 24, 57, 82, 20]. This fuel cycle is attractive due to the similarity to existing technology (mainly LWRs) and the availability of LEU from current supply chains. Because of this, many companies are seeking to commercialize an MSR utilizing an open fuel cycle and LEU fuel, making this an active area of research.

Fast spectrum MSR (FSMSR) fuel cycles diverge from LWRs even more than thermal MSRs. The increased neutron yield in the fast spectrum combined with high actinide loading can lead to high plutonium conversions but also lighter plutonium isotopic distribution due to the higher fission to capture ratio. The hard spectrum opens several fuel cycle options

for FSMSRs, each with their own advocates. The first option is a once-through burner fuel cycle [26]. The once-through fuel cycle would require refueling, but it would have higher fuel utilization and a more manageable waste output. Another option for FSMSR fuel cycle is the Breed-and-Burn (B&B) fuel cycle [36, 54]. Much of the proposals for B&B fuel cycle have been for traveling wave reactors and standing wave reactors in the sodium cooled fast reactor design space [52]. The bonded fuel salt in an FSMSR takes away the material constrains of the traveling wave design, and the well-mixed nature of the fuel inherently shuffles the core like a standing wave reactor would. Fuel salt is continuously siphoned off a small fraction of fuel salt and replaced with depleted uranium bearing salt in the FSMSR B&B refueling strategy. This siphoning creates a consistently breeding fuel salt mass that manages the changes in criticality over burnup, but it also produces a stream of uranium and plutonium that would need to be monitored. It is possible to lower the amount of breeding to reduce the criticality swing while also remaining critical for the lifetime of the reactor vessel [84]. Since this approach would also limit refueling, fuel storage, and safeguarding requirements, it is the method explored in this study.

It should be noted that a great deal of historic research on MSRs has focused on thermal spectrum reactors using a thorium fuel cycle. Reactors that operate entirely on the thorium cycle will have a negligible amount of plutonium production and different safeguarding requirements. Additionally, reactors that burn U-233 and refuel with near pure U-233 would have minimal isotopic drift during operation, but introduce different safeguarding challenges. There are some designs that would mix thorium in with an LEU fuel salt. For these reactors, the delayed neutron fraction may follow a similar trend as reactors that transmute U-238 to Pu-239 since, as can be seen in Table 4.1, U-233 has a lower delayed neutron fraction than U-235 [28]. However, separating isotopes is significantly more difficult than chemical separation, and therefore, it is not explored in this study.

4.2 Neutronic Modeling Methodology

As of this writing, no physical examples of MSRs with significant burnup exist. However, several modeling codes, benchmarked against solid fuel reactors, have been developed with

Table 4.1: Delayed neutron fraction for various isotopes.

Isotope	Delayed Neutron Yield (ν_d) Thermal/Fast	Delayed Neutron Fraction (β) Thermal/Fast
U-233	0.00667/0.00731	0.0026/0.0026
U-235	0.01668/0.01673	0.0067/0.0064
U-238	-/0.0460	-/0.0164
Pu-239	0.00645/0.0063	0.0022/0.0020
Pu-240	-/0.0090	-/0.0029
Pu-241	0.0157/0.0152	0.0054/0.0047

additional features and modifications to capture the unique characteristics of MSR burnup. For both the thermal MSR and the FSMSR, this study employs Serpent 2.1.32 to model the neutronic parameters and fuel cycle, consistent with the methodology in the previous chapter [51]. In this chapter, the models are extended to encompass the full core region, enabling accurate accounting of fuel volumes and neutron leakage. More importantly, this approach allows precise representation of SQ removal, specifically plutonium. Furthermore, the dynamic models introduced in the next chapter are designed to maintain consistency with the neutronic and burnup models.

This section explores the modeling method and key assumptions. Additionally, for the sake of reproducibility, all Serpent inputs and outputs are uploaded to a GitHub repository [81]

4.2.1 Thermal Spectrum Molten Salt Reactor Neutronic Modeling Methodology

The primary goal of modeling the thermal MSR is to create a design with results broadly applicable to other reactor designs, while accurately accounting for plutonium diversion. To achieve this, this research utilizes the NERTHUS reactor model [29]. NERTHUS is an open-source thermal MSR reactor model inspired by the Molten Salt Demonstration Reactor (MSDR) and incorporates elements from private sector reactor designs [12]. While much of the material remains consistent with the original study, the fuel cycle calculations have been modified to reflect a once-through, low-enriched uranium (LEU) fuel cycle. Specifically, this study adopts the Sourdough fuel cycle described in Reference [82]. The Sourdough fuel cycle minimizes online reprocessing; however, the plutonium vector would not be significantly different from a fuel cycle that has minor reprocessing of fission products.

Geometry

The reactor uses interlocking graphite moderator plates to channel fuel salt through the actively fissioning core region, as seen in Figure 4.1. The fuel salt enters at the bottom of the core into the bottom axial reflector. The salt then flows up through the central core

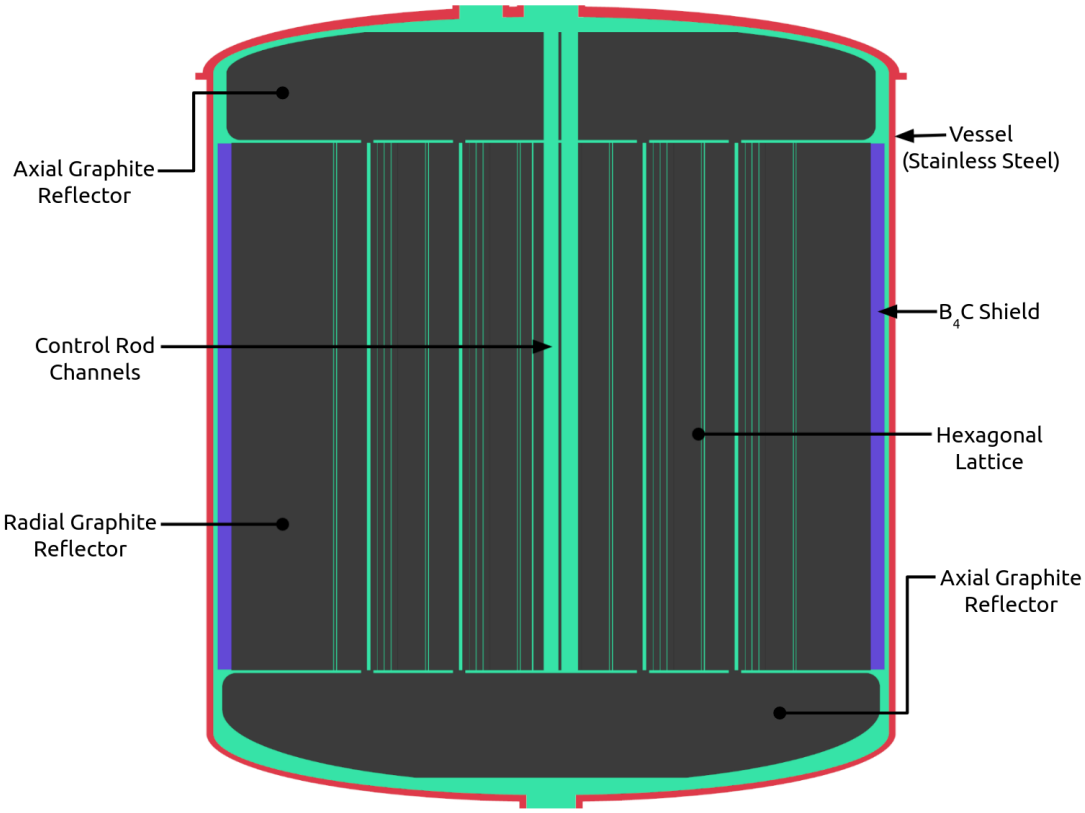

Figure 4.1: The cross section of the thermal MSR [29]

lattice and the outside of the radial reflector for cooling purposes. The fuel then flows past the top radial reflector and out of the core. The fuel salt in the external circuit and heat exchangers is not accounted for in the geometry, but it is accounted for in the material cards for power density and inventory calculations. Serpent allows for materials to have a defined volume separate set in the material card, separate from the actual volume in the geometry. The ratio of fuel salt in the core to fuel salt outside of the core is 1:1.5.

The core lattice is comprised of hexagonally repeating groups of graphite plates called "Logs." These Logs form a fuel cell in lattice as seen in Figure 4.2. The plates in a Log can be separated into two types: the "Slabs" and the "Yolks." The Yolks are oriented so that one side will meet in the center of the hexagonal cell, and branch outwards to alliterate vertices. In between the Yolks, four of the Slabs are stacked back to back. Each Slab has nubs protruding from one side to create an interstitial space between the Slabs and the Yolks. It is through this interstitial space that the fuel salt flows. The Logs, as well as the Yolks and Slabs, run the entire length of the lattice.

The center Log of the lattice does not have any Yolks or Slabs. Instead, there are four large channels, meant for control rods and other instrumentation, as well as several smaller channels that facilitate heat transfer. The radial reflector consists of graphite with a B_4C shield around the outer edge to reduce neutron damage to the vessel. Beyond the reflector is a fuel salt upcomer, which is meant to cool the reflector. Just before the radial boundary, there is a stainless steel vessel wall, and the boundary condition beyond the vessel wall is vacuum. There is another version with the same geometry but no B_4C shield or upcomer to test the effectiveness of an external device for frequency response measurements. All dimensions for the geometry at operational temperature are given in Table 4.2.

When core temperatures drift from operational temperature, it is assumed that only the graphite and B_4C shield change in dimensions and the fuel salt fills the rest of the space inside the vessel. The equation for the expansion of graphite with temperature is given by Equation 4.1.

$$L = L_0 \cdot (1 + \alpha \cdot \Delta T) \tag{4.1}$$

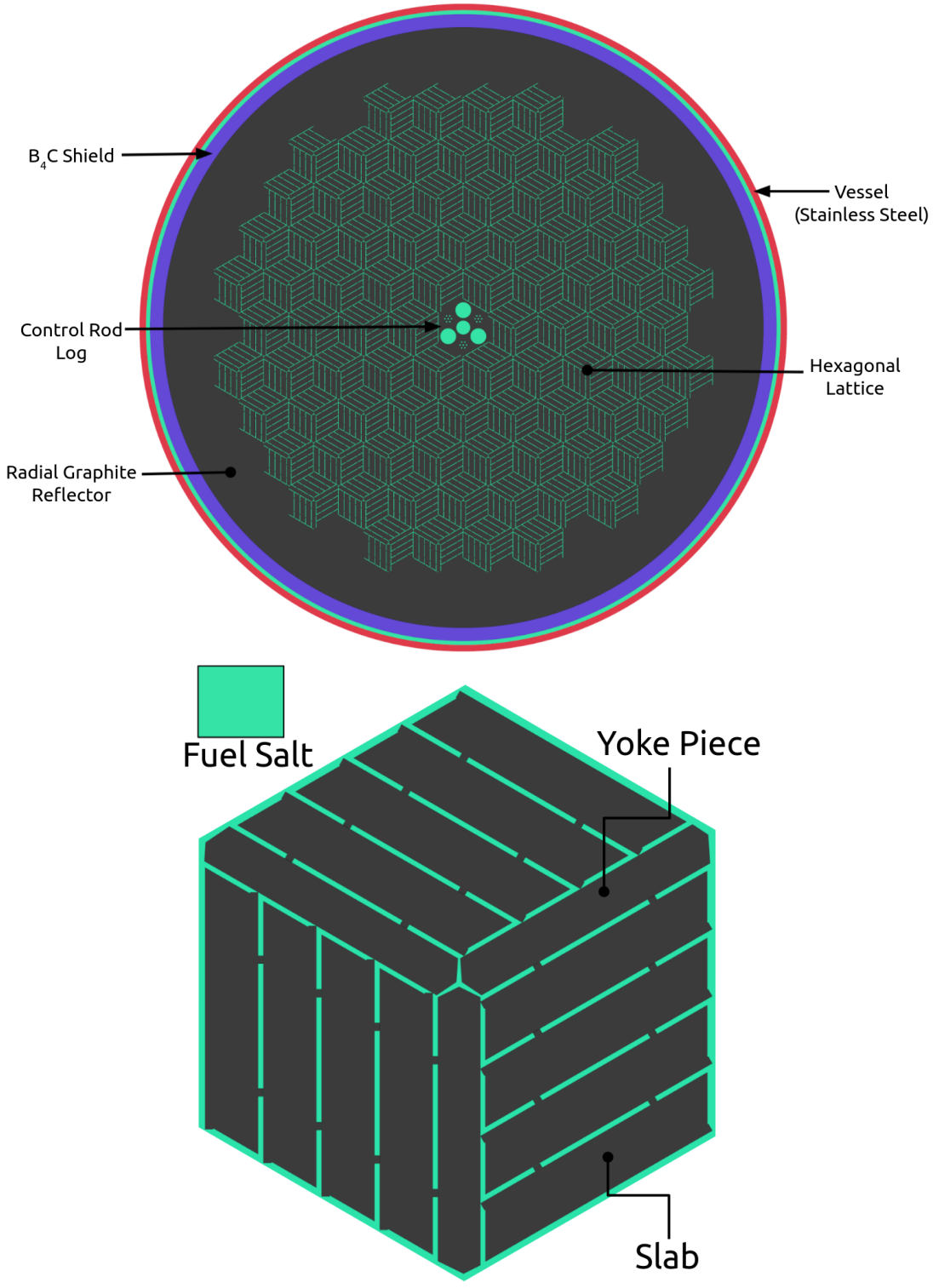

Figure 4.2: The hexagonal lattice of the thermal MSR [29].

Table 4.2: Physical dimensions of the thermal MSR.

Component Dimension	Length (cm) Volume (m^3)
Lattice Height	378
Lattice Radius	≈220.5
Log Apothem	19.055
Slab/Yolk Thickness	3.2
Axial reflector thickness	50
Core Height	482
Radial reflector thickness	≈10
B_4C Shield Thickness	10
Vessel inner radius	243
Vessel Wall Thickness	3
In/Out-Core Fuel Volume	5.468/8.202

Where L is the length of dimension of graphite in cm at the given temperature, L_0 is the length at operational temperature, α is the thermal expansion coefficient ($3\times10^{-6}\ \frac{m}{m\,K}$ for graphite). The B_4C shield is assumed to expand as if it is an extension of the radial graphite reflector. ΔT is the difference of current temperature of the graphite to operational temperature.

Materials

There are four main materials used in the modeling of the thermal MSR: fuel salt, graphite moderator/reflector, B_4C neutron shield, and SS-316. While the most important material to accurately capture is the fuel salt, the other materials in the model can have a significant effect on the neutron spectrum. Therefore, a proper accounting of the material concentration used in the thermal MSR models is presented in Table 4.3, and ENDF/B-VII.1 is employed for the material libraries.

The fuel salt is LiF–BeF–UF_4 (72–16–12 mole%). The lithium is enriched to 99.999 wt% Li-7 (arbitrary) to reduce parasitic neutron absorption and tritium production. The enrichment of the uranium in the fuel salt is initially 2.1 wt% U-235. The density for the fuel salt is calculated using molar weighting for the operational temperature of 900K. The density of the fuel salt is calculated using the known melt composition molar volumes at 600 and 800 [86]. The resulting density is 3.35 g/cm^3 at operational temperature, but the density is changed with temperature for feedback calculations.

The moderator and reflectors are made of graphite with an assumed 2 ppm boron impurity. The density of the graphite is 1.8 g/cm^3 at the base temperature and changes with volume expansion to conserve mass. The operational temperature of all graphite is assumed to be 950K. The mass conservation and operational temperature is the same radial shield composed of B_4C. The density of B_4C is 3.636 g/cm^3. The SS-316 vessel has a density of 7.9 g/cm^3, and it is assumed that the vessel does not change temperature from 900K in this analysis.

Table 4.3: Weight percentages of the materials in the thermal MSR Serpent model.

Fuel Salt		Graphite Moderator		Radial Shield		SS-316	
Element	wt%	Element	wt%	Element	wt%	Element	wt%
Li-6	3.4e-6	B-10	4e-7	B-10	9.3	C	0.08
Li-7	7.91	B-11	1.6e-6	B-11	37.2	N-14	0.1
Be	2.26	C	99.9998	C	53.5	Si	0.75
F	45.22					P	0.0045
U-234	0.08					S	0.03
U-235	8.72					Cr	17
U-236	0.04					Mn	2
U-238	35.78					Fe	65.495
						Ni	12
						Mo	2.5

Burnup Calculation

MSRs exhibit distinctive operational characteristics and burnup behavior compared to solid-fueled reactors, which require consideration in any simulations. The liquid fuel allows online material removal and additions, adding complexity to material safeguarding. Moreover, various options for online fuel processing further complicate the process.

For this study, the focus is on a once-through fuel cycle without active reprocessing. This choice is made because it closely resembles contemporary LWRs and presents fewer barriers to market entry.

The Sourdough strategy is employed for refueling the thermal MSR [82]. In the Sourdough strategy, there is no active reprocessing, and the reactor is refueled with a chemically identical salt with a higher uranium enrichment than the initial fuel salt. The volume of the fuel salt will grow over time depending on the level of uranium enrichment. This study uses the enrichment of 19.75 wt% for the base case, since it will minimize fuel salt growth over burnup. While changing refuel enrichment during operation is not explicitly done here, Chapter 7 explores the possible effects different make-up uranium assay has on fission rates.

Even though there is not active reprocessing in this study, the liquid nature of the fuel will cause some elements to volatilize or otherwise separate from the fuel salt. These elements can be divided into chemical groups, which would have their own removal rate; this has been greatly explored for fluoride salts [32, 65]. This study uses the expected removal rates for isotopes that will passively separate from the fuel salt. Serpent treats online removal as additional decay constants in Bateman equations [69]. The removal constants used in the burnup calculation are presented in Table 4.4. While these volatilization rates are expected for an MSR with a fluoride carrier salt, there is uncertainty with the exact value as well as small variations between designs. Predicting the exact chemical behavior is difficult with today's understanding, as much of the chemistry inside a high temperature, highly radioactive fuel mixture is extremely difficult to precisely predict [3]. However, discussion of the impact of the chemical uncertainties would need a sensitivity study.

Table 4.4: Chemical reprocessing groups for the Thermal MSR burnup calculation.

Chemical group	Included Elements	Removal Constant λ (s^{-1})
Noble Gasses	Kr, Xe	0.05
Noble Metals	Se, Nb, Tc, Ru, Rh, Pd, Ag, Sb, Te	0.05
Volatile Halides	Zr, Cd, In, Sn	1.9e-9
Seminoble Metals	Br, I	5.8e-8

4.2.2 Fast Spectrum Molten Salt Reactor modeling

The second major reactor type explored in this study is the FSMSR. FSMSRs are typically designed specifically to breed large quantities of plutonium during operation. Consequently, these reactors exhibit a similar kinetic drift to thermal MSRs. However, their hard spectrum suppresses the production of heavier plutonium isotopes, leading to behavior in FSMSRs that is unique when compared to their thermal counterparts. The significant actinide inventory and high-quality plutonium only emphasize the need for robust safeguarding regimes for these reactors.

This subsection outlines the methods and assumptions used in modeling the FSMSR fuel cycle. While there are various designs in the literature, this study adopts an simplified FSMSR design that exhibits some breed-and-burn characteristics. This design features a fast spectrum initially fueled with LEU, breeding sufficient plutonium to eliminate the need for refueling with new fissile material. Similarly to thermal MSRs, FSMSRs are not closed systems. However, comparing them is somewhat complicated due to inherent design differences, such as the absence of a moderator and differences in core size. Furthermore, FSMSRs exhibit lower sensitivity to fission product poisons due to their hard spectrum. This chapter will delve into the effects of these factors on the FSMSR fuel cycle and what that would mean for using the neutronics/kinetics as a means to detect plutonium removal.

Geometry

The FSMSR modeled here is a single-fluid, homogeneous salt mixture reactor, and the fuel circulates rapidly in and out of the core. Thus, the reactor core geometries tend to be free of intrusions and be shaped as neutronically efficient as possible. Therefore, the base geometry of the reactor is assumed to be a sphere. The inlet, outlet, and ex-core fuel do not appear in the geometry constructed for neutron transport, but the mass is still accounted for in the material cards. Since several designs in the literature more closely resemble a cylinder, several comparison cases use a square cylinder (height equal to diameter) geometry. The study [84] this model is based on explores the neutronics for various geometries and what effect that has on the neutronics. The study showed that the neutronics is linked to the

change in k_{eff}, and thus the results in this study should be applicable to most FSMSRs using a breed-and-burn fuel cycle. A 100 cm wide reflector made of cast iron is placed around the core region. Inlets and outlets are not modeled, since they would appear in the least neutronically important areas of the reactor.

Materials

All materials in this study are kept the same as in Reference [84]. However, since this study only pertains to a single geometry FSMSR geometry explored, there is only one salt composition needed. The carrier salt is the binary salt NaCl-UCl_3 with a molar ratio of 2–1. There are two main FSMSR projects that look into using this binary salt: REBUS-3700 and TerraPower's MSFR [58, 59]. The REBUS-3700 uses a higher fissile load with some transuranics for fissile, but Terrapower's MSFR will start with an initial load of LEU fuel like the reactor modeled here. The initial load of LEU is the only fissile material explored with no makeup fuel added during burnup. Their reactor design does use a liquid lead reflector, which is not the case for the modeled reactor.

An FSMSR utilizing chloride salt may necessitate the use of enriched chlorine. Chlorine poses a potential issue due to parasitic neutron absorption by the Cl-35 isotope, leading to decreased neutron economy. Furthermore, the reaction produces Cl-36, complicating waste disposal owing to its bio-availability and half-life of 300,000 years. Consequently, the chloride in this model is enriched to 99.999% Cl-37. While the chlorine enrichment is set arbitrarily high, the difference in burnup compared to other enrichments of 97% or higher would be minimal [35]. The uranium enrichment is determined through a criticality search for each configuration investigated separately, ensuring that the multiplication factor k_{eff} is within 1.005±0.001. This places the enrichment of the uranium at approximately 12.5 wt% U-235. The temperature of the fuel salt is 900 K. The reflector around the core region is made up of cast iron of natural isotopic distribution. The reflector's temperature is at 873 K. This model uses the JEFF-3.3 libraries with these temperatures for nuclear reaction data. The density of the fuel salt is calculated using molecular weighting. The density at this temperature is calculated using molecular weighting. The molten salt compendium [42] contains experimental values of NaCl-UCl_3 density as a function of temperature at four

different molar fractions of UCl_3. The fuel salt in this study is NaCl-UCl_3 (66.66-33.34) with a density of 3.164 g/cm^3 while the reflector is cast iron of density 7.034 g/cm^3.

Burnup Calculation

Many have investigated FSMSRs for their potential in B&B fuel cycles. Utilizing its fuel cycle would allow long periods of operation with minimal refueling [36, 55]. B&B fuel cycles often continuously siphon fuel salt and replace it with depleted uranium loaded salt. The effects of this action dampen excess reactivity while allowing breeding to continue on indefinitely. Siphoned fuel would also be excellent fuel material to start an additional reactor. However, it has been shown that a smaller core can have a smaller excess reactivity [55]. Additionally, reactors will not operate indefinitely, and there may not be other reactors built with designs close enough to accept breed fuel salt. The refueling equipment and excess fuel storage may also add a cost to the system. Instead, designers may want a reactor that breeds just enough to maintain criticality throughout the reactor lifetime. In this case, the cost and risk associated with a refueling system would be minimized. Therefore, none of the results shown have refueling of any kind.

Even though there are no refueling or other online material additions in the models investigated, there is passive fission product removal. This assumption results in a small decrease in density over burnup. However, the initial mass of the fuel to begin with is so large that the density drop is negligible (<0.1%). Like in the thermal MSR system, the FSMSR fuel cycle in this study has no active fission product removal. In the fast spectrum, neutron loss to fission product absorption will be minimal when compared to a thermal spectrum. As a result, a designer may wish to minimize the material removal from an FSMSR fuel salt, as it adds cost and complexity. Certain volatile species, such as fission product gases, will naturally remove themselves from the fuel salt regardless. The elements removed from the fuel salt, along with their removal constants, are shown in Table 4.5 and are comparable to other MSR fuel cycle studies [67, 13].

Since the volume of fuel salt is so much higher for the FSMSR when compared to the thermal MSR, the power is also set higher. In this study, the burnup calculation is set to a constant power rate of 3 GW_{th}. This volume card in the serpent file accounts for a 1:1 ratio

Table 4.5: Chemical reprocessing groups for the FSMSR burnup calculation.

Chemical group	Included Elements	Removal Constant λ (s^{-1})
Noble Gasses	Kr, Xe	0.05
Noble Metals	Se, Nb, Tc, Ru, Rh, Pd, Ag, Sb, Te	0.05

of fuel salt in to out of core. Overall, the in to out of core fuel salt ratio is lower than the thermal MSR. However, it is more in line with other FSMSR designs being proposed, and the total fuel volume is significantly higher.

4.3 Parameter Evolution over Burnup

This section presents how the reactor's neutronic parameters evolve over burnup. Quantifying this evolution is important as it will establish a baseline for normal operation for diversion to be compared to. Additionally, there will be a significant drift in reactor behavior over burnup. In fact, this could be used as a form of burnup measurement.

This section also compares and contrasts the results between the fast and thermal designs where possible. While both reactors remain critical over the burnup calculation, the similarities end there. The primary cause steams from the differences in neutron spectrum. It is apparent from Figure 4.3 that the FSMSR's flux is significantly harder than the thermal MSR's neutron spectrum.

Figure 4.4 depicts the effective multiplication factor over burnup for the thermal MSR with 19.75% enriched makeup uranium. The refueling rate for the thermal MSR is calculated so that a constant refueling rate would keep the multiplication factor remains around the same level at the end of cycle as at the beginning. The calculated refueling rate is 0.0175 %/day (2.025e-09 frac/sec) of the total fuel volume. There is, at first, a small drop followed by a longer rise in reactivity. The multiplication factor eventually drops back close to the initial level. This jump is an artifact of the constant refueling rate and the slow build up of fission product poisons. The current version of Serpent (v2.1.33) does not allow for changing material flow rates over burnup. During actual operation, the reactor operator may wish to deal with the excess reactivity by lowering the refueling rate during early burnup. However, the overall refueling rate would not vary significantly from the value presented here.

The thermal reactors multiplication factor's behavior contrasts with that of the fast reactor's seen in Figure 4.5. These results are with no refueling and only passive fission product removal. The result is that this reactor remains critical for ≈40 full-power years on

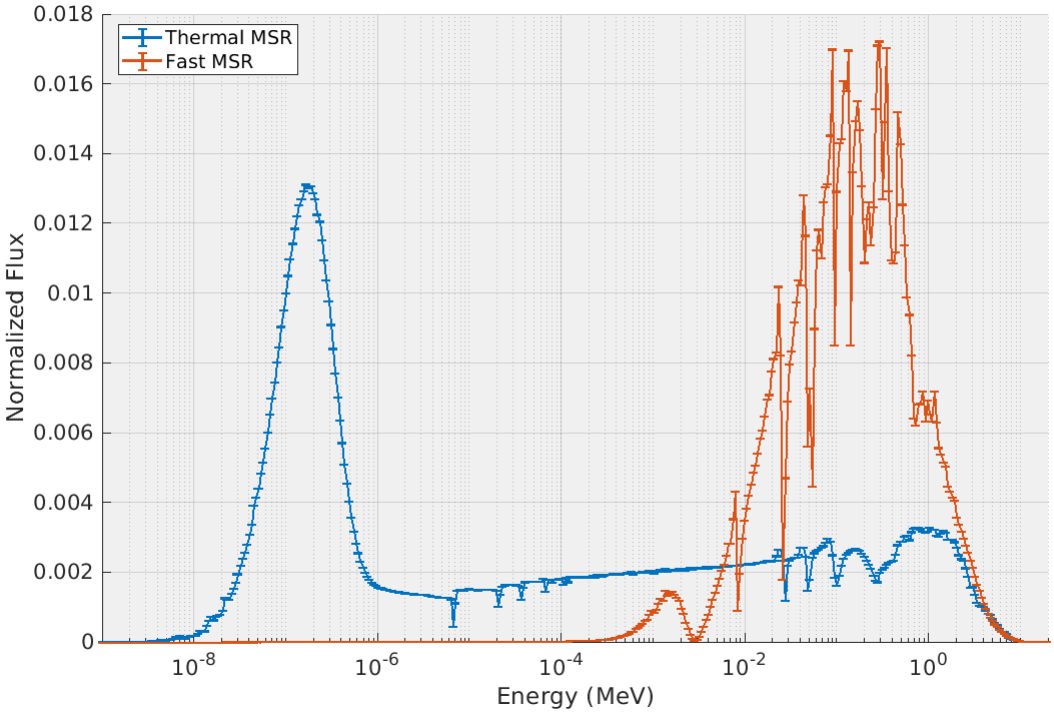

Figure 4.3: The relative neutron spectrum of the thermal and fast spectrum MSRs.

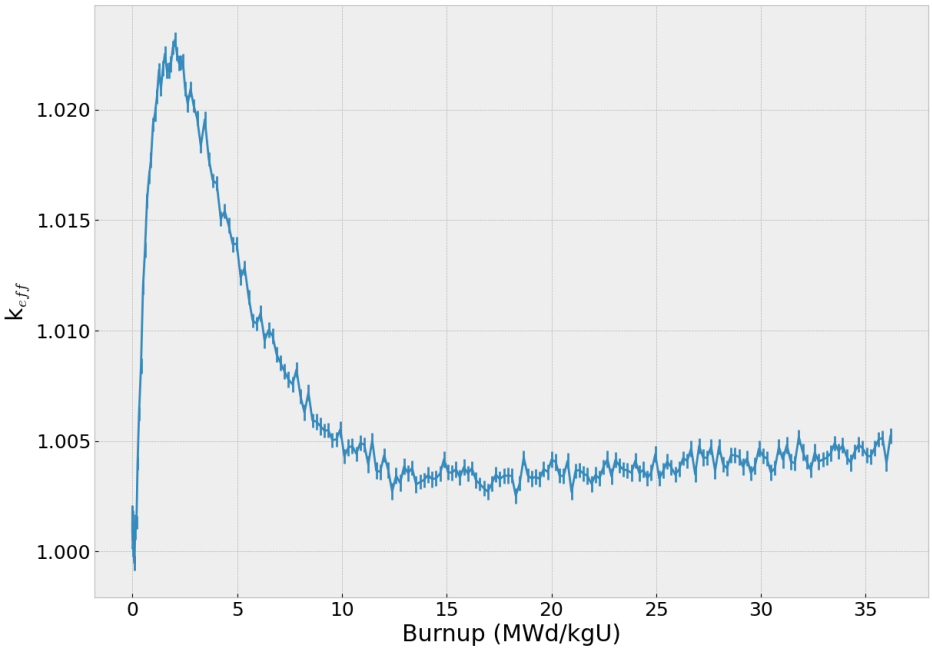

Figure 4.4: The multiplication factor over burnup in the thermal MSR.

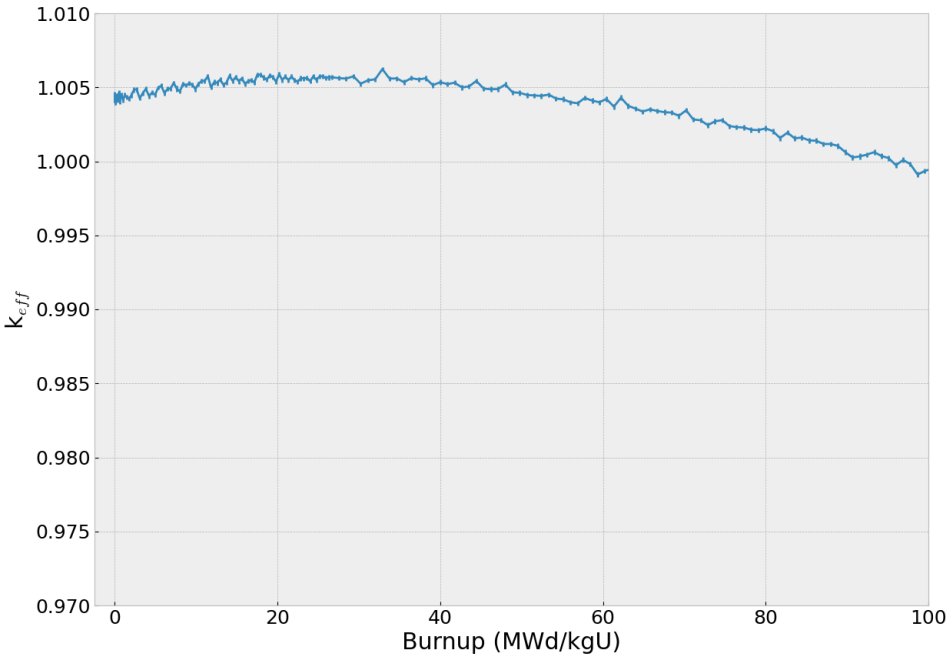

Figure 4.5: The multiplication factor over burnup in the FSMSR.

just the material in the reactor from startup. In the FSMSR, the breeding is such that the multiplication factor gently increases before slowly falling back. The large mass of initial actinides and fast circulating fuel acts similar to that of a standing wave reactor. Any batch reprocessing or refueling that would occur after the reactor becomes subcritical is not explored.

The difference in refueling and neutron spectrum causes there to be significant differences in the makeup of the fission chain. Figure 4.6 shows what fraction of the fissions is the result of each major actinide for the thermal and fast MSR. Due to the refueling, the thermal MSR reaches a quasi steady state relatively quickly for Pu-239 and later for Pu-241. This behavior is not present in the fast spectrum reactor due to the lack of refueling. The Fast MSR also has a much slower buildup of transuranics due to the higher fission ratio in the fast spectrum. As a result, Pu-241 does not majorly contribute to the chain reaction for the fast reactor, while U-238 does. For both reactors, the change in what isotope is fissioning is directly related to the neutronic parameters.

4.3.1 Neutronic Parameters

Two of the most important parameters in neutron kinetics are the delayed neutron fraction and mean neutron generation time. The mean neutron generation time is the average amount of time it takes for a neutron to reproduce. This is shorter for fast reactors when compared to thermal reactors, since the neutron in thermal reactors must slow down in a moderator before causing a fission. However, whether it be fast or thermal systems, the generation time is too fast for human (or even machine) intervention. Luckily, a small number of fission products emit neutrons during their decay. These neutrons from fission product decay make up the delayed neutrons. The chain reaction can be kept such that it is only critical with these neutrons, and thus changes in reactor operation will be on human time scales.

Needless to say, these parameters strongly affect the time-based behavior of the chain reaction and thus the frequency response of an MSR. Both parameters will change significantly over burnup and during plutonium diversion. In the case of mean neutron generation time, the build up of fission products reduces the life time of a neutron, and thus the mean neutron generation time must decrease as well to maintain criticality. The

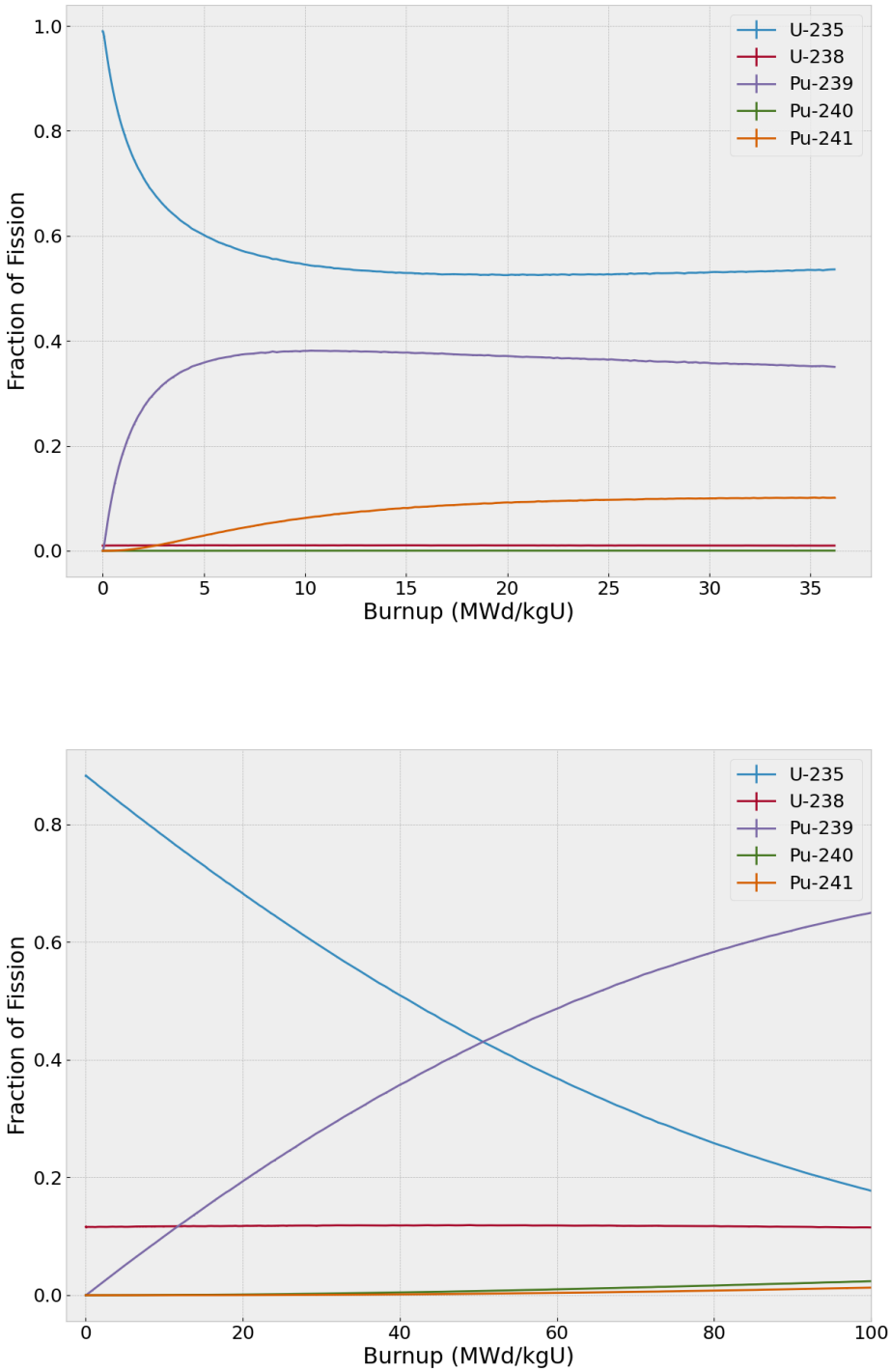

Figure 4.6: The fission fraction for each major actinide in the thermal MSR (top) and fast MSR (bottom)

different actinides have different cross section and neutron yields, which also greatly affect mean neutron generation time. For delayed neutrons, they are directly tied to the fission product yield, which can change drastically between actinides and neutron spectrum.

Both the FSMSR and the thermal MSR display a significant change in mean neutron generation time over burnup. As can be seen in Figure 4.7, the thermal spectrum reactor neutron generation time quickly drops to a bit under half of the original value. The change for the fast spectrum reactor is not nearly as rapid or as dramatic. This distinct behavior is the result of the parasitic absorption from fission products, which has a higher impact in the thermal spectrum.

Delayed neutron fraction also has a distinct evolution over burnup. Delayed neutrons are the result of the decay of fission products, so variation in the fission yield is the main driver of delayed neutron fraction divergence. The two main factors influencing this are the isotope fission fraction and the neutron spectrum. While the neutron spectrum does get harder with burnup, this factor is negligible when compared to the transmutation of heavier actinides. Hundreds of fission products emit neutrons, but for dynamic calculations, all the precursors are lumped into six delayed neutron precursor groups. Figure 4.8 shows each of the six groups and the corresponding decay constants, where each group is numbered so that the first group is the fastest decaying and the sixth is the slowest. There are some notable differences between the reactors even at the initial, pre-burnup state. Both reactors experience their delayed neutron fraction drop. Save group six in the thermal MSR, the time constants remain constant. However, even though each decay constant group fraction drops, they do maintain the same relative proportion to each other. As a result, the single group decay constant drops for the thermal MSR while it steadily increases for the fast reactor.

4.3.2 Temperature Feedback Coefficients

The main factor in distinguishing kinetic calculations from dynamic calculations is the inclusion of all temperature feedbacks. For an MSR, there are many mechanisms in which temperature affects reactivity that change with burnup. First and foremost is the Doppler feedback. Since the Doppler feedback is the product of resonance absorption from non-fissioning actinides, the introduction of transuranics requires tracking the change in

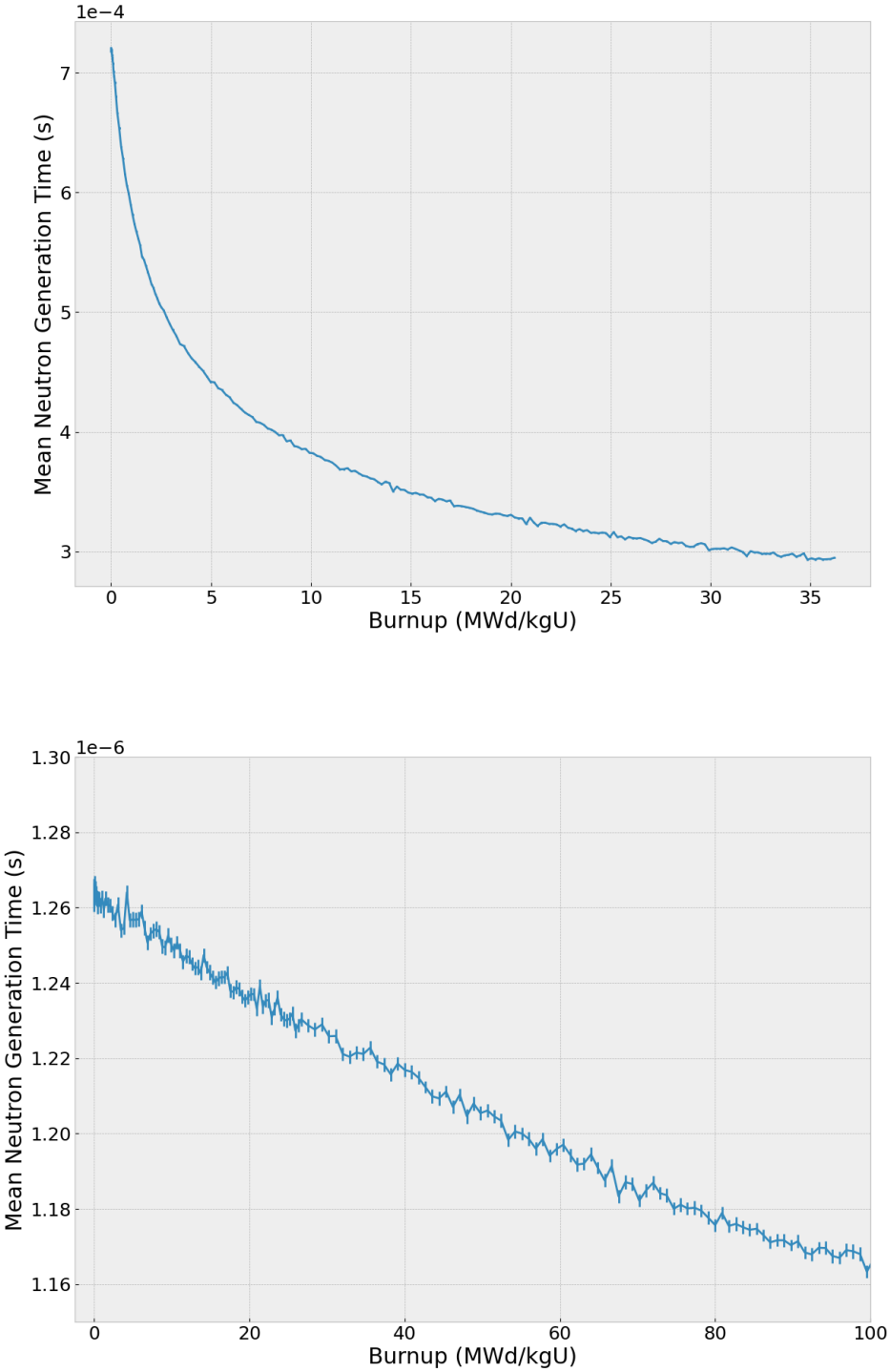

Figure 4.7: The evolution of the mean neutron generation time with burnup for a thermal (top) and fast (bottom) MSR.

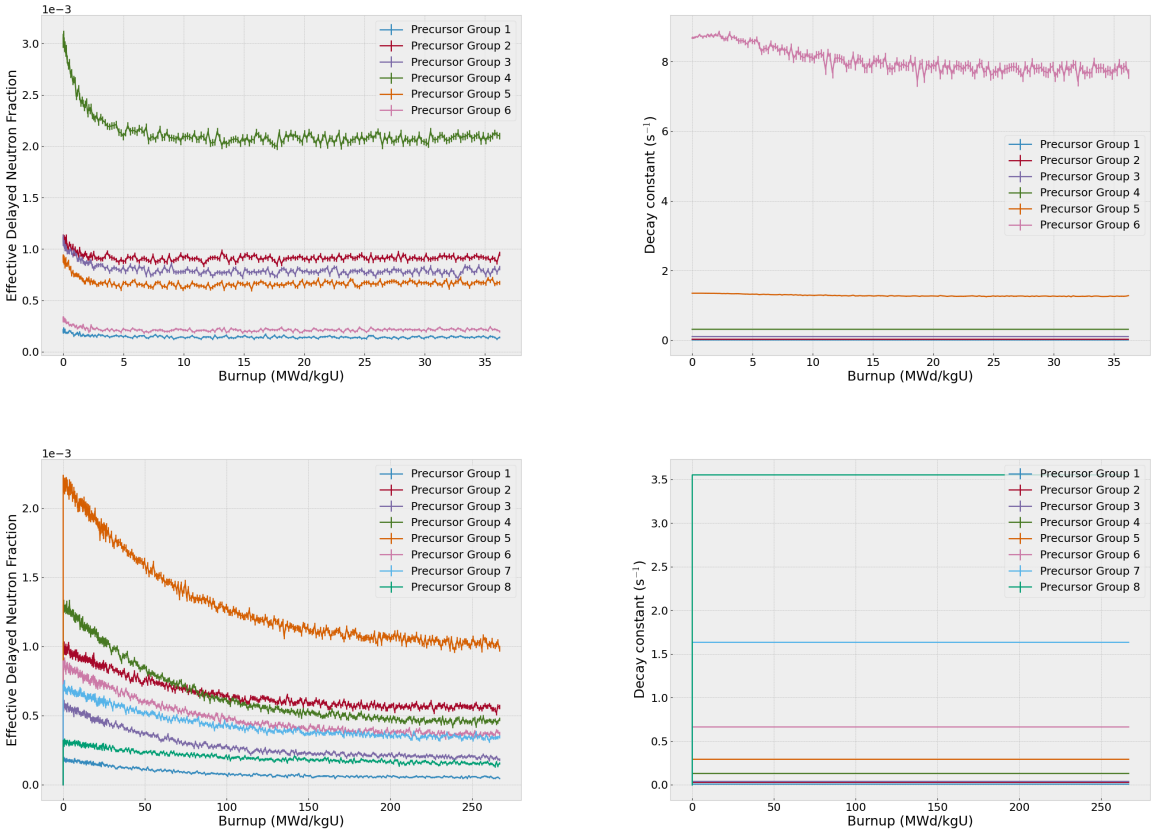

Figure 4.8: The six group delayed neutron precursor calculation for the thermal (top) and fast (bottom) MSR.

the Doppler feedback coefficient with burnup. An increase in fuel temperature causes Doppler broadening and also fuel salt expansion. When the salt expands, it not only alters the fuel to moderator ratio but also drags fissile material out of the core. The introduction of soluble fission product poisons cause the expansion coefficient (usually called void feedback coefficient) to not be static as well. Lastly, there is the moderator feedback coefficient. Graphite at higher temperature cannot moderate as effectively as it can at lower temperatures. Given all of these physical effects, the need to track the graphite temperature reactivity coefficient becomes apparent.

The thermal MSR is split into two main temperature feedback coefficients: the total fuel and graphite feedback coefficient. The fuel feedback coefficient itself can be split into the moderator and void coefficient. Figure 4.9 shows each of the calculated feedback coefficients throughout burnup for the thermal MSR. It should be noted that, overall, the reactor has a negative temperature feedback in both the fuel and the graphite moderator. The thermal MSR has a positive void coefficient, though. It is common to under moderate reactors since most reactors are LWRs. In those reactors, the only appreciable thermal expansion is in the liquid moderator. The void coefficient is in the fuel, not the moderator, for an MSR, thus causing under moderated reactors to have a positive void coefficient. However, the Doppler feedback is significantly more negative, making the overall fuel negative when combined. As the fuel undergoes burnup, the total fuel decreases in magnitude while the graphite feedback decreases then increases. This behavior will have a distinct effect on the reactor's dynamic response over burnup.

The calculations for the FSMSR are slightly different. There is no internal moderator and therefore no moderator calculation performed. The Doppler and void feedback coefficients are shown separately here, as well as some high reactivity insertions [17]. This distinction is not appreciable for the frequency response. Figure 4.10 plots both the void and Doppler feedback, as well as the total fuel feedback as a function of burnup. Since the fast spectrum reactor criticality is heavily connected to neutron leakage, the fuel salt has a strong void feedback coefficient. The Doppler feedback is not as strong as the void feedback. The Doppler coefficient also slightly increases over burnup but remains negative throughout operation.

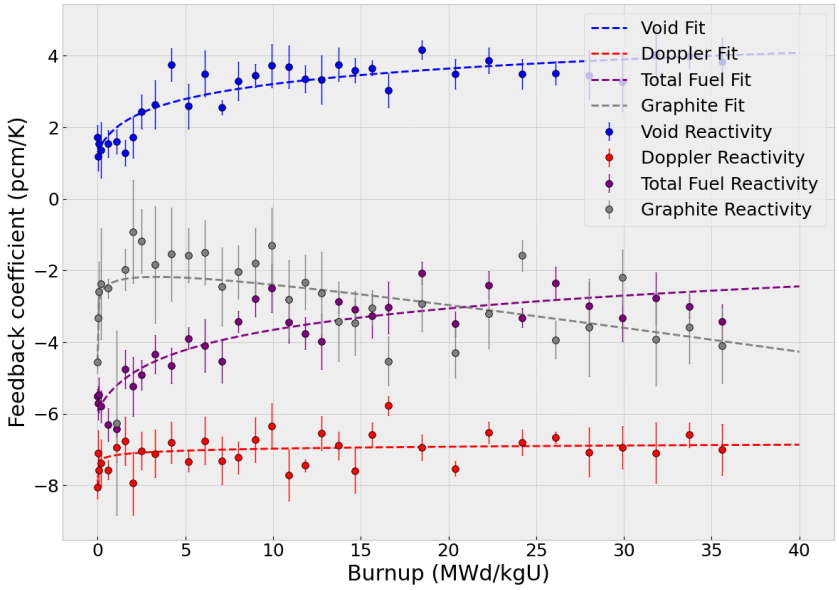

Figure 4.9: The temperature feedback coefficients for the thermal MSR over burnup.

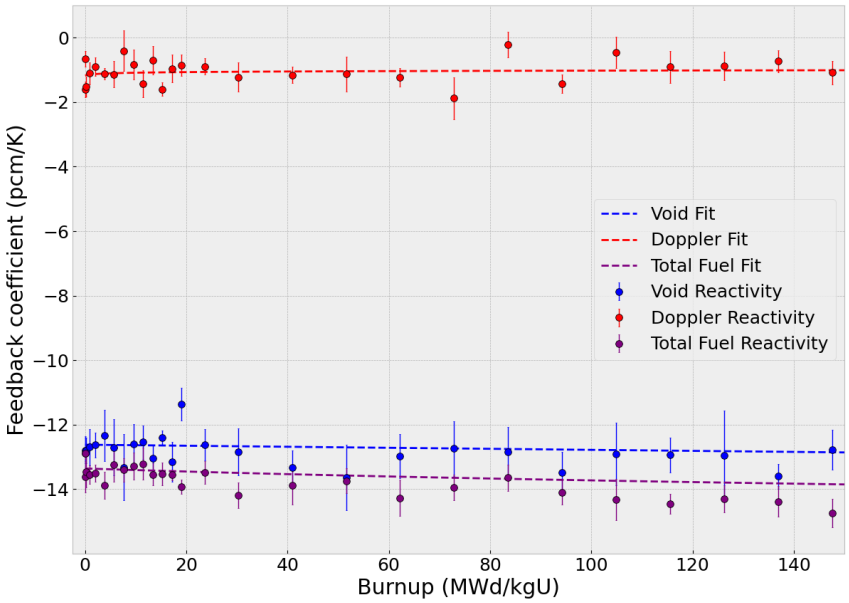

Figure 4.10: The temperature feedback coefficients for the fast spectrum MSR over burnup.

The total feedback dampens with burnup since the void feedback's trend outweighs the Doppler's.

4.3.3 Fission Product Poisons

Fission product poisons have a major impact on the dynamic behavior of the reactor. They can come from direct yield or decay from other fission product, and as a result, there are prompt and delayed effects on the dynamic response of the reactor. The dynamic modeling methodology is discussed in the next chapter, but in summation, it tracks the production and neutron absorption of Xe-135 and Sm-149. The parameters passed on are the yield of these isotopes and parent isotopes, as well as the operational reactivity drain (operational neutron absorption in terms of reactivity). These parameters will also change significantly with burnup and the introduction of transuranics.

The fission yield of relevant fission product poisons in the thermal reactor is shown in Figure 4.11. Both I-135 and Pm-149 remain relatively stable while somewhat increasing. The Xe-135 yield doubles in magnitude, but levels off after 5 MWd/kgU of burnup. The Sm-149 direct yield is considered negligible for these calculations. Figure 4.12 shows a similar trend for the fission product poison yield in the FSMSR. However, the yields never truly stabilize since the fission fractions never reach a steady state.

The operational reactivity drain shows significant differences between the thermal and fast systems. Figure 4.13 depicts the reactivity from Xe-135 and Figure 4.14 shows Sm-149. Due to the rapid removal of noble gases out of the fuel salt, Xe-135 absorbs a relatively small amount of neutrons ($\leq$5 pcm). Running the same calculations without any gas removal results in operational reactivity drain of over 2000 pcm for Xe-135. Sm-149, on the other hand, absorbs significantly more neutrons during operation. Samarium is soluble in molten salt systems, and its neutron absorption cross section in the fast spectrum is not as small as xenon's.

For the FSMSR, relative neutron absorption by fission product is significantly less than that for the thermal reactor. Xe-135 absorption is so small ($\ll$1 pcm) that it is considered negligible for this research. Sm-149, however, still absorbs a significant amount of neutrons.

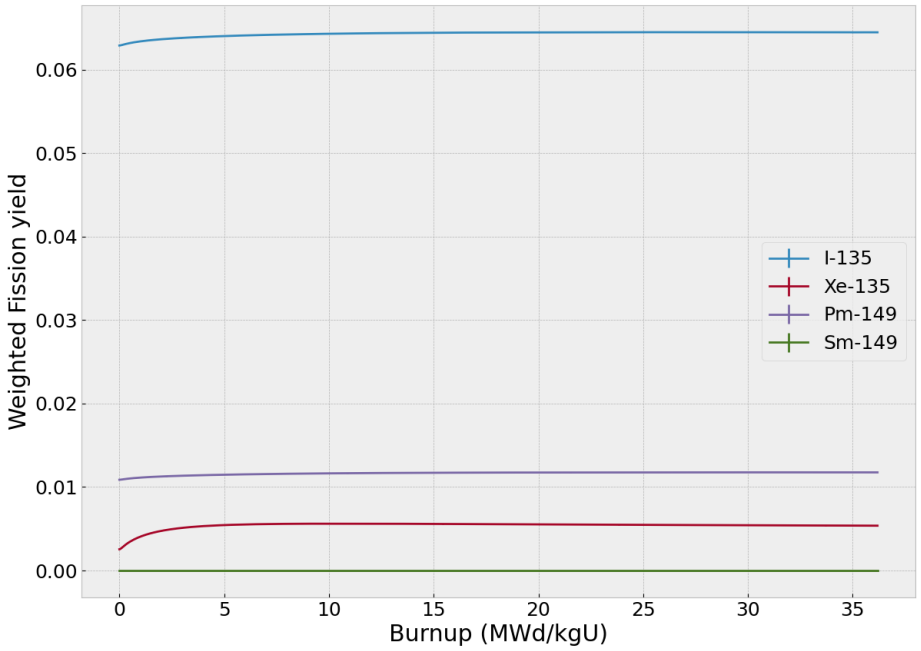

Figure 4.11: Fission yields for fission product poisons in the thermal MSR.

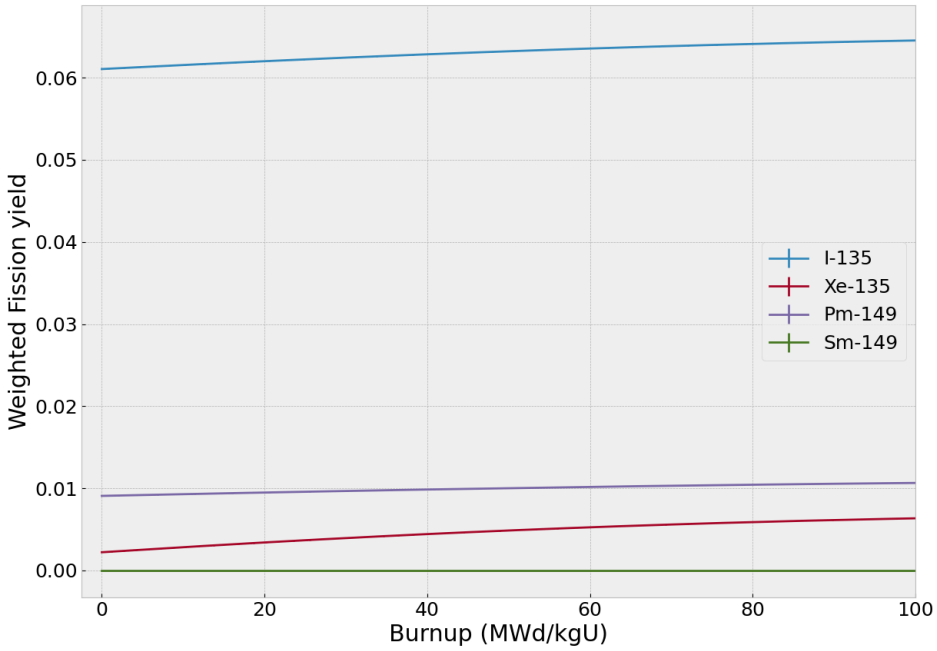

Figure 4.12: Fission yields for fission product poisons in the FSMSR.

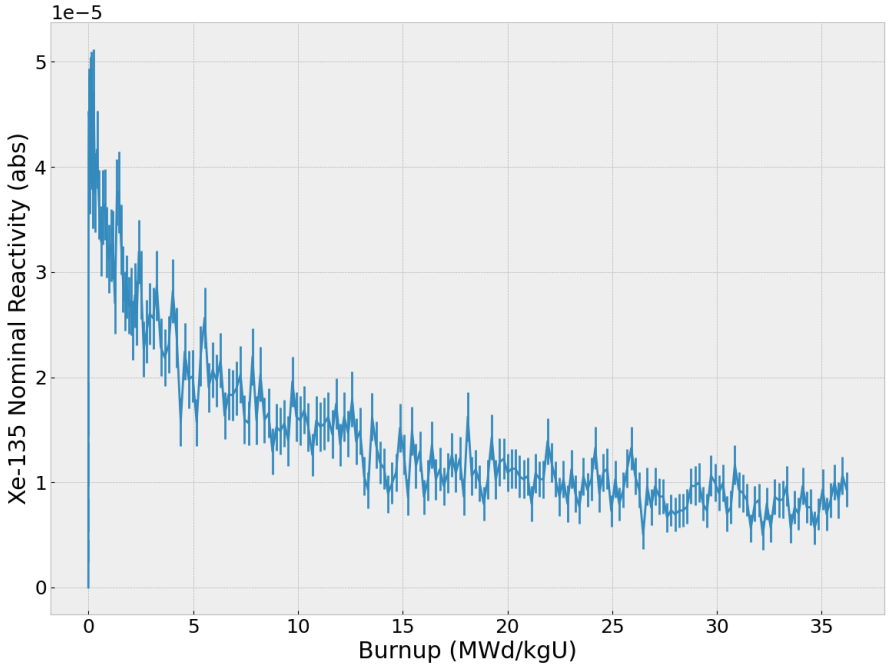

Figure 4.13: The operational reactivity absorbed by Xe-135 in the thermal MSR.

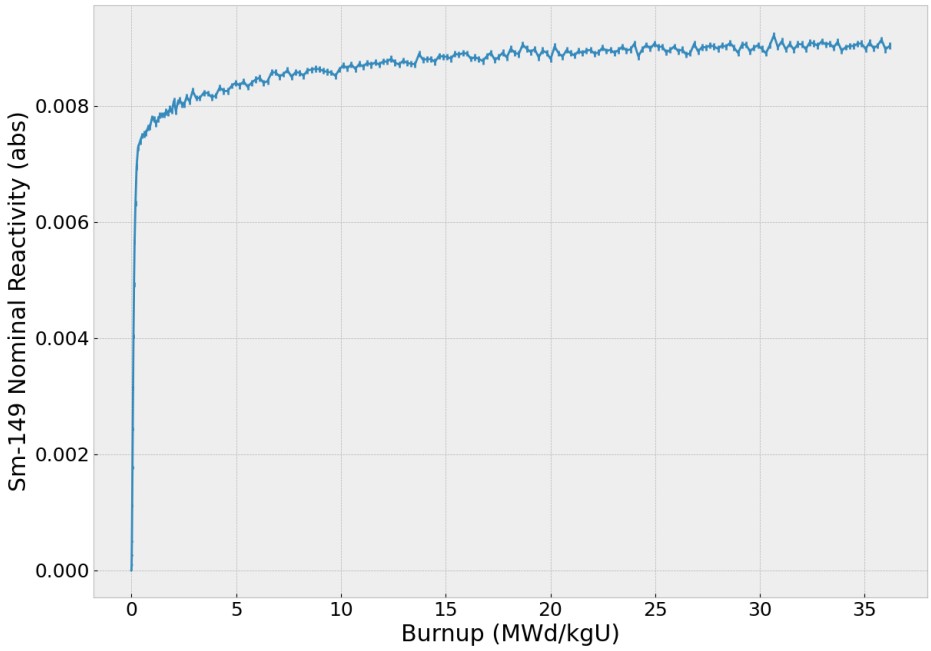

Figure 4.14: The operational reactivity absorbed by Sm-149 in the thermal MSR.

Figure 4.15 shows the relative amount of neutrons absorbed by Sm-149 in the FSMSR. Sm-149 absorbs an increasing amount of neutrons representative of the increasing Pm-149 fission yield.

4.3.4 Decay Heat

The fraction of total power that is the result of fission product decay heat will evolve with burnup. Similar to the fission product poisons and delayed neutron precursors, this change is mainly driven by the change in fission product yields. To further complicate the matter is the chemical volatilization in a molten salt medium. Some fission product decay chains contain gases and noble metals that leave the fuel salt. Therefore, it is necessary to split the heat contribution into distinct chemical groups to determine if the energy contributes to heating the fuel salt. Figure 4.16 shows the contribution to heat that all FP based off of their chemistry. Most of the elements remain in the fuel salt, but a not so insignificant portion of the decay comes from elements that remove themselves through either volatilization or deposition.

Noble metals and semi-noble metals are expected to plate/deposit throughout the primary fuel circuit. Therefore, the energy they produce will still go towards heating the fuel salt. The heat from volatilized such as gasses and some fluoride compounds is considered lost. The same goes for any daughters that are the product of decay after the parent left solution. Figure 4.17 depicts the resulting operation decay heat contribution for the thermal MSR, and Figure 4.18 shows the same for the FSMSR. As the fission chain becomes more dependent on plutonium, power generation becomes less dependent on fission product decay heat. One important feature to note is the slight bump in the decay heat for the thermal MSR in Figure 4.17. This anomaly occurs when there is a change in step size in the simulation while there is online user input material changes. This issue has been brought to the attention of the developers. However, in the modeling presented here, the step size increase was decreased until the bump was no longer as pronounced.

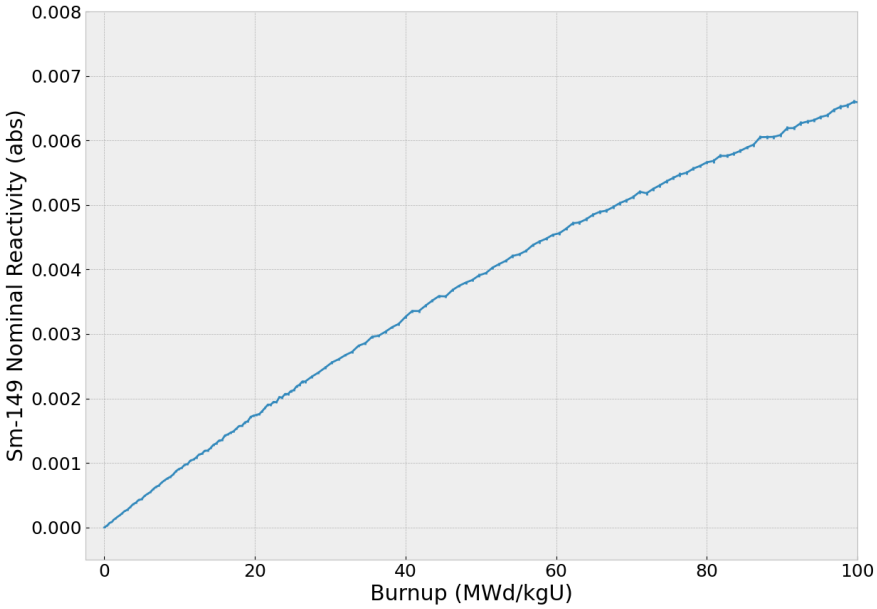

Figure 4.15: The operational reactivity absorbed by Sm-149 in the FSMSR.

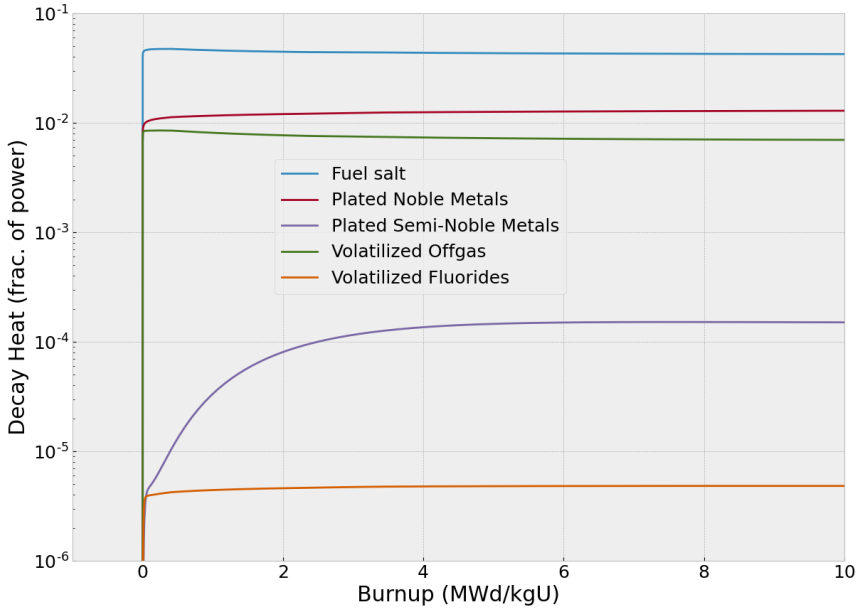

Figure 4.16: Decay heat relative to the operational power of the thermal MSR, sorted by what remains in the fuel salt and the isotopes that do not.

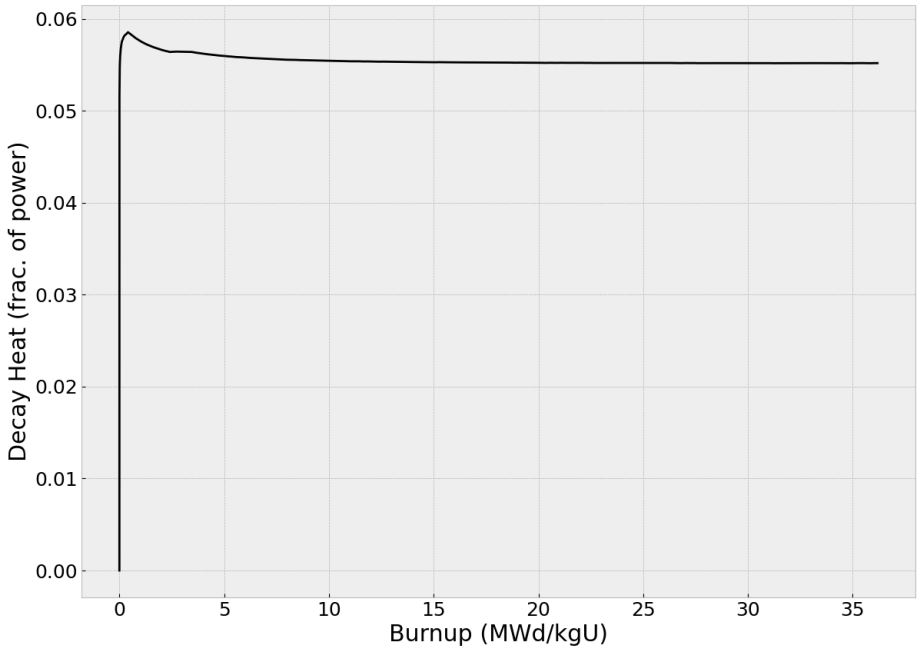

Figure 4.17: Fraction of power in the thermal MSR resulting from fission product decay.

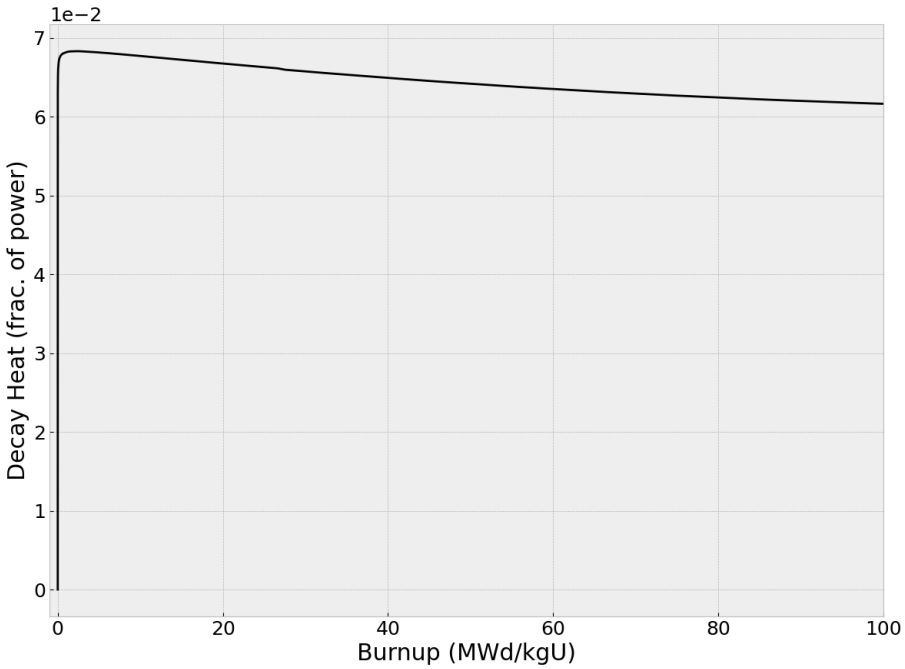

Figure 4.18: Fraction of power in the FSMSR resulting from fission product decay.

4.4 Plutonium Diversion

While burnup has an expected trend shown in key parameters, the diversion of plutonium will undoubtedly disrupt this trend. How and to what degree exactly the disruption will manifest itself is the subject of this section. From Chapter 3, the kinetic parameters, mean neutron generation time and delayed neutron fraction, are strongly linked to the presence of plutonium. However, further investigation shows that other parameters will also have their own effect. Additionally, while the diversion in the previous chapter is at a single point in burnup, the diversions here occur at different burnup intervals to understand any burnup dependencies.

4.4.1 Plutonium Grade during Burnup

When looking at the neutronics, it is safe to assume that both the percentage and grade of plutonium will have important implications. The grade of plutonium is defined by the presence of Pu-240. Chapter 3 already demonstrated the link by showing more noticeable responses with higher percentages of plutonium removed. However, there is little research done on higher burnup plutonium (e.g. reactor grade and fuel grade). This is not without reason, since it is expected that higher Pu-240 content could make weapons making difficult if not infeasible [48]. However, material accountancy programs do not make distinctions and still require tracking of special nuclear material regardless of the quality. As previously established, the frequency response is tightly linked to what isotopes are fissioning. As heavier isotopes of plutonium build up (and the grade deteriorates), plutonium diversion would affect the frequency response differently. Therefore, it is important to distinguish the response during diversions at different grades of plutonium.

Assessing plutonium breeding is where the thermal MSR and FSMSR differ drastically. Figure 4.19 shows the total mass of plutonium in the thermal spectrum MSR, while Figure 4.20 shows the same but for the FSMSR. The first noticeable difference between the reactors is the grade of the plutonium at any given point of burnup. Due to the higher fission-to-capture ratio in the fast spectrum, the plutonium in the fast spectrum consists of a higher percentage of Pu-239 than the thermal spectrum reactor for the same level of

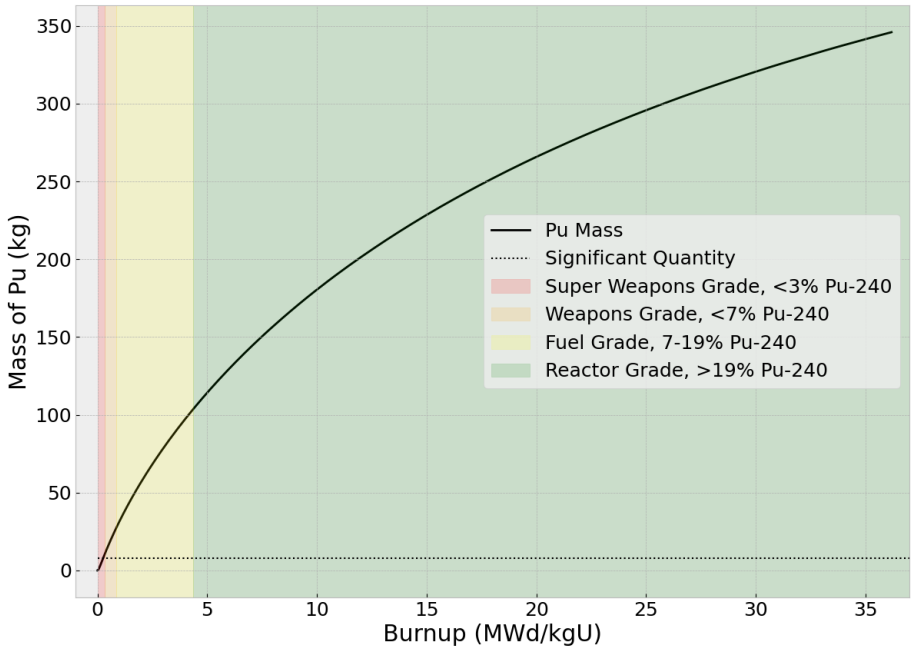

Figure 4.19: Total mass plutonium in the thermal spectrum MSR.

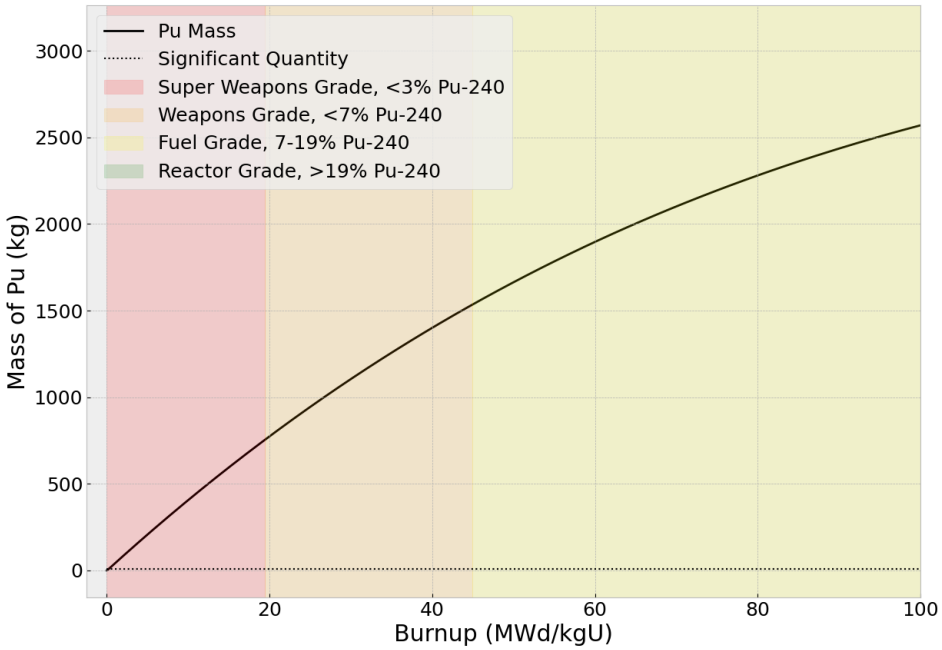

Figure 4.20: Total mass plutonium in the fast spectrum MSR.

burnup. Additionally, the well-mixed nature of the fuel means that all the plutonium is the same quality. There are no fuel pins with different quality that you would see in a solid fuel reactor. This means that there is only a short window of opportunity to remove weapons grade plutonium in the thermal MSR and a larger one for the FSMSR. The second major difference between the two reactors is the total mass of plutonium. Since the FSMSR needs a large body of fuel salt to go critical and maintain a favorable breeding ratio, the resulting total mass of the plutonium is much larger than some thermal MSRs. Even when taking the difference in power level into account, the FSMSR would have over 25 times as plutonium at 20 MWd/kg than the thermal MSR.

This discussion hints at a major limitation of the use of frequency analysis for bulk salt measurements (or any other bulk salt measurements). The requirements for diversion measurements are in terms of mass, while bulk measurements are in terms of concentration. Therefore, a removal of an SQ of plutonium will have a smaller impact on the total Pu:U ratio in larger fuel salt mass. Figure 4.21 and Figure 4.22 depict the percentage of plutonium that is removed from the bulk fuel salt when an SQ (8 kg) of plutonium is removed for the thermal and fast reactors, respectively. A removal of plutonium at higher quality in the thermal spectrum MSR accounts for a large proportion of the total plutonium. This percentage drops with lower plutonium quality. Removal in the FSMSR, however, has little impact on the plutonium mass. Even at the early stages of burnup, when a SQ makes up a noticeable percentage of plutonium, the total fissions do not rely heavily on plutonium. These effects are quantified in Table 4.6.

4.4.2 Plutonium Diversion Effect on Parameters

While the removal of an SQ may affect the total mass of plutonium, for this study, the change in the key parameters affecting the reactor response is what is most important. In this study, the parameters in Section 4.3 are the assumed to be the major parameters that will shift the frequency response over burnup and during diversion. To simulate plutonium diversion, reductions in plutonium concentration as detailed in Table 4.6 are applied at five distinct burnup intervals. A new Serpent calculation is executed incorporating the updated material composition, allowing for approximately one day to attain steady-state fission product heat

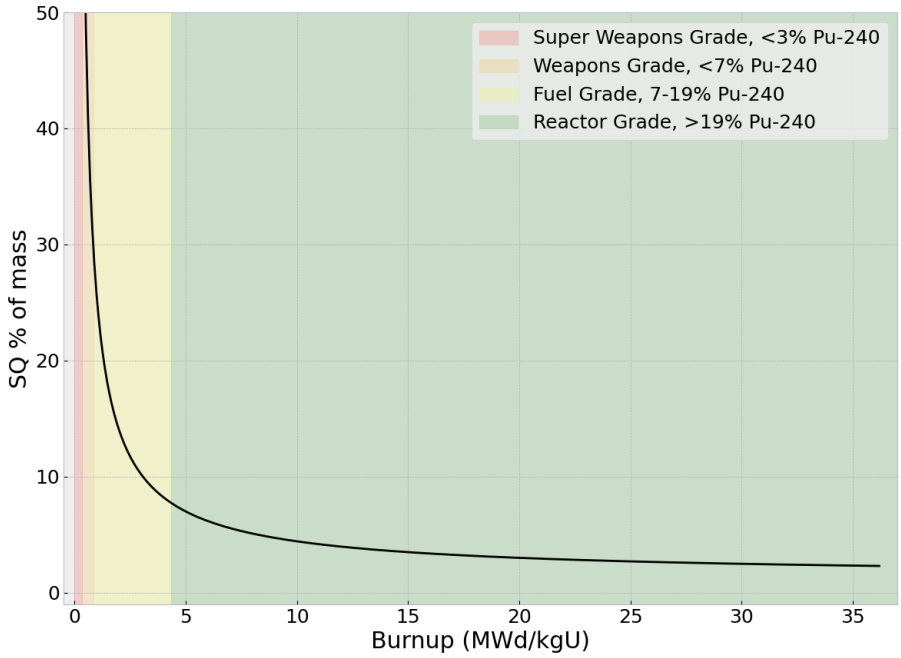

Figure 4.21: The percentage that an SQ (8kg) of plutonium represents of the total plutonium in the thermal MSR fuel salt.

Table 4.6: The amount of plutonium needed to be diverted to form an SQ of plutonium for several levels of burnup.

Thermal MSR			
Burnup GWd/MTHM (FP Days)	SQ % of Pu	% Pu-240	Pu % of fission
0.32 (23.2)	79.40	2.9	7.2
0.89 (65)	28.24	7.3	17.3
1.553 (114)	17.31	11.0	24.5
4.978 (366)	7.66	19.1	38.7
32.19 (2368)	2.42	19.0	45.6
FSMSR			
Burnup GWd/MTHM (FP Days)	SQ % of Pu	% Pu-240	Pu % of fissions
0.31 (42)	7.61	0.1	0.5
0.82 (112)	2.72	0.1	1.0
2.67 (366)	0.83	0.4	2.7
19.43 (2662)	0.12	3.0	19.0
45.34 (6210)	0.05	7.1	40.4

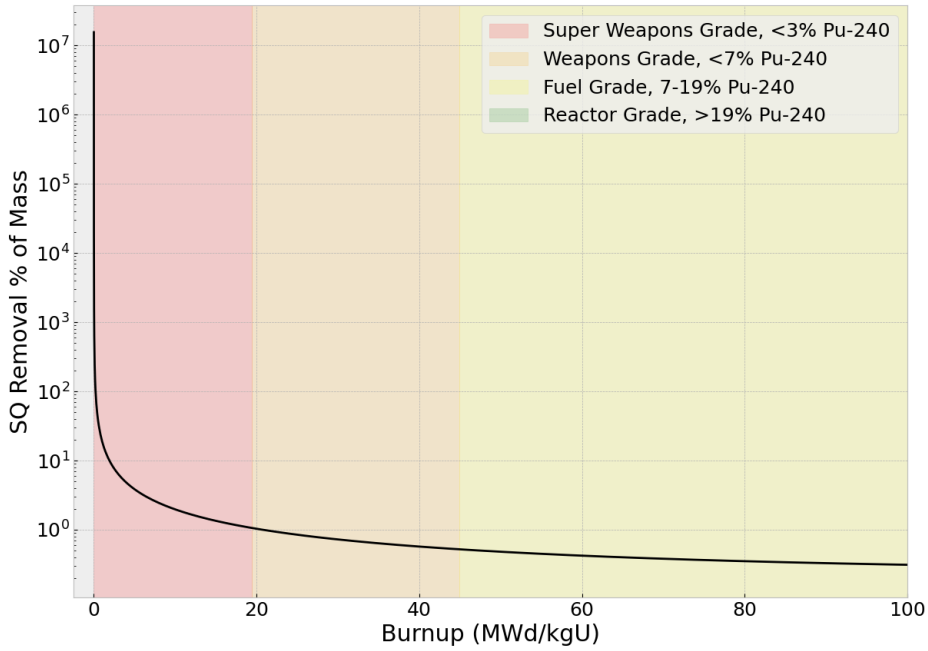

Figure 4.22: The percentage that an SQ (8kg) of plutonium represents of the total plutonium in the fast spectrum MSR fuel salt.

levels. The diversion of plutonium occurs at varied burnup stages, representative of the diverse qualities of bred plutonium.

All diversion case results are provided in Appendix A. Monitored parameters include kinetic parameters, delayed neutron fraction, mean neutron generation time, and parameters related to significant fission product poisons. Feedback coefficients, influenced by actinide presence, are expected to undergo changes during diversion. However, the minor differences in actinide content, on the order of a few percent, render precise calculation challenging given computational constraints. Serpent calculations suggest that the alterations in feedback coefficients are inconclusive, if not negligible. Similar observations apply to decay heat groups, where significant shifts in individual fission products' heat production amalgamate into indistinguishable changes when combined. Notably, Serpent simulations indicate appreciable variations in heat production from longer-lived fission products, contrary to expectations. However, the resulting change in total fission product heat production is below 2%. These longer-lived fission products exhibit prolonged equilibration times, potentially contributing to the observed discrepancies. Figure 4.17 highlights challenges in decay heat calculations, particularly with sudden changes. Consequently, decay heat production results are omitted to avoid conflating modeling limitations with real-world reactor behavior. Instead, it is assumed that decay heat production changes with burnup, but not during plutonium diversion events.

Appendix A.1 presents the thermal MSR's response to plutonium diversion. The most prominent impact of diversion is a reduction in the multiplication factor for early burnup. Notably, the earliest plutonium removal results in a reactivity decrease exceeding 1000 pcm, pushing the system into subcritical states. With no control rods inserted, compensatory measures necessitate a temperature decrease exceeding 150°C. A comparable, albeit less pronounced, reactivity decrease occurs during diversions at 65 and 114 full power days. To maintain reactor reactivity within a 100 to 200 pcm range of the original level, additional refuel uranium (of equivalent enrichment as refuel stock) is introduced into the fuel salt. Appendix A.2 presents the outcomes of this adjustment. The influence on the multiplication factor is negligible for fuel and reactor grade plutonium, hence such cases were not reevaluated with supplemental uranium.

In the thermal MSR, plutonium diversion appreciably affects the effective delayed neutron fraction. The removal of plutonium correlates with an increase in the delayed neutron fraction, as expected due to plutonium's lower delayed neutron fraction. This effect is exacerbated when makeup uranium is introduced to counteract reactivity changes. Furthermore, the six delayed neutron precursor groups have their own changes. The initial group, characterized by the longest half-life (55 seconds), experiences a substantial increase in its fraction until the plutonium quality diminishes to reactor grade. However, in liquid-fueled systems like MSRs, delayed neutron precursors undergo cycling in and out of the core. Consequently, a new parameter, termed β_{circ}, emerges, which is further investigated in Chapter 5. While certain longer-lived delayed neutron precursors may exert less influence on the reactor's dynamic response, their impact may be more noticeable in the external loop.

During plutonium diversion in the thermal MSR, the mean neutron generation time consistently increases. This parameter is intricately linked to k_{eff}, the effective multiplication factor. Therefore, in cases where k experiences a significant drop, particularly evident during high-quality plutonium diversion at lower burnup stages, the increase in mean neutron generation time becomes more exaggerated than in reliability. Introducing makeup uranium into the fuel mixture mitigates this increase, although it remains observable even under minimal changes in neutron multiplication, suggesting a distinct rise during diversion events.

Finally, properties concerning fission product poisons undergo marked alterations during plutonium diversion. The cumulative yield of I-135 increases but remains relatively stable (¿1%) when compared to the direct yield of Xe-135. The direct yield of Xe-135 can change by up to 8.5% with early burnup plutonium diversion. However, the direct yield of Xe-135 is an order of magnitude lower than the cumulative yield of I-135, suggesting that the steady-state concentration of Xe-135 would not undergo substantial changes. Nonetheless, given the strong linkage between frequency response and feedback timing, disparities may become apparent. Both xenon and samarium exhibit an increase in steady-state reactivity worth. With less fissile material available to absorb neutrons, the likelihood of neutron absorption by fission product poisons amplifies.

In contrast to the thermal spectrum MSR, the fast spectrum MSR exhibits minimal differences in the selected parameters during plutonium diversion. As mentioned earlier, the

large mass associated FSMSRs fuel salt means that a SQ of plutonium makes a smaller impact on the overall ratio of isotopes. Referring back to Table 4.6, it becomes apparent that the percentage of plutonium requiring diversion is notably lower, translating to a correspondingly reduced fraction of fissions. Consequently, there are no discernible changes in the neutronic parameters during diversion events. While some small variations are observed in certain delayed neutron precursor groups, these differences lack consistency across simulations. It is plausible that any observed disparities are merely artifacts of statistical fluctuations inherent in Serpent calculations.

While the fuel cycle described here is representative of a large portion of FSMSR designs in the space, it's important to acknowledge that other FSMSRs may not possess such a significant heavy metal mass. For instance, a burner FSMSR operating at a higher level of uranium enrichment would experience a similar, albeit less pronounced, buildup of plutonium. This plutonium would also exhibit a comparable isotopic distribution as observed in the B&B fuel cycle FSMSR.

To explore the implications of diversion in smaller reactors, several scenarios involving incremental removal of plutonium were simulated. Appendix A.3 presents the results of these simulations on FSMSR neutronics. A notable observation is that the effects of plutonium diversion on FSMSR neutronics are considerably less pronounced compared to thermal MSRs. While neutron multiplication exhibits a decrease in reactivity at higher levels of plutonium removal, the stronger temperature feedback coefficient in FSMSRs necessitates a smaller temperature drop to compensate for reactivity loss. The Doppler temperature feedback coefficient remains relatively steady for many diversion cases, but experiences a rapid increase with higher percentages of plutonium removal. All other neutronic parameters demonstrate minimal to negligible changes, which would be challenging to detect.

4.5 Conclusions

In summary, this chapter presents thermal and fast spectrum MSR models that encompass a significant portion of the design space. Both reactors commence operation with LEU and undergo plutonium breeding during burnup. The accumulation of plutonium and

fission products induces a natural drift in parameters relevant to reactor dynamics. The ramifications of this drift on reactor dynamic behavior will be investigated in Chapter 6. Whether plutonium diversion is discernible in reactor dynamic parameters depends on the reactor type and conditions of the diversion.

Thermal MSRs exhibit distinct alterations in dynamic parameters during plutonium diversion. Attempts to mitigate reactivity drops by introducing makeup uranium from the refuel stockpile accentuate most of these differences. Conversely, in FSMSRs with a sufficient mass to sustain a B&B fuel cycle, no measurable changes occur in parameters due to the minimal impact on the total fission rate. Only at higher percentages ($\geq$10%) of plutonium removal do dynamic parameters manifest signs of diversion, albeit with more subdued changes compared to thermal MSRs.

Chapter 5

Dynamic Models for Thermal and Fast Molten Salt Reactors

From the work in the previous chapter, we see that there are substantial changes in both MSR's operating parameters during burnup and diversion. However, what is not as clear is how each of the parameters interacts with each other and impacts the reactor behavior. This especially applies to the reactor's frequency response. Therefore, this study needs another modeling tool to better understand the parameters that influence the frequency response. Although there are several tools that show the behavior of a reactor neutron population in an MSR, there are three main requirements for this study:

1. **Accuracy:** The model would need to capture all the underlying physics. Any modeling methodology would need to be benchmarked against MSR experiments. However, we are limited to data only from the MSRE as a reference.

2. **Reactor inclusive:** Thermal MSRs and FSMSRs differ in many ways; the modeling tool used here would need to be broad enough to accurately depict both types of reactors. Additionally, MSRs have a large design space, so to facilitate safeguard research in the field, the model would ideally cover as much of the design space as possible.

3. **Computationally inexpensive:** A scoping study to find sensitive frequencies could take thousands of runs. This study shows results for tens of thousands of transient

calculations. Therefore, each run needs to consume only minimal computational resources.

This chapter details the chosen dynamic modeling methodology that fits these requirements. The methodology chosen is a non-linear, modified point kinetics model using nasalized masses to simulate heat transfer. This methodology has been developed over years at the University of Tennessee, Knoxville, and has been validated against the MSRE [74, 47]. In later years, relevant features have been tested and added, such as a once-through steam generator (OTSG) and decay heat generation [75, 61]. As a result, some of the explanations and theories behind the work are split between papers but eventually compiled into paper on the NERTHUS reactor, a design with a set of tools to aid in research [29]. However, several features that appear in these studies are unrelated aspects of MSRs frequency response during normal operation and material diversion. Therefore, this chapter will aggregate and condense the model to the features relevant for this study. Furthermore, the chapter details exactly how the methodology is applied to both the fast and thermal spectrum MSRs. As established in Chapter 3, the frequency response shows the greatest potential containing safeguarding signatures. Therefore, it is necessary at this time to explore what exactly the frequency response is and how that is captured in this modeling methodology.

5.1 Background on Frequency Response and MSR Dynamic Modeling

Past research in frequency analysis goes back to some of the earliest research reactors. It was known that the frequency of a reactivity insertion would affect the response in the neutron chain, and there was a concern that, for certain frequencies, the reactor could be unstable [46]. To probe for any sensitivity, these early experiments built dedicated equipment into the neutron reflector region to initiate a sinusoidal reactivity insertion. Building equipment in the core with no other function was eventually dropped due to financial concerns, at which point, new methodology was used to initiate a frequency response with a control rod and pseudo-random binary sequences. This method was adopted for the MSRE and yielded usable results

within a fifteen minute window [77]. Pseudo-random binary sequences were implemented on a wider scale of LWRs, and the frequency response was used to determine reactor core operational parameters such as heat transfer and temperature feedback coefficient.

The use of frequency analysis dropped over the years. One of the main causes for this drop in use is due to nonlinear behavior resulting from the phase change of water. The only reactors deployed commercially in the United States are LWRs, and the focus of reactor response analysis shifted towards behavior during accidents, particularly for LWRs. However, a phase change is not necessarily inherent to advanced reactors as it is to LWRs. There are a number of frequency effects in sodium-cooled fast reactors, and molten salt cooled pebble bed reactors may use frequency analysis for maintenance purposes [79, 49, 63, 38]. While in these other studies, the frequency analysis is used to derive reactor parameters for maintenance and safety purposes, this study extends this reasoning for MC&A.

Frequency analysis is often predicted via a dynamic model before any experimentation. There are a number of ways to predict the behavior of neutrons when subjected to a reactivity transient, whether they be periodic or not. The most common method is coupling point kinetics with thermal hydraulics for temperature feedback. This method was adopted by ORNL during the MSRP [47, 9, 78]. ORNL modified the point kinetic equations to account for the delayed neutron precursors flowing out and back into the core. The thermal hydraulics were modeled by nodalizing the fuel salt into a series of well mixed tanks and time delays. There have been many different takes on combining modified point kinetics with accompanying thermal hydraulics other than nodalization [89]. However, in more recent times, there have been some attempts at coupling Monte Carlo calculations with thermal hydraulics codes [6, 17]. Taking this multiphysics approach may increase accuracy with the trade-off of greatly increasing computational expense. However, it has been theorized that, in FSMSRs, the compressibility of the fuel salt filled with bubbles can affect the reactor response to large reactivity insertions [17]. Recent sensitivity analyses have shown that point kinetic equations still reasonably agree with these multiphysics calculations, though [18]. Additionally, there is no real-world data of a FSMSR's behavior to properly validate the models against.

In this study, the modeling approach adopted is the non-linear point kinetics, nodalized thermal-hydraulics method developed over the years at the University of Tennessee. This method has been applied to a wide variety of MSR designs. It was first validated against the frequency response of the MSRE [74]. The method was further expanded to encompass the balance of plant [75]. However, one of the results of the study indicated that only the steam generator was relevant to the reactor neutronic response. A later study included heat generated from fission products by grouping fission product heat in a similar fashion as delayed neutrons [61]. Representation of a once through steam generator (OTSG) and decay heat are included in a model that encompasses both the thermal and fast MSRs.

5.2 Governing Theories in Nodal Dynamic Modeling

While many of these methods have been published in previous years, the individual aspects of the MSR model are spread across multiple publications. Additionally, there are extraneous features (for frequency analysis) within some of these publications that are excluded here. Therefore, all the necessary theory and governing equations required to perform frequency analysis are reproduced here, along with the appropriate context.

5.2.1 Modified Point Kinetics Equations and Power Production

Given the timescale of the transients (ranging from a few seconds to hours), this model employs modified point-reactor kinetic equations (PKEs) with reactivity feedback. The PKEs are a series of coupled ordinary differential equations that capture changes in the neutron population, assuming that the neutron population is proportional to reactor power. These equations have primarily been used for solid-fueled reactors in the past, and many of the underlying assumptions and treatments of the equations remain the same here. However, MSRs feature liquid fuel that flows in and out of the core, which carries delayed neutron precursors with it. To address this issue, the PKEs were modified to include new terms accounting for the delayed neutrons lost to the external loop [47]. The modified PKEs suitable for MSRs are given in Equation 5.1 and Equation 5.2.

$$\frac{dn(t)}{dt} = \frac{(\rho(t) - \beta)}{\Lambda} n(t) + \sum_{i=1}^{6} \lambda_i C_i(t) + S(t) \tag{5.1}$$

$$\frac{dC_i(t)}{dt} = \frac{\beta_i}{\Lambda} n(t) - \sum_{i=1}^{6} \lambda_i C_i(t) - \frac{C_i(t)}{\tau_C} + \frac{C_i(t - \tau_L) e^{-\lambda_i \tau_L}}{\tau_C} \tag{5.2}$$

Where:

- t = time (s)
- $n(t)$ = relative to steady-state (operational) neutron population at time t
- $\rho(t)$ = reactivity at time t
- $S(t)$ = neutron added from external source relative to steady state (rel.)
- Λ = mean neutron generation time (s)
- β = delayed neutron fraction
- $i = i^{th}$ delayed neutron precursor group
- λ_i = decay constant for the corresponding delayed neutron precursor group (s^{-1})
- $C_i(t)$ = delayed neutron precursor group concentration (rel.)
- τ_C = core transit time (s)
- τ_L = external loop transit time (s)

Equation 5.1 is the same for both liquid and solid fueled reactors and represents the neutron population relative to operational steady-state. The delayed neutron precursor concentration is represented by Equation 5.2. It is in Equation 5.2 that the difference between liquid and solid fueled reactors becomes apparent. The third term in Equation 5.2 represents the loss of the delayed neutron precursors to the external loop, and the fourth term represents the circulation of the delayed neutron precursors back into the core after an appropriate amount of decay.

This study takes the neutron population and assumes that it is linked to fission power (e.g. if the neutron population is half of normal operation, then half the number of fission are occurring). It is common to assume that the total power is directly proportional to the neutron population. However, this ignores the contribution from fission product decay heat. Earlier work at ORNL accounts for fission product heating by splitting heat production into direct fission heat and constant heat production from decay heat [9]. This study takes this one step further by leaving the decay heat as a variable itself, the theory of which is explained in Section 5.3.

Most importantly, the reactivity is a variable that accommodates insertions with time. This reactivity can come from either inherent sources (e.g. temperature feedbacks) or actuated sources (e.g. control rod movement, accidents). The PKEs account for both actuated and inherent reactivity through the term $\rho(t)$ in Equation 5.1. The temperature feedbacks are treated as linear and scaled to the difference between the current temperature and normal operating temperature. Actuated reactivity is inserted as pure reactivity and can take any shape that can be represented as a time series (constant, function, step changes, etc.). For frequency analysis, the model inserts reactivity in the shape of a sine wave with magnitude +/-1 pcm.

While not a physical form of reactivity, the modeling methodology requires the accounting of ρ_{circ} (also known as ρ_0). ρ_{circ} is the reactivity lost due to the delayed neutron precursors that decay out of the core. This reactivity will not change so long as the flow is consistent, but the model requires ρ_{circ}, otherwise the temperature will drop to counteract it. The term ρ_{circ} is additionally useful for adjusting the neutronic parameters. The delayed neutron fraction is effectively lowered by ρ_{circ} and thus gives rise to the new term β_{circ}, which is analogous to β_{eff} in solid fueled reactors. Delayed criticality is particularly dependent on ρ_{circ}, which is defined by Equation 5.3.

$$\rho_0 = \beta - \sum_{i=1}^{6} \frac{\beta_i}{1 + \frac{1}{\lambda_i \tau_c}[1 - e^{-\lambda_i \tau_l}]} \tag{5.3}$$

The circulating fuel also affects the change in delayed neutron fraction during a plutonium diversion. For instance, if the overall β_{eff} drops by 1%, the change in β_{circ} may be smaller or

greater depending on how much of the drop is in or outside of the core. As a result, changes in the longer-lived delayed neutron precursors are felt less, and changes in the shorter lived precursors are felt more. An example of how core and loop transit time can affect changes to β_{circ} is given in Table 5.1.

5.2.2 Nodal Representation Theory and Heat Transfer

Historical models of MSRs, including the MSRE, used a lumped parameter method, which was limited by computational power of the time, so parameters were represented by differential equations within a system of equations. The scientists would then apply the Laplace transform to the system to make it suitable for the analog computers of the era. The result was a linearized model of the reactor that used nodes to represent the masses present in the reactor. Over time, more sophisticated models that incorporate mass flow and heat transfer coupled with neutronics have been developed [6, 50]. However, these methods tend to be complex to construct and require substantial computational resources. Recently, the nodalized methodology has been successfully implemented on modern digital computers [74]. This non-linearized methodology has been shown to be reasonably efficient despite requiring less computing power, making it particularly suitable for the purposes of this research.

A nodalized approach consists of a set of lumps representing mass in a reactor. Each mass node tracts temperature with respect to time. The underlying theory of heat production and transfer in a nodalized methodology, or Mann's model, is first explored in Reference [8], and this modeling approach has been widely implemented in the field. In summation, each node tracks changes in temperature resulting from heat transfer or internal heat generation. Liquid flow is modeled as a series of well-mixed tanks and time delays. Each liquid node mixes inlet temperature with current temperature, has internal heat production, and heat transfer to calculate change in temperature. The temperature of each node is assumed to be the outlet temperature. The node temperature being the same as the outlet temperature can lead to some inaccuracies with heat transfer if liquid to solid nodes are one-to-one. Thus, the Mann's model was conceptualized to achieve heat transfer based off an average temperature. In Mann's model, each solid to liquid heat transfer is represented by two liquid nodes to

Table 5.1: Percent change in β_{circ} when 1% of the β_{total} drop occurs in just one delayed neutron precursor groups (longer half life to shorter half life).

τ_c (s)	1	3	1	3
τ_l (s)	1	1	3	3
1 (55.5 s)	-0.922	-0.963	-0.728	-0.839
2 (21.9 s)	-0.926	-0.966	-0.743	-0.850
3 (6.3 s)	-0.944	-0.975	-0.809	-0.898
4 (2.2 s)	-0.986	-0.996	-0.966	-1.002
5 (0.5 s)	-1.151	-1.070	-1.554	-1.296
6 (0.1 s)	-1.397	-1.160	-2.157	-1.497

every one solid node. The outlet of the first fuel node is the average temperature of both liquid nodes and is therefore temperature in the temperature difference driven heat exchange. Figure 5.1 depicts how this heat transfer occurs. While Mann's model is reasonably accurate for most cases, irregularities may arise if the heat transfer area is too large in comparison to the specific heat capacity and mass flow rate. To address this, the dimensionless term "section length" was formulated and shown in Equation 5.4. The smaller the section length, the more accurate the simulation becomes; results become nonphysical if the section length exceeds 2. In such cases, heat transfer would need to be modeled with multiple successive heat transfer areas.

$$S_L = \frac{hA}{W_l C_p} \tag{5.4}$$

Where:

- S_L = section length
- h = heat transfer coefficient
- A = the area over which the conductive heat transfer occurs
- W_l = mass flow rate of the liquid
- C_p = specific heat capacity

If the section length requirements are met, Equation 5.5 can be applied to track the temperature of any given node.

$$\frac{dT_n}{dt} = \frac{K_n P_0 n(t)}{m_n C_p} + \frac{P_{dh}(t)}{m_{f,tot} Cp} + (\frac{hA}{m_n Cp})(T_s - T_{avg}) + \frac{W_n}{m_n}(T_{n-1} - T_n) \tag{5.5}$$

Where:

- K = fraction of fission power deposited in node n
- P_0 = nominal fission power generation
- m_n = mass of node n

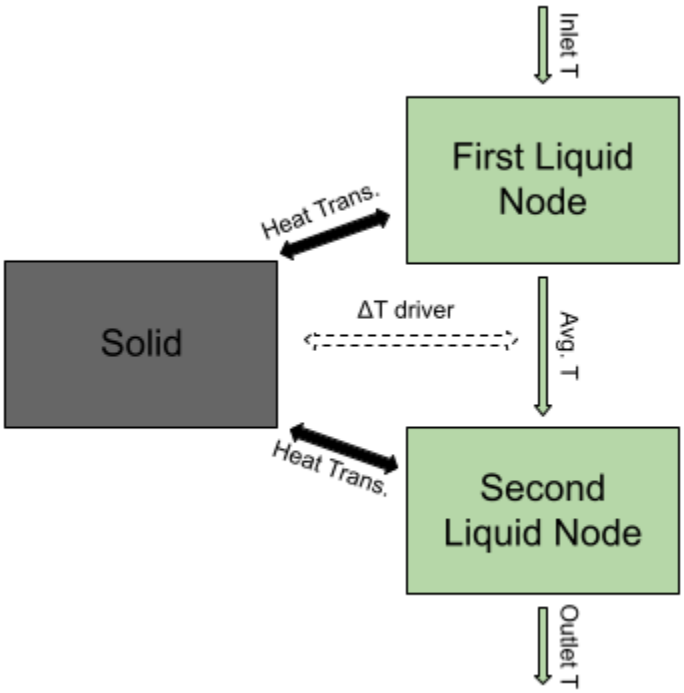

Figure 5.1: Diagram of heat transfer between liquid and solid nodes.

- $P_{dh}(t)$ = decay heat power at time t
- $m_{f,tot}$ = total fuel salt mass
- T_s = temperature of the adjacent solid node
- T_{avg} = average temperature of the two liquid nodes (outlet temperature of first fluid node)
- W_n = flow rate in liquid node
- T_{n-1} = node inlet temperature
- T_n = node outlet temperature

Equation 5.5 comprises multiple terms, each representing distinct contributions to the node's change in temperature. The first term accounts for heat generated from fission, which is assumed to be proportional to the neutron population in Equation 5.1. The second term represents heat generated by the decay of radioactive fission products. The third term models heat transfer between liquid and solid nodes (note that the temperature difference is between the first fluid node). Finally, the fourth term accounts for temperature changes resulting from the mixing of liquid from preceding liquid nodes. Whether a term is included or not in the equation depends on the physical characteristics of the mass the node is intended to represent. For instance, only the fuel nodes contain heat generation from fission products, and solid nodes have no mixing term.

5.3 General MSR Nodalized Model Representation

5.3.1 Core and Coolant Representation

To ensure accurate modeling, the nodalization must be in agreement with the physical reactor. This begins with the core, where both fast and thermal reactors can be modeled using a single Mann's model, as illustrated in Figure 5.1. In a thermal MSR, the solid node represents the graphite moderator, while in the FSMSR, it corresponds to the neutron

reflector. After leaving the core, the fuel salt enters the primary heat exchanger, which is modeled using two Mann's models to maintain a low section length and ensure accurate heat transfer representation. For the piping between the core and the heat exchanger where the salt flows, an additional node is included to account for the heat generated by the decay of fission products. This node incorporates time delays on either side to model the transit time of the salt accurately.

Due to concerns about steam generator failure, MSRs almost always include a secondary salt loop [34]. The secondary salt is chosen to be chemically compatible with the fuel salt to prevent contamination in the event of accidental mixing. For fast spectrum MSRs (FSMSRs), the secondary salt must also remain free from moderating materials to maintain the reactor's fast neutron characteristics. Unlike the fuel salt, the secondary salt does not produce internal heat and only facilitates heat transfer.

The molten salt reactor research program also introduced a tertiary molten salt loop composed of HITEC salt, a design that is incorporated into the planned demonstration reactors [12]. This tertiary loop serves several purposes. First, it lowers the temperature of salt entering the steam generator which was a limiting factor during the time of the MSRP. Second, it acts as a safety measure; in the event of a steam generator failure, water can safely boil out of the HITEC salt without directly interacting with the reactor systems. Finally, it mitigates tritium release to the environment. Tritium, generated during reactor operation (either from neutron absorption of Li-6 or from ternary fissions), diffuses through metal barriers at the operating temperature of an MSR and follows a temperature gradient in the coolant salts. Once tritium reaches the HITEC salt, it forms tritiated water, which can then be safely captured and removed from the system. This study assumes that both fast and thermal reactor designs include a HITEC salt loop.

The model concludes with a once-through steam generator (OTSG), a component that has been used in previous reactor models and will be discussed in detail in the next section. Overall, this dynamic model layout mirrors the configuration of the NERTHUS reactor model, as depicted in Figure 5.2. While the NERTHUS model was designed to be broadly applicable, certain adjustments were made to streamline the current digital model.

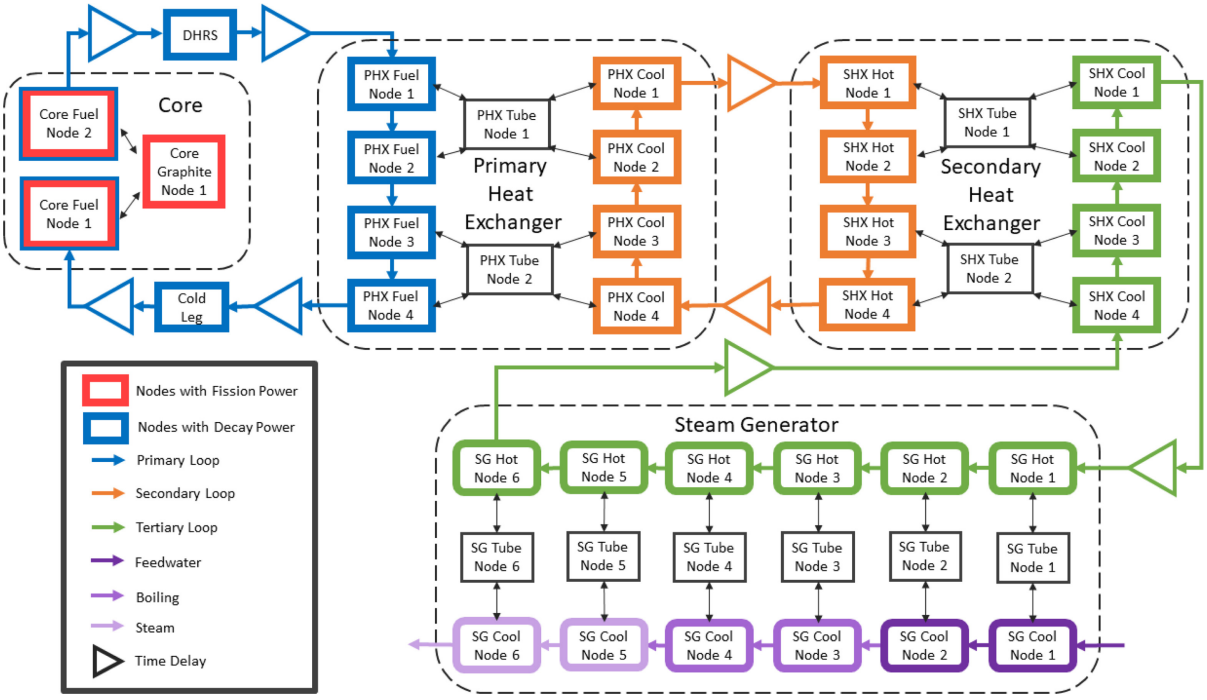

Figure 5.2: Nodalization of the reactor dynamic models [29].

Specifically, superfluous features, such as those used for calculating frequency responses (e.g., pump trips, load following), have been removed to decrease run time and increase reliability.

5.3.2 Once-Though Steam Generator

For power generation, this model employs an OTSG, a key component that was not included in the study presented in Chapter 3. The representation of an OTSG used here has been under development for several years[19]. For its implementation in MATLAB, both the OTSG and the rest of the balance-of-plant were developed and coupled with an MSR concept [75]. This modeling approach mirrors that effort. However, the feedwater flow to the OTSG is actively controlled, resulting in a significant impact on the system's frequency response. Beyond the OTSG, the balance-of-plant has no measurable effect on the frequency response. This behavior is illustrated in Figure 5.3, which highlights the need to include a OTSG's (or other power generating system) in assessing a reactor frequency response.

The OTSG is divided into six heat transfer nodes, distributed across three distinct regions based on the state of the cooling water. Each region contains two nodes. The first region is the subcooled region, where the high mass of water heats up to its boiling point. The second region, the saturated region, represents the area where water is boiling, and the temperature remains constant while the flow rate to the steam nodes changes. Finally, the steam region captures the behavior of steam as it continues to heat before exiting the OTSG. The lengths of these regions vary dynamically with changes in heat flux. Figure 5.4 illustrates the nodalization structure of the OTSG. All equations governing the OTSG are provided in the appendix of Reference [75]. Additionally, because this model does not include load-following capabilities as the feedwater flow rate is held constant.

5.3.3 Decay Heat Production

The inclusion of decay heat has been noted as important in the past. The dynamic analysis of the MSRE used a first order time lag (or that all heat is produced by a single nucleus) [9]. The approach used in this study instead follows the methodology in Reference [61]. In the paper, fission products that produce heat are lumped together into groups the same way

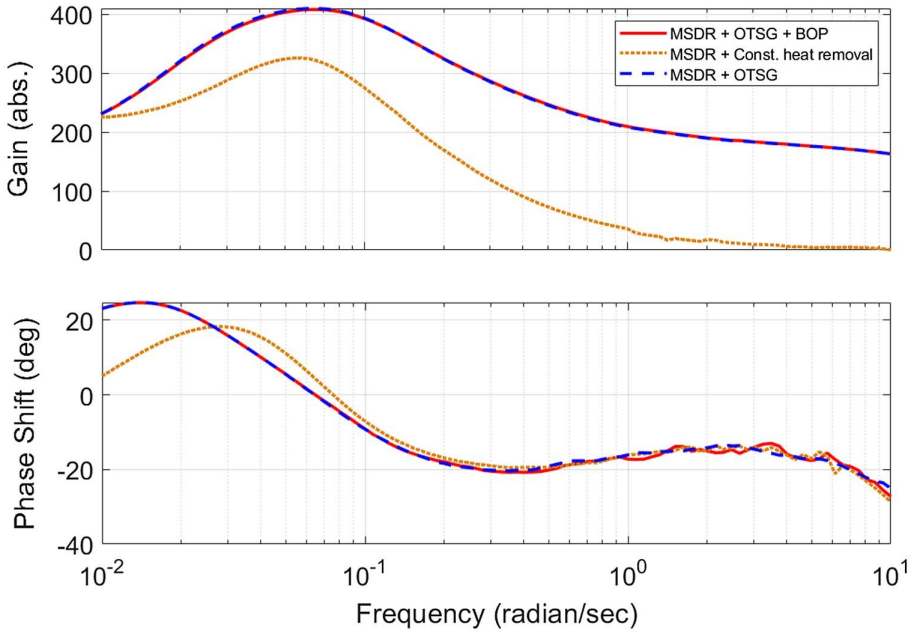

Figure 5.3: Example of how the introduction of a steam generator can change the frequency response from a previous study [75].

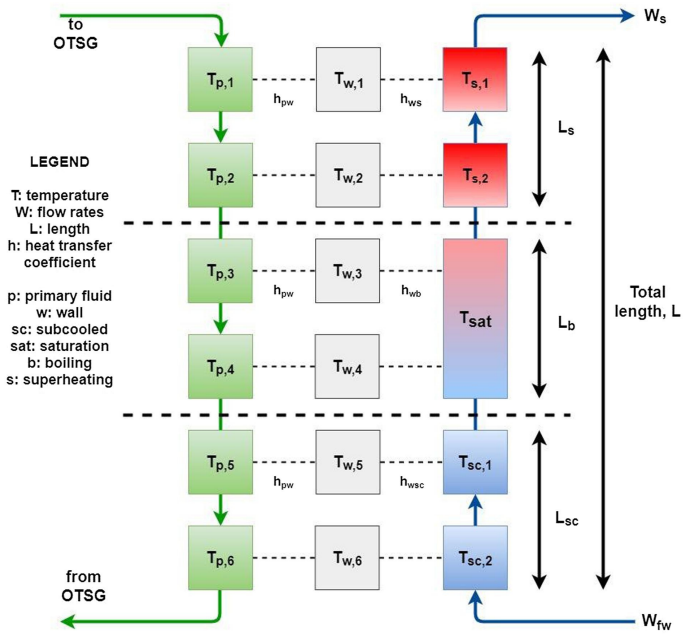

Figure 5.4: A diagram of how the OTSG is nodalized [75].

delayed neutron precursors are. As a result, this study does not look at the inventory of isotopes, but only the heat produced by the fission products. The lump decay heat precursors are fit to the amount of power produced during normal operation and after fission power is shut down. However, while Reference [61] matched referenced data fairly well, it relied on data from solid-fueled reactors which diverges from MSRs due to online FP vitalization. This study, instead, used the data generated in Section 4.3.4. From the material concentration of the fuel at each point, a decay curve is generated for each point of burnup when fissioning ceases. The precursor groups are fit to the steady-state power and decay curve, of which an example can be seen in Figure 5.5. For all decay curves, four precursors are sufficient enough to fit the decay curves with $< 1\%$ error on the integral.

Fitting four decay heat precursor groups to the decay heat curve can be represented by Equation 5.6 and 5.7. This fitting approach mirrors how the U.S. Nuclear Regulatory Commission approaches decay heat production [4]. However, this equation here greatly reduces complexity while maintaining accuracy for dynamic modeling purposes. As can be seen in Figure 5.6, the inclusion of decay heat does change the calculated frequency repose and differs from both not including decay heat and constant decay heat.

$$\frac{d\alpha_i(t)}{dt} = \gamma_i n(t) - \alpha_i e^{\lambda_i t} \tag{5.6}$$

$$P_{dh}(t) = \sum_{i=1}^{4} \alpha_i(t) \tag{5.7}$$

Where:

- P_{dh} = Power resulting from FP decay heating
- α_i = decay heat contribution of group i
- γ_i = fission yield of group i
- λ_i = decay constant of group i (s^{-1})
- t = time (s)

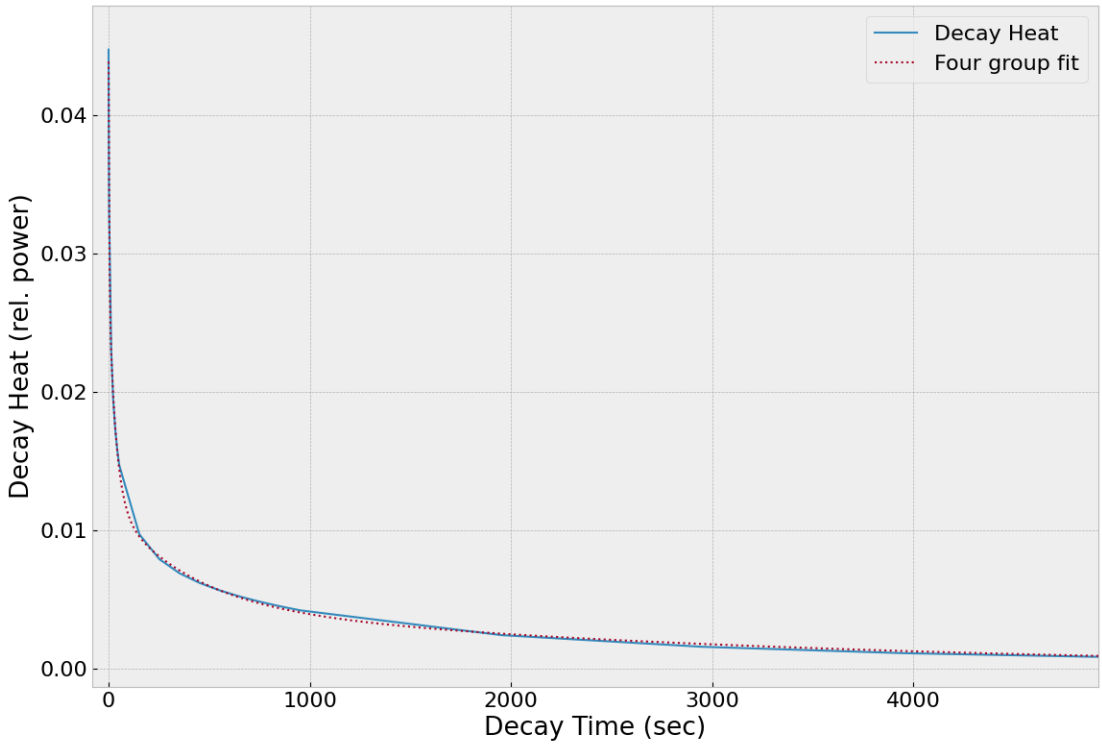

Figure 5.5: Example of four group decay heat precursors fitting Serpent calculated decay heat in terms of operational power with time zero when fission stops.

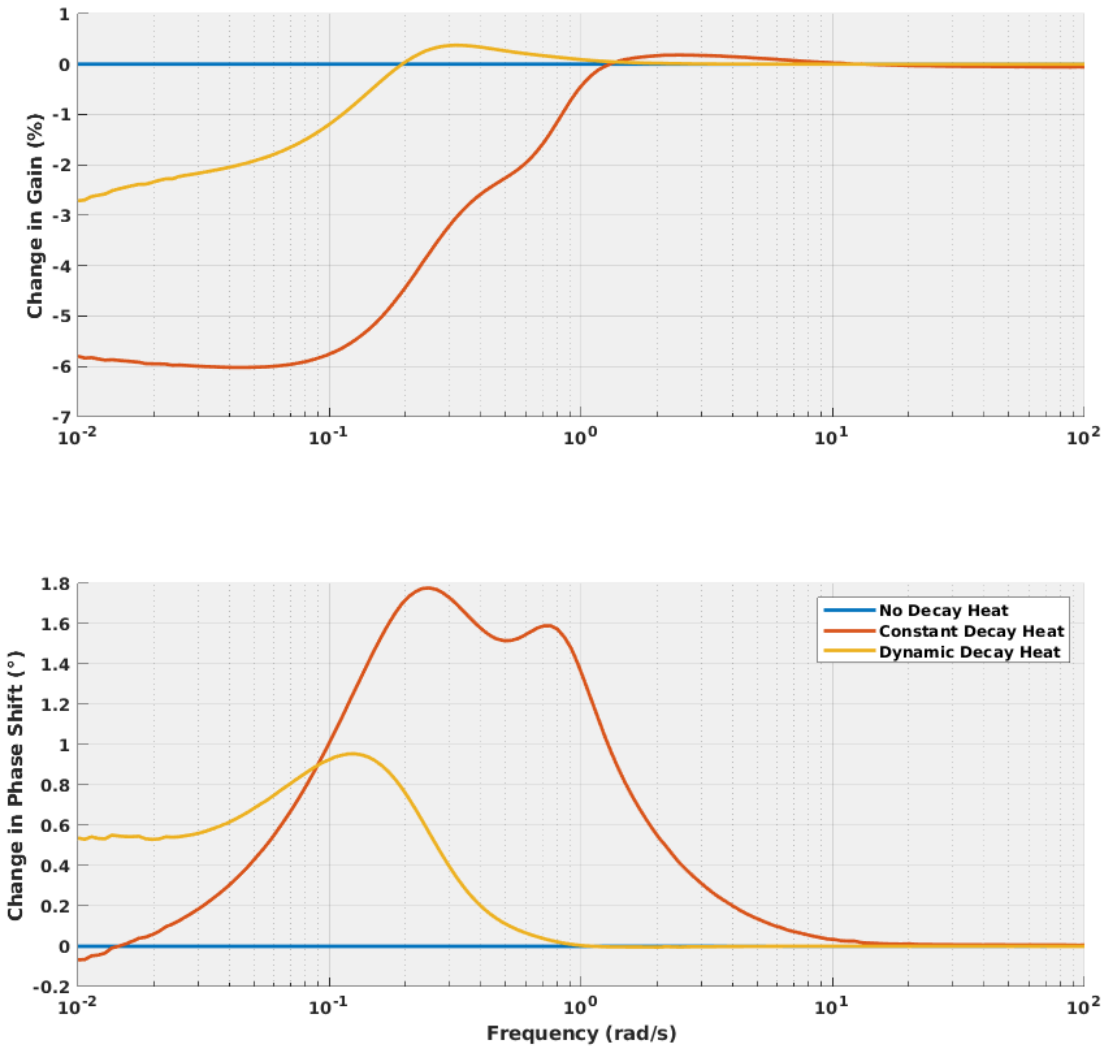

Figure 5.6: How the inclusion of different methods for accounting for decay heat changes the frequency response of a reactor for both Gain (top) and phase shift (bottom) relative to not including decay heating.

The digital model includes heat generation from FP decay, which is assumed to occur uniformly throughout the fuel salt with no spatial differentiation. Additionally, this methodology does not distinguish FPs that have plated out or agglomerated within the reactor fuel system from FPs that remain dissolved in the fuel salt. Heat generated by insoluble FPs, such as noble metals, is treated equivalently to that generated by soluble FPs. Depending on deposition behavior, noble metals and other plated-out FPs could cause local hot spots that are not modeled here due to the current limited understanding. Only volatile FPs, which leave the system, are excluded from the heat generation calculations. These assumptions ensure a simplified yet consistent approach to perform the rapid iterations of calculations in this study.

5.3.4 Reactivity Feedback Mechanisms

Since the neutron chain reaction is represented by Equation 5.1, feedback to the reaction is modeled entirely through reactivity. Aside from user-defined reactivity insertions, the system incorporates two internal reactivity feedback mechanisms. The first is temperature feedback, calculated by multiplying the temperature coefficient by the difference between the current and nominal temperatures. For the fuel salt, Doppler and void coefficients are combined into a single value for total fuel salt feedback coefficient. This assumption may not be acceptable in some cases with larger reactivity insertions in fast spectrum reactors, but for the reactivity insertion presented will not see this effect (see Reference [17]). In the thermal MSR, temperature feedback also includes contributions from the graphite moderator, whereas in the FSMSR, only the fuel temperature feedback is considered.

The second feedback mechanism arises from FP poisons. As the reactor undergoes burnup, neutron-absorbing FPs accumulate in the system. This study takes into account the two most prominent FP poisons: Xe-135 and Sm-149. Xe-135, with its exceptionally high neutron absorption cross-section, is typically the dominant FP poison. However, in liquid-fueled reactors, its impact is significantly mitigated because Xe-135, being a noble gas, evolves out of the system continuously.

With Xe-135 effectively removed from the system, Sm-149 becomes the most prominent FP poison. As a lanthanide, Sm-149 is soluble in both fluoride and chloride molten salts.

Unlike Xe-135, Sm-149 is stable and must absorb a neutron to leave the system. The Sm-149 and precursor populations are calculated using the equations provided below. Direct yield of Sm-149 is ignored since the direct yield is insignificant compared to Pm-149's yield.

For implementation in the code, Equations 5.8-5.11 were used to calculate the change in atoms total:

$$\frac{dI}{dt} = \gamma_I F_0 n(t) - \lambda_I I(t) \tag{5.8}$$

$$\frac{dXe}{dt} = \gamma_{Xe} F_0 n(t) + \lambda_I I(t) - \lambda_{Xe} Xe(t) - \rho_{Xe} F_0 n(t) Xe(t) \tag{5.9}$$

$$\frac{dPm}{dt} = \gamma_{Pm} F_0 n(t) - \lambda_{Pm} Pm(t) \tag{5.10}$$

$$\frac{dSm}{dt} = \lambda_{Pm} Pm(t) - \rho_{Sm} F_0 n(t) Sm(t) \tag{5.11}$$

Where:

- $I(t)$ = I-135 atoms in the fuel salt
- $Xe(t)$ = Xe-135 atoms
- $Pm(t)$ = Pm-149 atoms
- $Sm(t)$ = Sm-149 atoms
- λ = Decay constant of the respective isotope (s^{-1})
- F_0 = nominal fission rate (fiss./s)
- γ = fission yield (frac.)
- ρ = steady state reactivity drain from FP poison (abs.)

Most parameters are derived from the neutronic model (i.e., yield, fission rate, steady-state absorptions) while others are from assuming steady-state (i.e., initial values). As

the concentration of FP poisons in the fuel salt changes, it is assumed that the reactivity changes linearly. The result is Equation 5.12, which inserts positive reactivity when FP concentrations are lower than steady state and negative reactivity when higher.

$$\rho(t) = \frac{(FP_0 - FP(t))}{FP_0}\rho_0 \tag{5.12}$$

Where:

- $\rho(t)$ = reactivity from FP poison at time t
- FP_0 = pseudo steady state FP poison atom quantity
- FP_0 = FP poison atom quantity at time t
- ρ_0 = steady state reactivity drain from FP poison (abs.)

5.4 Physical Parameters used in MSR Modeling

A complete list of all thermophysical parameters used in this study is provided in Appendix B. For the thermal MSR, parameters are drawn from a combination of the NERTHUS reactor paper and data from the MSRP. Parameters of the FSMSR are primarily sourced from the Molten Salt Fast Reactor (MSFR) thermal hydraulics study, which include key properties such as heat capacity and total fuel volume [66]. Pairing the fuel volume from the neutronics study resulting in instability due to the low power density. To address this issue, the parameters were adjusted to blend these values, ultimately achieving a power density within a stable operational range.

It is assumed that none of the thermophysical parameters change over burnup. While some parameters would normally change over burnup due to build up of FP species in the salt. However, this change is expected to be relatively small, and therefore ignored.

5.5 Discussion

Both models developed in this study are available online on GitHub [81], allowing anyone to download and run a frequency response analysis for their chosen reactor design. Users need only modify the thermophysical and neutron parameters to reflect the characteristics of their specific reactor. While the current implementation is tailored for liquid-fueled reactors, the underlying methodology remains valid for other reactor types with appropriate adjustments. The next chapter will present the results generated from these models, specifically examining when and under what conditions plutonium diversion becomes apparent.

Chapter 6

Frequency Response during Burnup and Plutonium Diversion

The neutronic parameters calculated in Chapter 4 are utilized in the model discussed in Chapter 5. Traditionally, frequency response are analyzed using Laplace transforms of linear models. However, due to the non-linear nature of this model, the frequency of the sinusoidal reactivity insertion is varied to generate Bode plots. For each case, the reactivity insertion consists of a sinusoidal pure reactivity input with a magnitude of ± 1 pcm. This small reactivity perturbation ensures the system's response remains within the linear regime. The reactor's power response mirrors the sine wave with a power response of the same frequency but with a shifted phase and gain in amplitude. In this study, a sine wave is fitted to the power response, from which the response gain and phase shift are determined.

6.1 Thermal MSR Frequency Response

6.1.1 The Effect of Burnup on the Thermal MSR Frequency Response

The thermal MSR model presented in this study closely resembles the earlier results detailed in Chapter 3. Chapter 3 only tracked changes to the delayed neutron fraction and the mean neutron generation time. The more detailed approach includes a comprehensive evolution of

parameters such as the delayed neutron fraction, mean neutron generation time, decay heat, FP poisons, and temperature feedbacks. Additionally, the dynamic model that assesses the frequency response includes the steam generator. By integrating these additions, the model provides a more accurate representation of the system's behavior. This allows for a direct comparison between the detailed results from this study and the outcomes derived from the earlier simplified methods, thus also determining whether or not the extra effort is worth it.

Figure 6.1 illustrates the gain profile of the thermal MSR, which exhibits the characteristic double-peak structure typical of such systems. This double peak is a defining feature that reflects the system's dynamic response across different frequency ranges. The evolution of gain over the reactor's burnup period is shown in Figure 6.2. Generally, the gain increases across all frequencies as burnup progresses. However, a distinctive pattern emerges: while the mid-range frequency gain stabilizes after the initial burnup phase, the gain for both low and high frequencies continues to rise.

The increase in gain at lower frequencies, as observed in this detailed model, was not evident in the simplified approach presented in Chapter 3 (see Figure 3.4). While the high-frequency changes were noted in the earlier model, they were slightly exaggerated compared to the results from the comprehensive model. The gain changes in the mid-range frequencies, however, show good agreement between both the simplified and full models. Overall, these findings suggest that incorporating additional parameters such as burnup effects and steam generation dynamics is crucial for accurately assessing the changes in the reactor's frequency response.

The phase shift over the course of burnup is illustrated in Figure 6.3, revealing significant changes across different frequency ranges. At low frequencies, a large positive phase shift is observed, while at higher frequencies, there is a pronounced negative phase shift. Additionally, a distinctive bump in the phase shift, characteristic of circulating liquid fuel systems, is evident. Although the changes in phase shift over burnup are subtle and difficult to notice in Figure 6.3, a plot of the differences in Figure 6.4 provides a clearer depiction of these variations. Depending on the frequency, the phase shift can either increase or decrease during burnup. This nuanced behavior contrasts with the predictions of the simplified model, which only anticipated an overall increase in phase shift. The results, therefore, indicate that

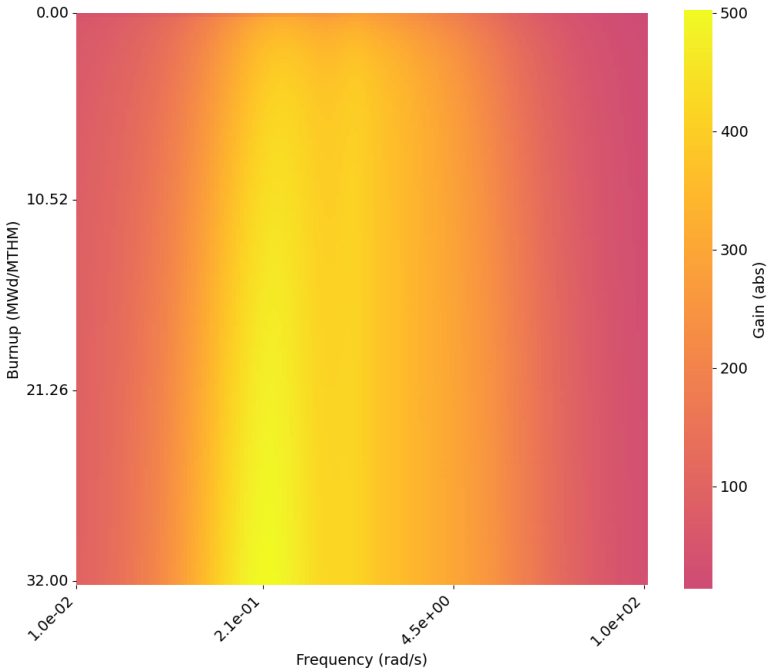

Figure 6.1: Gain in the reactor response over burnup of the thermal MSR.

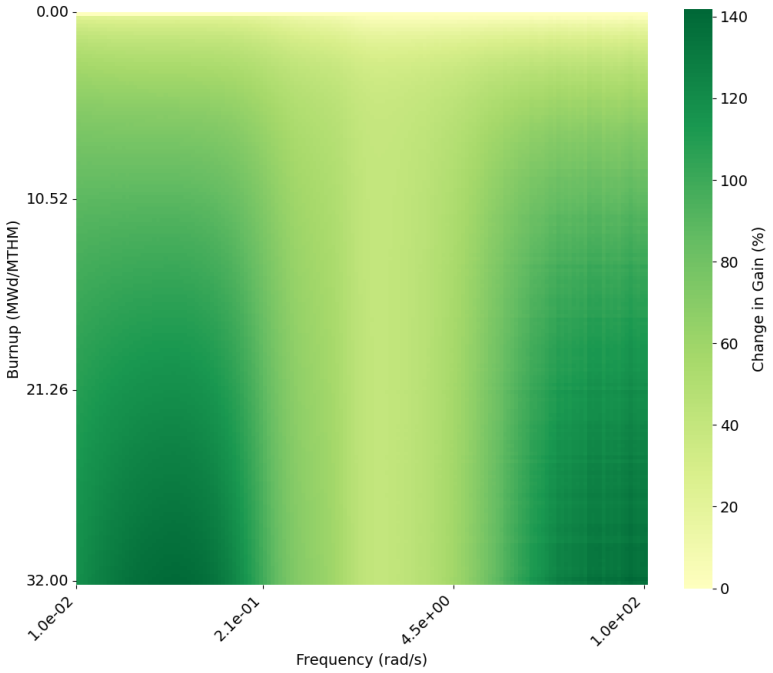

Figure 6.2: Percentage change in frequency response gain over burnup of the thermal MSR.

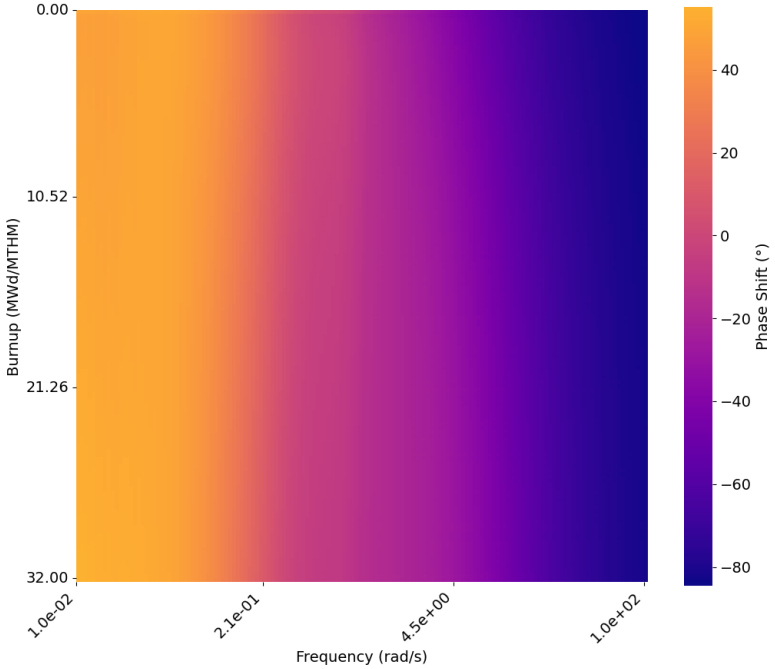

Figure 6.3: The shift in phase of reactor frequency response over burnup of the thermal MSR.

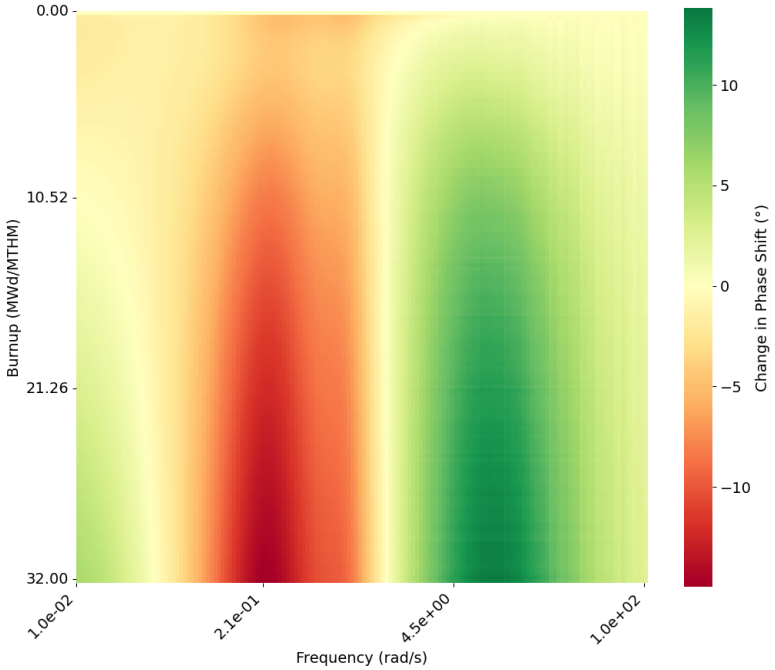

Figure 6.4: The absolute change in the phase shift over burnup of the thermal MSR.

by measuring the response to certain frequency, one could infer the level of burnup the fuel salt has undergone. However, the results also indicate that there may be value in higher fidelity modeling.

6.1.2 Plutonium Diversion's Effect on the Thermal MSR Frequency Response

Plutonium diversion also impacts the reactor's frequency response, as demonstrated in Figure 6.5. At this stage, the thermal MSR has reached a burnup level of 0.32 MWd/MTUi, corresponding to the first entry in Table 4.6. At this relatively low burnup, the plutonium is composed of $\geq$95% Pu-239, and diverting a significant quantity removes the majority of the plutonium present. This results in a noticeable deviation in the reactor's dynamic response. Figure 6.6 highlights this deviation, showing the gain as a percentage difference from nominal operation and the phase shift as a direct degree change. For the gain, a significant drop of $\approx$6% is observed at higher frequencies, while lower frequencies show minimal change. Additionally, the phase shift experiences a modest decrease across all frequencies, peaking in the mid-range frequencies.

Figures 6.5 and 6.6 also include the scenario where the reactor is refueled with uranium enriched to 19.75 wt%. This addition of uranium compensates for the removed plutonium just enough to maintain reactor criticality. Since the reactor's response depends on the ratio of isotopes contributing to fission, it follows that the differences in the frequency response would be more pronounced. This hypothesis aligns with the results from the simplified model in Chapter 3. Indeed, some frequency ranges show exaggerated effects, such as an increased gain in the mid-range frequencies and a phase shift at high frequencies that flips from negative to positive. On the other hand, other frequencies exhibit dampened effects, like the reduced gain at high frequencies. These findings underscore the necessity of considering factors beyond the delayed neutron fraction and mean neutron generation time when evaluating the impact of plutonium diversion on reactor neutronics.

This diversion was repeated at several burnup stages, with Pu-240 concentrations varying from weapons-grade to reactor-grade plutonium. The differences in gain and phase shift

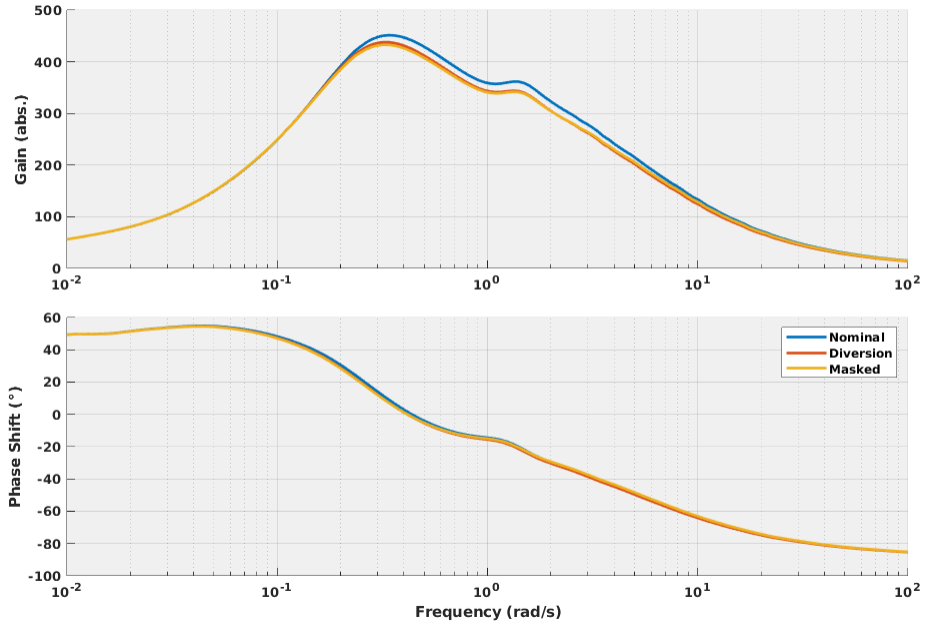

Figure 6.5: The frequency response of the thermal MSR at 0.32 MWd/MTUi for nominal operation and during plutonium diversion both with and without makeup uranium to account for criticality drop.

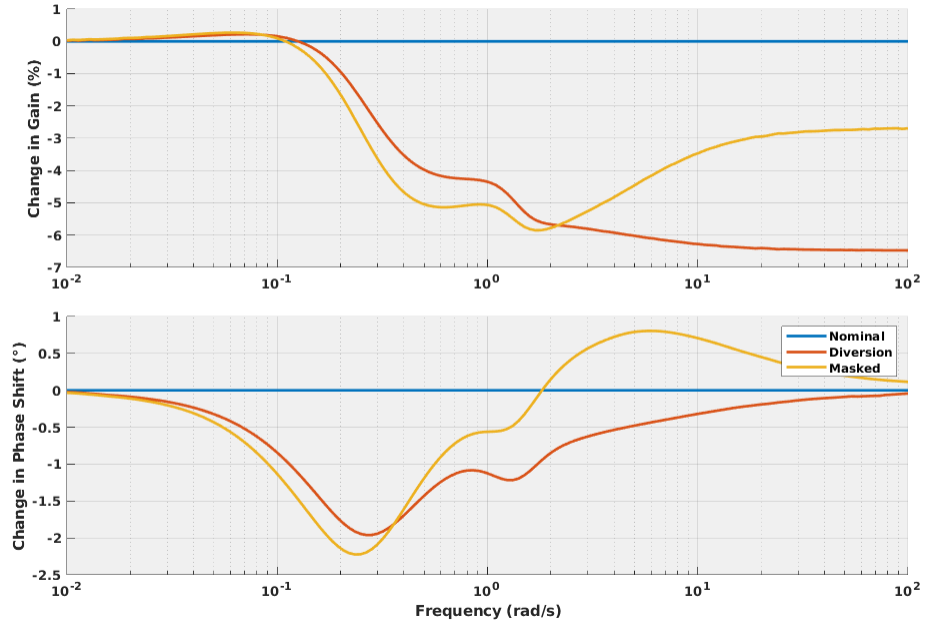

Figure 6.6: The change that plutonium diversion causes in frequency response from nominal operation at 0.32 MWd/MTUi.

are depicted in Figure 6.7. Each case exhibits unique behavior depending on the grade of plutonium removed. Weapons-grade plutonium diversion, having the largest shift in fissile isotopes, caused the most significant impact on the frequency response. Lower-grade plutonium diversions, while less dramatic, still left discernible signatures in the frequency response.

When examining the changes in frequency response across different scenarios, certain trends emerge. Notably, the gain change for masked diversion runs is smaller at higher frequencies compared to unmasked runs. For instance, in the SQ diversion of fuel-grade plutonium (yellow), the masked run shows a reduced impact on the frequency response. However, the mid-range frequencies reveal greater disparities in masked weapons-grade diversions.

Another notable observation is the frequency response at higher burnup (32.19MWd/MTU). The changes in frequency response are inverted compared to other diversion cases. This contrast is particularly striking given that the 4.98MWd/MTU diversion also involves reactor-grade plutonium. The key difference lies in the Pu-241 content, which contributes to over twice as many fissions in the higher burnup case. This inversion suggests that the buildup of Pu-241 could complicate the detection of diversion signatures, as it may reach a point where no significant changes are observed across much of the frequency range. This underscores the importance of monitoring the entire frequency range and maintaining detailed records of past reactor responses to ensure accurate detection.

6.2 FSMSR Frequency Response

6.2.1 The Effect of Burnup on the FSMSR Frequency Response

The fast reactor presents unique characteristics that distinguish it significantly from its thermal counterpart. Unlike thermal reactors, where Pu-239 concentration reaches an equilibrium, Pu-239 concentration increases throughout burnup in FSMSRs. Additionally, the grade of plutonium never lowers to reactor grade and only gets to fuel grade after over half of the reactor lifetime has passed. Another key factor is the large volume of fuel salt in

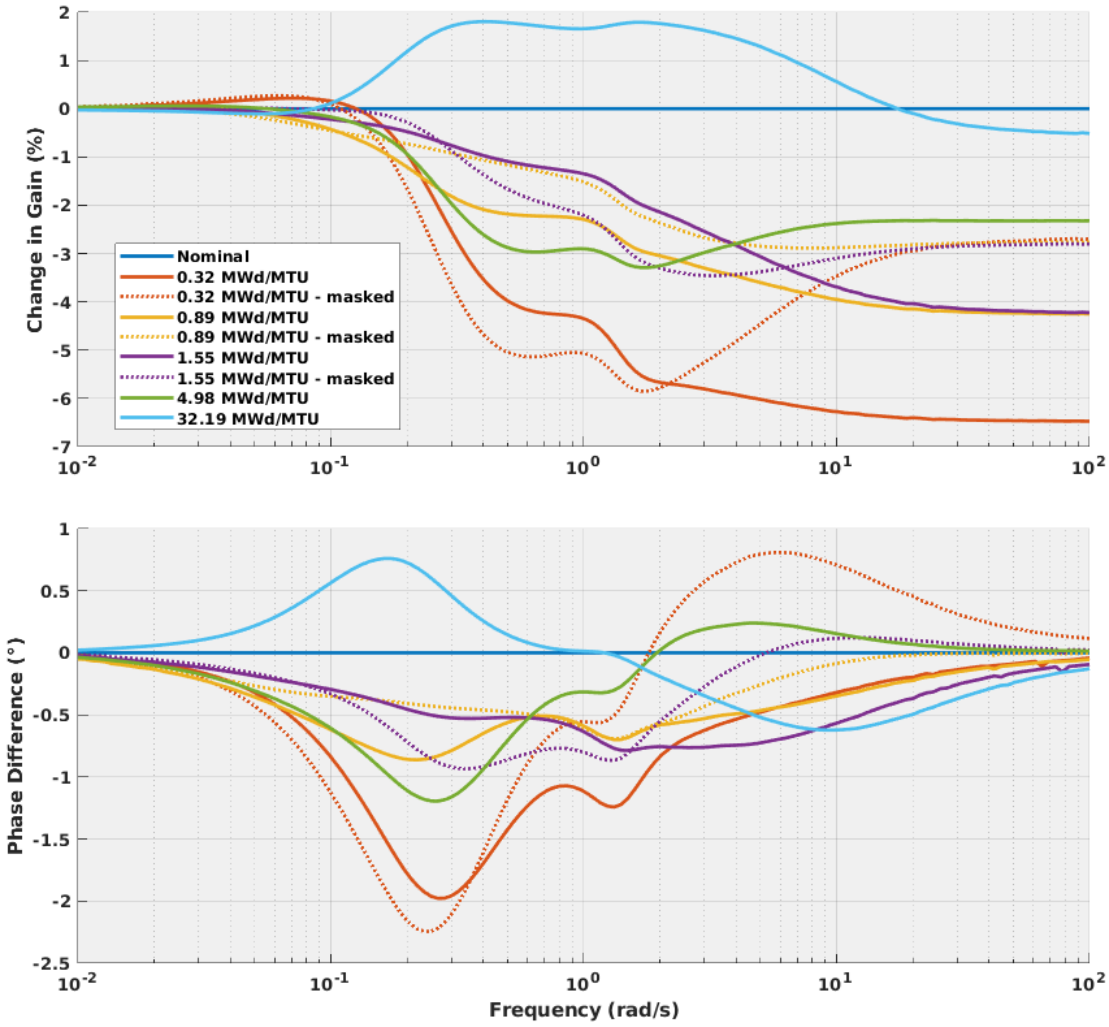

Figure 6.7: Change in the thermal MSR frequency response at different levels of burnup during plutonium diversion.

fast reactors, which slows the isotopic evolution over time. Although the changes in isotopics are gradual, burnup eventually exerts its influence on the reactor's behavior. This effect is evident in the gain trends illustrated in Figures 6.8 and 6.9. At higher frequencies, the response gain is elevated and continues to rise with increasing burnup. However, the overall change in gain for the fast reactor is approximately half that of the thermal reactor, even over extended burnup periods. Interestingly, a slight decrease is observed in the gain for lower frequency insertions.

The phase shift behavior, depicted in Figures 6.10 and 6.11, reveals additional insights. A notable peak occurs in the mid-range frequencies, and this peak becomes more pronounced as burnup progresses. Despite these changes, the phase shift for other frequencies remains relatively constant. This behavior highlights the distinct dynamics of fast reactors, emphasizing the importance of tailored analysis for accurately assessing their frequency response under varying operational conditions.

6.2.2 The Effect of Plutonium Diversion on the FSMSR Frequency Response

As stated in Chapter 4, the FSMSR has a negligible change in relevant parameters. This is somewhat expected given the substantial volume of fuel salt required to achieve criticality and fill the external circuit for heat removal. However, this is an expectation based on the large amount of fuel needed to sustain criticality and breeding. However, to see where the frequency response in a safeguarding context may be applicable to a less massive FSMSR, increasing percentages of plutonium were removed from the fuel salt of the FSMSR serpent model. The frequency response for increasing plutonium removal is presented in Figures 6.12 and 6.13

Simulated results reveal that only one specific scenario resulted in a noticeable (>1%) change in frequency response - specifically, when 25% of the plutonium was removed. In contrast, other diversion cases fell within the zone of error for fuel calculations, indicating that the reactor's sensitivity to plutonium withdrawal may be lower than anticipated. These findings have significant implications for fast spectrum molten salt reactors compared to

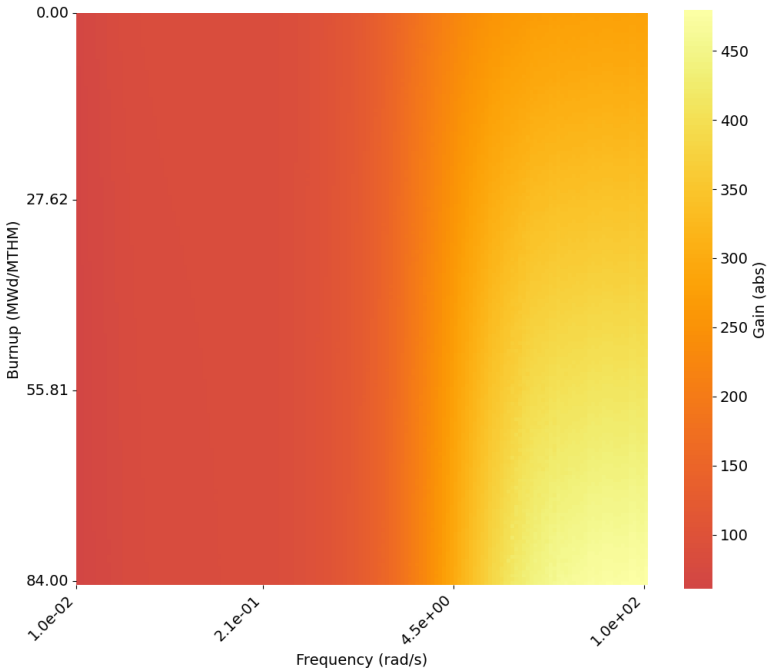

Figure 6.8: Gain in the reactor response over burnup for the FSMSR.

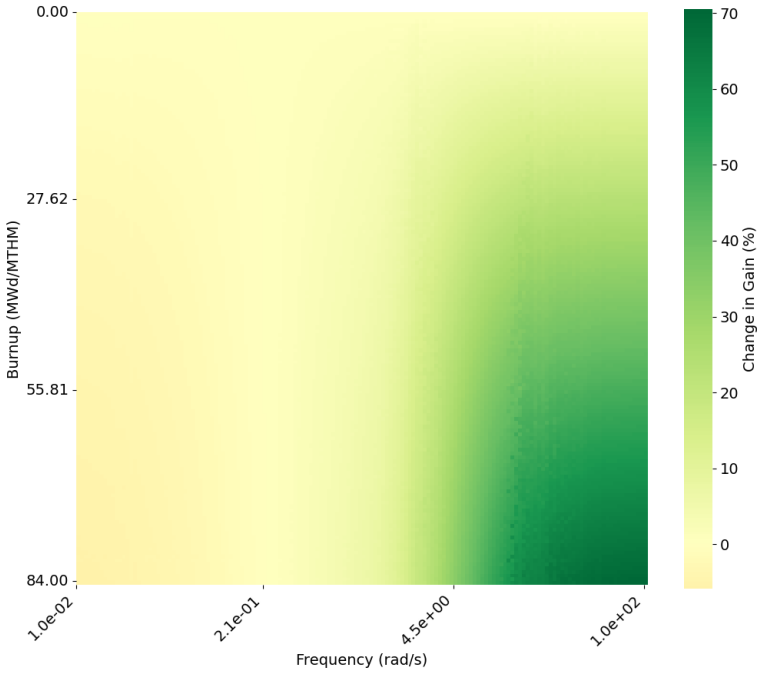

Figure 6.9: Percentage change in frequency response gain over burnup for the FSMSR.

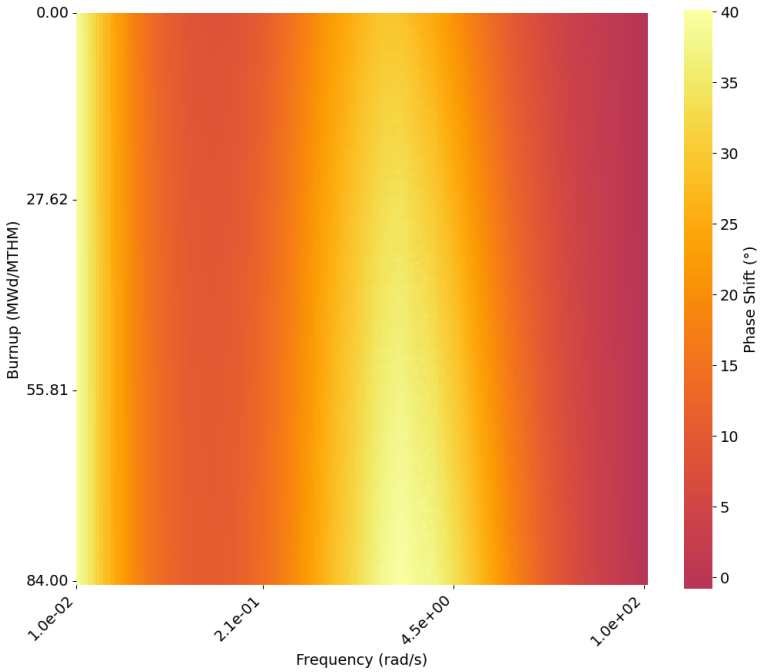

Figure 6.10: Phase shift in frequency response of the FSMSR over burnup.

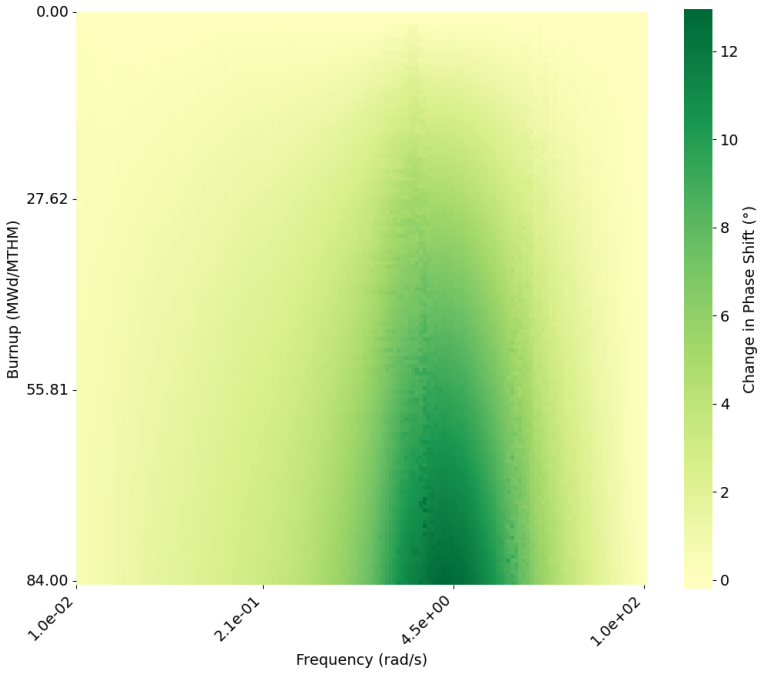

Figure 6.11: Degree change in phase shift of the FSMSR during burnup.

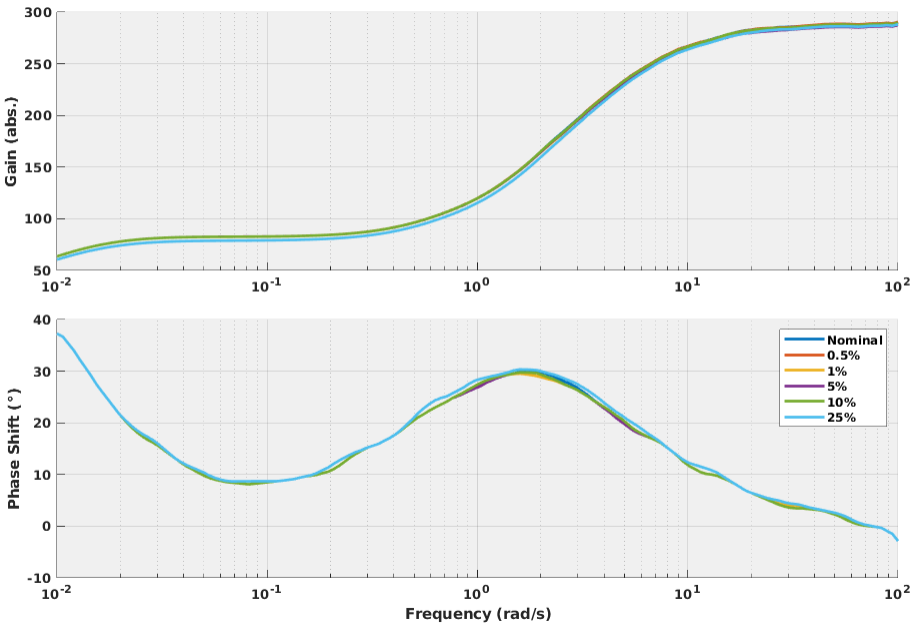

Figure 6.12: The frequency response of a FSMSR with different levels of plutonium removed.

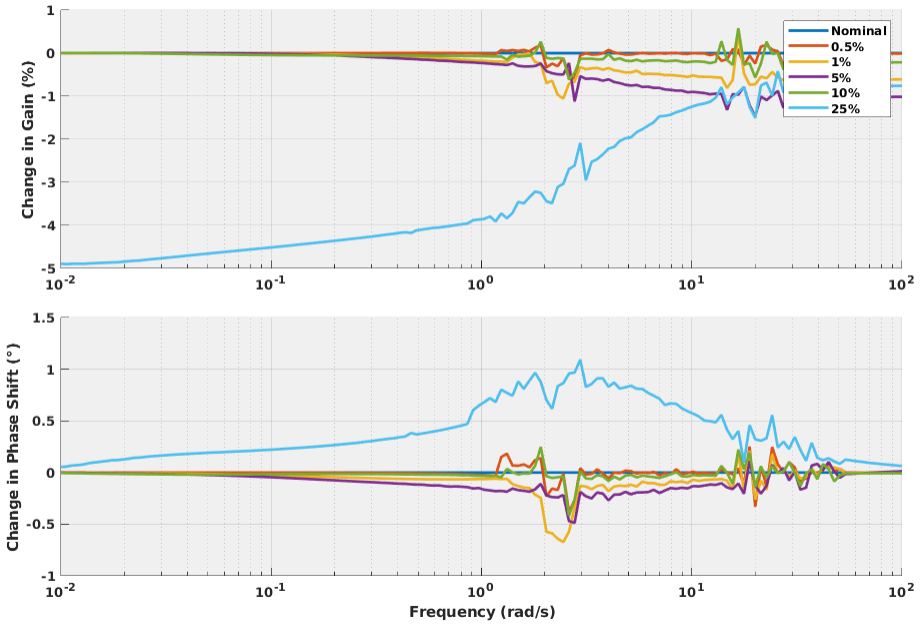

Figure 6.13: The relative change in the frequency response of a FSMSR due to plutonium diversion of increasing amounts.

thermal MSRs, which are generally more sensitive to such perturbations. The relatively low sensitivity to plutonium diversion in this reactor design suggests that the frequency response may not be the best signature to use for safeguards in an FSMSR.

Chapter 7

Conclusions

This study explored the utility of frequency analysis as a tool for detecting the diversion of plutonium in MSRs. Firstly, it was determined that this methodology is well suited for SMR sized, thermal MSRs. The sensitivity observed in the thermal MSR suggests frequency response may be useful for a safeguarding regime as a signature. In contrast, FSMSRs showed reduced sensitivity in their frequency response, primarily due to their larger fuel salt volume requirements for achieving criticality. However, even when accounting for percentage diversion cases, FSMSRs appear to have diminished responsiveness to plutonium removal.

This study revealed that frequency response is a valuable method for tracking burnup in both reactor systems. Additionally, the study found that the removal of plutonium does not entirely reverse changes in the frequency response as previously anticipated. Some alterations persist due to residual fission products, indicating complex interactions within the reactor environment that merit further exploration.

While this research establishes an approach for evaluating frequency responses to detect potential plutonium diversion, it also highlights areas for future research. Further work is needed to refine these methods and explore additional variables that could affect frequency response in a nuclear reactor.

In summary, the findings suggest that frequency analysis offers a promising avenue for enhancing the security and operational oversight of MSRs. Continued research will be vital to fully harness this technique's potential and address remaining questions about its application across different reactor types.

7.1 Future Work and Considerations

7.1.1 Detector Systems

This study has explored the frequency response of two distinct MSRs as a potential signature of plutonium removal. However, it is essential to note that the results presented only show the theoretical behavior of the chain reaction to plutonium withdrawal and do not provide a method for detecting it. To utilize this signature for monitoring purposes, an appropriate detector system would need to be implemented. Furthermore, for international safeguards purposes, these detectors must also be independently operated by the IAEA to ensure reliability and accuracy.

For the MSRE, neutron population assessment has been conducted using external neutron detectors, which could also be employed here. However, a crucial aspect of utilizing this signature is ensuring that the reactivity transient is initiated independently from any control mechanisms. In the case of the MSRE, control rod movement is used to initiate analysis, but alternative methods would need to be explored. Previous studies have investigated devices in the reflector region for initiating reactivity transients, but these designs may not be compatible with the specific reactor configuration [83]. An external oscillator that could induce a sinusoidal reactivity insertion around the maximum point has been proposed and tested in this study. Each design, however, would need to evaluate whether such a device can be implemented without compromising reactor stability or safety.

7.1.2 Different Fuel Cycles

The term "Molten Salt Reactor" encompasses a vast design space, encompassing various fuel cycles and configurations. The MSRP, for example, initially aimed to develop a thorium breeder fuel cycle at ORNL. More recently, the MSR being built in the Gobi Desert is focused on utilizing thorium as its primary fuel.

Several companies are also exploring different fuel cycles that incorporate thorium, further expanding the design space of MSRs. It is essential to note that all these fuel cycles share a common challenge: producing U-233 from a chain reaction based on other fissile materials

like U-235. This is because there is only one stockpile of U-233 in the US, which is currently being disposed of.

Another common fuel cycle is the waste burning reactor, which aims to recycle and reprocess used nuclear fuel from the US's current stockpile of around 90,000 metric tons. In a waste burner reactor, some of the uranium, plutonium, and minor actinides from LWR used nuclear fuel are utilized as a fuel source. The resulting composition would feature heavier-than-uranium isotopes in higher proportions than typical reactors, while very heavy isotope concentrations may be increased. As commercialization draws near for MSRs, it is crucial to consider which reprocessing methods will be adopted.

New and inventive approaches to reprocessing for the fuel salt are being developed, and a commercially viable MSR is likely to employ one of these methods. As the market evolves, applying the methodology presented here to different fuel cycles could provide value.

7.1.3 Tailored Diversion Scenarios

This study assumes a step-reduction in plutonium concentration diversion scenario, which aligns with batch reprocessing approaches commonly employed in MSRs. However, MSRs utilize online reprocessing, thus allowing protracted material diversions, and early analysis indicates these scenarios should be more difficult to detect [70]. Despite this, the methodology can still be applied to model protracted losses so long as it is properly implemented into the fuel cycle calculation.

The study does not delve into the specifics of how plutonium is initially removed from the reactor, as the method of removal significantly influences the neutron effects. For instance, electrochemical reduction in a chloride-based system involves a specific order of reduction: noble/platinum metals first, followed by uranium, neptunium, and then plutonium. This sequence affects the neutronics, which must be explored. Fluoride systems, on the other hand, exhibit a different reduction order, with limited published information available. The actinide and fission products removed by fluoride/chloride volatility will have their own effects. Whichever method is deemed plausible, incorporating these effects could yield new signatures not captured in this study.

7.1.4 Effectiveness in Solid Fuel Reactors

Much of the traditional item counting methods, in the current safeguards, were developed with solid fuel in mind. In contrast, liquid fuel in MSRs requires innovative approaches to tracking actinide inventory, thus the as frequency analysis method for material accountability in this study. However, the frequency analysis is not limited to liquid-fueled reactors and could be applied to solid-fueled reactors as well.

In solid-fueled reactors that challenge current safeguarding methodologies, such as pebble-bed reactors with a multi-pass fuel cycle, the fuel is distributed among solid particles, which brings a spatial component to the removal of plutonium-bearing pebbles. Since MSRs have circulating fuel that mixes online, the concentration of plutonium or other special nuclear material in the fuel happens uniformly. In a pebble-bed reactor, a pebble may have lower or higher importance in the neutron chain, dependent on the placement in the core. Additionally, the weight would change as a pebble moves through the bed and thus have varying importance as the pebble moves through. These spatial aspects would represent a complicating factor that would need to be studied.

7.1.5 Neutron Noise

In this study, while focusing on the frequency response of MSRs to potential plutonium diversion, it is crucial to acknowledge that the presented neutronic model does not currently account for neutron noise, or the fluctuations in neutron counts that would be read by the detector. The overall level of noise present in the system significantly influences both expected error margins and measurement times.

Historically, some exploration into neutron noise has been conducted [62]; however, its behavior in MSRs presents challenges. The neutron noise within these reactors is intricately linked to various factors such as mechanical vibrations from components like molten salt pumps, which would need to be defined. However, the noise is also dependent on the neutronic parameters. A notable characteristic of liquid-fueled reactors is the presence of circulating delayed neutron precursors, which introduce distinctive behaviors into the neutron noise profile. This raises the question of whether or not a diversion of an SQ

of nuclear material affects the neutron noise. If so, it could potentially serve as a passive alternative or complement to frequency analysis for safeguarding purposes. This aspect opens up new avenues for research, suggesting that incorporating neutron noise considerations could enhance the precision and reliability of material accountancy methods in MSRs.

7.1.6 Transient Modeling

The methodology used for modeling the transient response was selected because it is a well-established approach that is both computationally efficient and capable of capturing changes in reactor neutronics. As discussed in Chapter 5, alternative methodologies could also be employed, provided they follow the framework outlined in this study. While different modeling techniques may offer unique advantages, the fundamental process remains the same.

A significant challenge for all these approaches is the lack of high-quality experimental data for validation. There are only a handful of frequency response data points from the MSRE that can be used for comparison. However, by modern standards, this data is insufficient for rigorous validation. For example, the Bode plots from the MSRE lack error bars, making it difficult to assess the reliability of the measurements. These data limitations inherently constrain the understanding of the validity of any modeling approach. The only viable solution to overcome this challenge is to construct and operate an MSR test reactor to generate high-fidelity experimental data, which could then be used to benchmark computational models.

Bibliography

[1] (1972). *The Structure and Content of Agreements Between the Agency and States Required in Connection with the Treaty on the Non-Proliferation of Nuclear Weapons, INFCIRC/153 (Corrected),*. International Atomic Energy Agency, Vienna. 7

[2] (1999). *Design Measures to Facilitate Implementation of Safeguards at Future Water Cooled Nuclear Power Plants*. Number 392 in Technical Reports Series. International Atomic Energy Agency, Vienna. xi, 7, 8, 9

[3] (2017). Molten salt chemistry workshop. Technical report, Oak Ridge National Lab., TN (United States). 43

[4] (2018). *Spent Fuel Heat Generation In An Independant Spent Fuel Storage Instalation*. U.S. Nuclear Regulatory Commission. 89

[5] (2019). *International Safeguards in the Design of Reprocessing Plants*. Number NF-T-3.2 in Nuclear Energy Series. International Atomic Energy Agency, Vienna. 10

[6] Abou-Jaoude, A., Harper, S., Giudicelli, G., Balestra, P., Schunert, S., Martin, N., Lindsay, A., Tano, M., and Freile, R. (2021). A workflow leveraging moose transient multiphysics simulations to evaluate the impact of thermophysical property uncertainties on molten-salt reactors. *Annals of Nuclear Energy*, 163:108546. 76, 80

[7] Andreades, C., Cisneros, A. T., Choi, J. K., Chong, A. Y., Fratoni, M., Hong, S., Huddar, L. R., Huff, K. D., Kendrick, J., Krumwiede, D. L., et al. (2016). Design summary of the mark-i pebble-bed, fluoride salt–cooled, high-temperature reactor commercial power plant. *Nuclear Technology*, 195(3):223–238. 3

[8] Ball, S. (1963). Approximate models for distributed-parameter heat-transfer systems. In *Joint Automatic Control Conference*, number 1, pages 131–139. 80

[9] Ball, S. and Kerlin, T. (1965). Stability analysis of the molten-salt reactor experiment. Technical Report ORNL-TM-1070, Oak Ridge National Lab., Tenn. 18, 30, 76, 79, 87

[10] Beddingfield, D. H. and Hori, M. (2007). Nuclear safeguards challenges at reactors types that defy traditional item counting. In *JAEA-IAEA Workshop on Advanced Safeguards Technology for the Future Nuclear Fuel Cycle, Tokaimura, Japan*, pages 13–16. 9, 30

[11] Bettis, E., Cottrell, W., Mann, E., Meem, J., and Whitman, G. (1957). The aircraft reactor experiment—operation. *Nuclear Science and Engineering*, 2(6):841–853. 3

[12] Bettis, E. S., Alexander, L. G., and Watts, H. L. (1972). Design studies of a molten-salt reactor demonstration plant. 36, 85

[13] Betzler, B. R., Powers, J. J., and Worrall, A. (2017). Molten salt reactor neutronics and fuel cycle modeling and simulation with scale. *Annals of Nuclear Energy*, 101:489–503. 33, 47

[14] Bjornard, T., Bean, R., Durst, P. C., Hockert, J., and Morgan, J. (2010). Implementing safeguards-by-design. Technical report, Idaho National Laboratory (INL). 4

[15] Blandford, E., Brumback, K., Fick, L., Gerardi, C., Haugh, B., Hillstrom, E., Johnson, K., Peterson, P. F., Rubio, F., Sarikurt, F. S., et al. (2020). Kairos power thermal hydraulics research and development. *Nuclear Engineering and Design*, 364:110636. 3

[16] Casteleyn, K., Duinslaeger, L., Celdrán, P. A., Arboré, P., Chare, P., Dahms, E., Drinnhausen, O., Eberle, H., Enright, T., Guiot, A., et al. (2010). The euratom safeguards on-site laboratories at the reprocessing plants of la hague and sellafield. *JRC Reference Report*. 11

[17] Cervi, E., Lorenzi, S., Cammi, A., and Luzzi, L. (2019). Development of a multiphysics model for the study of fuel compressibility effects in the molten salt fast reactor. *Chemical Engineering Science*, 193:379–393. 57, 76, 92

[18] Cervi, E., Lu, X., Cammi, A., Di Maio, F., and Zio, E. (2022). Sensitivity-analysis-driven surrogate model for molten salt reactors control. *Journal of Nuclear Engineering*, 3(4):277–294. 76

[19] Chen, A. T.-l. (1976). *A digital simulation for nuclear once-through steam generators*. PhD thesis, The University of Tennessee, Knoxville. 87

[20] Choe, J., Ivanova, M., LeBlanc, D., Mohaptra, S., and Robinson, R. (2018). Fuel cycle flexibility of terrestrial energy's integral molten salt reactor (imsr). In *38th Annual Conference of the Canadian Nuclear Society and 42nd Annual CNS/CNA Student Conference, Saskatoon, SK, Canada, June*, pages 3–6. 4, 33

[21] Cipiti, B. B., Durán, F. A., Key, B., Liu, Y., Lozano, I., and Ward, R. (2012). Modeling and design of integrated safeguards and security for an electrochemical reprocessing facility. *SAND2012-9303, Sandia National Laboratories*. 10

[22] Coble, J. B., Skutnik, S. E., Gilliam, S. N., and Cooper, M. P. (2020). Review of candidate techniques for material accountancy measurements in electrochemical separations facilities. *Nuclear Technology*, 206(12):1803–1826. 13

[23] Cochran, R. G. and Tsoulfanidis, N. (1990). *The Nuclear Fuel Cycle: Analysis and Management*. American Nuclear Society. 10

[24] Constable, C., Lindley, B., and Parks, G. (2021). Maximising discharge burnup in an open cycle molten salt reactor. In *EPJ Web of Conferences*, volume 247, page 12002. EDP Sciences. 33

[25] Dai, Z. and Liu, W. (2013). Thorium-based molten salt reactor (tmsr) project in china. In *Proceedings of the conference on molten salts in nuclear technology*. 4

[26] Degtyarev, A., Myasnikov, A., and Ponomarev, L. (2015). Molten salt fast reactor with u–pu fuel cycle. *Progress in Nuclear Energy*, 82:33–36. 34

[27] Dion, M., Worrall, L. G., Croft, S., and Scott, L. (2021). Molten salt reactor signatures and modeling study. Technical report, Oak Ridge National Lab.(ORNL), Oak Ridge, TN (United States). 14

[28] Duderstadt, J. J. and Hamilton, L. J. (1976). *Nuclear reactor analysis*. Wiley. 34

[29] Dunkle, N., Richardson, J., Pathirana, V., Wheeler, A., Chvala, O., and Skutnik, S. E. (2023). Nerthus thermal spectrum molten salt reactor neutronics and dynamic model. *Nuclear Engineering and Design*, 411:112390. xv, xvi, 36, 37, 39, 75, 86

[30] Eash-Gates, P., Klemun, M. M., Kavlak, G., McNerney, J., Buongiorno, J., and Trancik, J. E. (2020). Sources of cost overrun in nuclear power plant construction call for a new approach to engineering design. *Joule*, 4(11):2348–2373. 4

[31] Forsberg, C. W. and Moses, D. L. (2009). Safeguards challenges for pebble-bed reactors designed by people's republic of china. *Global Nuclear Security Technology Division, http://www. osti. gov/bridge*. 4, 9

[32] Gehin, J. C. and Powers, J. J. (2016). Liquid fuel molten salt reactors for thorium utilization. *Nuclear Technology*, 194(2):152–161. 43

[33] Greenwood, M. S., Betzler, B. R., and Qualls, A. L. (2018). Dynamic system models for informing licensing and safeguards investigations of molten salt reactors. Technical Report ORNL/TM-2018/876, Oak Ridge National Lab.(ORNL), Oak Ridge, TN (United States). 17

[34] Haubenreich, P. N. and Engel, J. (1970). Experience with the molten-salt reactor experiment. *Nuclear Applications and technology*, 8(2):118–136. 3, 85

[35] He, L.-Y., Li, G.-C., Xia, S.-P., Chen, J.-G., Zou, Y., and Liu, G.-M. (2020). Effect of ^{37}cl enrichment on neutrons in a molten chloride salt fast reactor. *Nuclear Science and Techniques*, 31(3):1–12. 46

[36] Hombourger, B., Krepel, J., and Pautz, A. (2019). Breed-and-burn fuel cycle in molten salt reactors. *EPJ Nuclear Sciences & Technologies*, 5(ARTICLE):15. 34, 47

[37] Hombourger, B. A. (2018). Conceptual design of a sustainable waste burning molten salt reactor. Technical report, EPFL. 4

[38] Huddar, L., Kendrick, J. C., Poresky, C., Wang, X., and Peterson, P. F. (2018). Application of frequency response methods in separate and integral effects tests for molten salt cooled and fueled reactors. *Nuclear Engineering and Design*, 329:3–11. 76

[39] Inoue, T. and Koch, L. (2008). Development of pyroprocessing and its future direction. *Nuclear Engineering and Technology*, 40(3):183–190. 12

[40] Irish, E. and Reas, W. H. (1957). *The Purex Process: a Solvent Extraction Reprocessing Method for Irradiated Uranium*. Hanford Atomic Products Operation. 10

[41] Ishiguro, T., Van Rooijen, W., Shimazu, Y., and Mochizuki, H. (2014). Design of a passive residual heat removal system for the fuji-233um molten salt reactor system. *Annals of Nuclear Energy*, 64:398–407. 4

[42] Janz, G. J., Tomkins, R., Allen, C., Downey Jr, J., Garner, G., Krebs, U., and Singer, S. K. (1975). Molten salts: Volume 4, part 2, chlorides and mixtures—electrical conductance, density, viscosity, and surface tension data. *Journal of Physical and Chemical Reference Data*, 4(4):871–1178. 46

[43] Johnson, S. J. and Ehinger, M. (2010). Designing and operating for safeguards: Lessons learned from the rokkasho reprocessing plant (rrp). Technical report, Pacific Northwest National Lab.(PNNL), Richland, WA (United States). 11

[44] Jorgensen, L. (2017). Thorcon reactor. In *Molten Salt Reactors and Thorium Energy*, pages 557–564. Elsevier. 4

[45] Kane, C. and Pomper, M. A. (2014). Reactor race: South korea's nuclear export successes and challenges. *On Korea*, page 63. 3

[46] Kerlin, T. (1974). *Frequency response testing in nuclear reactors*, volume 11. Elsevier. 18, 75

[47] Kerlin, T., Ball, S., and Steffy, R. (1971). Theoretical dynamics analysis of the molten-salt reactor experiment. *Nuclear Technology*, 10(2):118–132. 75, 76, 77

[48] Kessler, G., Broeders, C., Hoebel, W., Goel, B., and Wilhelm, D. (2008). A new scientific solution for preventing the misuse of reactor-grade plutonium as nuclear explosive. *Nuclear Engineering and Design*, 238(12):3429–3444. 65

[49] Konomura, M. and Ichimiya, M. (2007). Design challenges for sodium cooled fast reactors. *Journal of Nuclear Materials*, 371(1-3):250–269. 76

[50] Lee, K., Jessee, M., Collins, B., Taylor, Z., and Graham, A. (2022). Transient convective delayed neutron precursors of 235u for the molten salt reactor experiment. Technical report, Oak Ridge National Lab.(ORNL), Oak Ridge, TN (United States). 80

[51] Leppänen, J., Pusa, M., Viitanen, T., Valtavirta, V., and Kaltiaisenaho, T. (2014). The serpent monte carlo code: Status, development and applications in 2013. In *SNA+ MC 2013-Joint International Conference on Supercomputing in Nuclear Applications+ Monte Carlo*, page 06021. EDP Sciences. 18, 19, 36

[52] Lopez-Solis, R. and François, J.-L. (2018). The breed and burn nuclear reactor: a chronological, conceptual, and technological review. *International Journal of Energy Research*, 42(3):953–965. 34

[53] MacPherson, H. (1985). The molten salt reactor adventure. *Nuclear Science and engineering*, 90(4):374–380. 3

[54] Martin, M., Aufiero, M., Greenspan, E., and Fratoni, M. (2017). Feasibility of a breed-and-burn molten salt reactor. *Transactions of the American Nuclear Society*, 116. 34

[55] Merk, B., Detkina, A., Atkinson, S., Litskevich, D., and Cartland-Glover, G. (2019). Evaluation of the breeding performance of a nacl-ucl-based reactor system. *Energies*, 12(20):3853. 47

[56] Merle-Lucotte, E., Heuer, D., Allibert, M., Brovchenko, M., Capellan, N., and Ghetta, V. (2011). Launching the thorium fuel cycle with the molten salt fast reactor. In *Proceedings of ICAPP*, pages 2–5. 4

[57] Moser, D., Wheeler, A., and Chvála, O. (2017). Lattice optimization for graphite moderated molten salt reactors using low-enriched uranium fuel. *Annals of Nuclear Energy*, 110:1–10. 33

[58] Mourogov, A. and Bokov, P. (2006). Potentialities of the fast spectrum molten salt reactor concept: Rebus-3700. *Energy conversion and management*, 47(17):2761–2771. 46

[59] Oak Ridge National Laboratory (2021). 2021 Virtual Molten Salt Reactor Workshop. 46

[60] Ottmar, H., Eberle, H., et al. (1991). *The Hybrid K-edge/K-XRF Densitometer: Principles-Design-Performance*. Citeseer. 11

[61] Pathirana, V., Chvala, O., and Wheeler, A. M. (2021). Scalable modular dynamic molten salt reactor system model with decay heat. *Annals of Nuclear Energy*, 154:108060. 75, 77, 87, 89

[62] Pázsit, I. and Jonsson, A. (2011). Reactor kinetics, dynamic response, and neutron noise in molten salt reactors. *Nuclear Science and Engineering*, 167(1):61–76. 112

[63] Poresky, C. (2017). Frequency response testing in the ciet facility. *Berkeley, CA*. 16, 76

[64] Ridley, G. and Chvala, O. (2017). A method for predicting fuel maintenance in once-through msrs. *Annals of Nuclear Energy*, 110:265–281. 20

[65] Robertson, R. C. (1971). Conceptual design study of a single-fluid molten-salt breeder reactor. Technical report, comp.; Oak Ridge National Lab., Tenn. 4, 43

[66] Rouch, H., Geoffroy, O., Rubiolo, P., Laureau, A., Brovchenko, M., Heuer, D., and Merle-Lucotte, E. (2014). Preliminary thermal–hydraulic core design of the molten salt fast reactor (msfr). *Annals of Nuclear Energy*, 64:449–456. 94

[67] Rykhlevskii, A., Betzler, B. R., Worrall, A., and Huff, K. D. (2019). Fuel cycle performance of fast spectrum molten salt reactor designs. Technical report, Oak Ridge National Lab.(ORNL), Oak Ridge, TN (United States). 47

[68] Scott, I., Abram, T., and Negri, O. (2015). Stable salt reactor design concept. In *Proceedings of the International Thorium Energy Conference: Gateway to Thorium Energy*. 4

[69] Seifert, L., Wheeler, A., and Chvala, O. (2021). Material Flows and On-line Reprocessing in Serpent (technical report). Technical report, University of Tennessee at Knoxville. 43

[70] Shoman, N. and Moosir, P. M. (2023). Novel strategies for safeguarding molten salt reactors. Technical report, Sandia National Lab., Albuquerque, NM (United States). 111

[71] Simpson, M. F. (2012). Developments of spent nuclear fuel pyroprocessing technology at idaho national laboratory. 12

[72] Singh, V. (2019). Study of the dynamic behavior of molten-salt reactors. Master's thesis, University of Tennessee, Knoxville. 19

[73] Singh, V., Lish, M. R., Wheeler, A. M., Chvála, O., and Upadhyaya, B. R. (2018a). Dynamic modeling and performance analysis of a two-fluid molten-salt breeder reactor system. *Nuclear Technology*, 202(1):15–38. 17

[74] Singh, V., Wheeler, A. M., Lish, M. R., Chvála, O., and Upadhyaya, B. R. (2018b). Nonlinear dynamic model of molten-salt reactor experiment–validation and operational analysis. *Annals of Nuclear Energy*, 113:177–193. 17, 18, 75, 77, 80

[75] Singh, V., Wheeler, A. M., Upadhyaya, B. R., Chvála, O., and Greenwood, M. S. (2020). Plant-level dynamic modeling of a commercial-scale molten salt reactor system. *Nuclear Engineering and Design*, 360:110457. xvi, 17, 75, 77, 87, 88

[76] Sowder, A. (2015). Program on technology innovation: Technology assessment of a molten salt reactor design—the liquid-fluoride thorium reactor (lftr). *Electric Power Research Institute*. 4

[77] Steffy, Jr., R. C. (1970). Experimental dynamic analysis of the msre with u-233 fuel. 76

[78] Steffy Jr, R. (1970). Frequency-response testing of the molten-salt reactor experiment. Technical report, Oak Ridge National Lab.(ORNL), Oak Ridge, TN (United States). 76

[79] Tenchine, D. (2010). Some thermal hydraulic challenges in sodium cooled fast reactors. *Nuclear Engineering and Design*, 240(5):1195–1217. 76

[80] Van Valkenburg, M. (1984). In memoriam: Hendrik w. bode (1905-1982). *IEEE Transactions on Automatic Control*, 29(3):193–194. 18, 30

[81] Wheeler, A. M. (2022). Dissertation repository. 36, 95

[82] Wheeler, A. M. and Chvála, O. (2021a). Molten salt reactor sourdough refueling and waste management strategy. *Journal of Nuclear Engineering*, 2(4):471–483. 33, 36, 43

[83] Wheeler, A. M. and Chvála, O. (2021b). Online monitoring of plutonium concentration via frequency analysis. *Proceedings of the INMM ESARDA Joint Virtual Annual Meeting*. 110

[84] Wheeler, A. M. and Chvála, O. (SUBMITTED). Neutronics for fast spectrum, molten salt reactors and evolution over burnup. *Progress in Nuclear Energy*. 34, 45, 46

[85] Wheeler, A. M., Chvála, O., and Skutnik, S. (2021). Signatures of plutonium diversion in molten salt reactor dynamics. *Annals of Nuclear Energy*, 160:108370. 17

[86] Williams, D. (2006). Assessment of candidate molten salt coolants for the ngnp/nhi heat-transfer loop. Technical report, Oak Ridge National Lab.(ORNL), Oak Ridge, TN (United States). 41

[87] Williamson, M. A. and Willit, J. (2019). Synthesis of molten chloride salt fast reactor fuel salt from spent nuclear fuel. Technical report, Argonne National Lab.(ANL), Argonne, IL (United States). 4

[88] Woo, S. M., Chirayath, S. S., and Fuhrmann, M. (2020). Nuclear fuel reprocessing: Can pyro-processing reduce nuclear proliferation risk? *Energy Policy*, 144:111601. 12

[89] Wooten, D. and Powers, J. J. (2018). A review of molten salt reactor kinetics models. *Nuclear Science and Engineering*, 191(3):203–230. 76

[90] Worrall, A., Betzler, B. R., Flanagan, G., Holcomb, D. E., Hu, J., Kovacic, D. N., Qualls, A. L., and Worrall, L. G. (2018). Molten salt reactors and associated safeguards challenges and opportunities. Technical report, Oak Ridge National Lab.(ORNL), Oak Ridge, TN (United States). 14

[91] Worrall, L. G., Worrall, A., Flanagan, G. F., Croft, S., Krichinsky, A. M., Pickett, C. A., McElroy Jr, R. D., Cleveland, S. L., Kovacic, D. N., Whitaker, J. M., et al. (2016). Safeguards considerations for thorium fuel cycles. *Nuclear Technology*, 194(2):281–293. 14

[92] Yu, C., Li, X., Cai, X., Zou, C., Ma, Y., Han, J., and Chen, J. (2015). Analysis of minor actinides transmutation for a molten salt fast reactor. *Annals of Nuclear Energy*, 85:597–604. 4

[93] Zhang, H., Choi, S., Zhang, C., Faulkner, E., Alnajjar, N., Okabe, P., Horvath, D. C., and Simpson, M. F. (2019). Square wave voltammetry for real time analysis of minor metal ion concentrations in molten salt reactor fuel. *Journal of Nuclear Materials*, 527:151791. 15

[94] Zhu, G., Zou, Y., Yan, R., Tan, M., Zou, C., Kang, X., Chen, J., Guo, W., and Dai, Y. (2019). Low enriched uranium and thorium fuel utilization under once-through and offline reprocessing scenarios in small modular molten salt reactor. *International Journal of Energy Research*, 43(11):5775–5787. 33

Appendices

A Plutonium Diversion Neutronic Parameters

A.1 Thermal MSR with Only Pure Pu Diversion

Diversion of super grade plutonium at 23.2 full powered days

Table A1: Change in reactor parameters when a SQ of plutonium is removed from a thermal MSR after a burnup of 0.316 GWd/MTHM (23.2 full power days).

	Nominal	Diversion	Change
k_{eff}	1.00624±0.00032	0.99448±0.00034	-1169 pcm
β_{eff}	0.00618±0.00005	0.00653±0.00006	5.63%
Λ	6.663e-04±8.3e-07	7.124e-04±8.3e-07	6.92%
I-135 yield	0.0631±0.0000	0.0629±0.0000	-0.23%
Xe-135 yield	0.0031±0.0000	0.0027±0.0000	-14.32%
Pm-149 yield	0.0110±0.0000	0.0109±0.0000	-0.68%
Xe ρ (pcm)	3.76±0.38	4.51±0.38	20.01%
Sm ρ (pcm)	728±5	770±5	5.86%

Table A2: Change in the six group effective delayed neutron fraction parameters when a SQ of plutonium is removed from a thermal MSR after a burnup of 0.316 GWd/MTHM (23.2 full power days).

Group		Nominal	Diversion	Change
1	β_1	0.000186±0.000009	0.000186±0.000009	11.81%
	λ_1	0.0125±0.0000	0.0125±0.0000	-
2	β_2	0.001036±0.000024	0.001078±0.000023	4.10%
	λ_2	0.0317±0.0000	0.0318±0.0000	-
3	β_3	0.000974±0.000022	0.001049±0.000023	7.76%
	λ_3	0.1095±0.0000	0.1095±0.0000	-
4	β_4	0.002847±0.000040	0.002998±0.000037	5.32%
	λ_4	0.3177±0.0001	0.3176±0.0001	-
5	β_5	0.000851±0.000019	0.000890±0.000021	4.60%
	λ_5	1.3521±0.0002	1.3523±0.0002	-
6	β_6	0.000285±0.000012	0.000303±0.000013	6.12%
	λ_6	8.7140±0.0164	8.6722±0.0085	-0.04%

Diversion of weapons grade plutonium at 65 full powered days

Table A3: Change in reactor parameters when a SQ of plutonium is removed from a thermal MSR after a burnup of 0.8867 GWd/MTHM (65 full power days).

	Nominal	**Diversion**	**Change**
k_{eff}	1.01773±0.00034	1.01108±0.00034	-653 pcm
β_{eff}	0.00576±0.00006	0.00592±0.00005	2.78%
Λ	5.990e-04±7.4e-07	6.256e-04±8.3e-07	4.45%
I-135 yield	0.0633±0.0000	0.0632±0.0000	-0.17%
Xe-135 yield	0.0039±0.0000	0.0036±0.0000	-8.49%
Pm-149 yield	0.0111±0.0000	0.0111±0.0000	-
Xe ρ (pcm)	3.29±0.34	4.01±0.38	22.10%
Sm ρ (pcm)	763±5	805±5	5.42%

Table A4: Change in the six group effective delayed neutron fraction parameters when a SQ of plutonium is removed from a thermal MSR after a burnup of 0.8867 GWd/MTHM (65 full power days).

Group		**Nominal**	**Diversion**	**Change**
1	β_1	0.000157±0.000010	0.000193±0.000011	22.75%
	λ_1	0.0125±0.0000	0.0125±0.0000	-
2	β_2	0.000956±0.000023	0.001026±0.000021	7.34%
	λ_2	0.0316±0.0000	0.0316±0.0000	-
3	β_3	0.000989±0.000021	0.000986±0.000022	-
	λ_3	0.1094±0.0000	0.1094±0.0000	-
4	β_4	0.002652±0.000036	0.002668±0.000033	-
	λ_4	0.3177±0.0001	0.3177±0.0001	-
5	β_5	0.000744±0.000019	0.000782±0.000020	5.03%
	λ_5	1.3514±0.0006	1.3521±0.0003	-
6	β_6	0.000264±0.000012	0.000268±0.000012	-
	λ_6	8.6863±0.0239	8.7112±0.0168	-0.03%

Diversion of fuel grade plutonium at 114 full powered days

Table A5: Change in reactor parameters when a SQ of plutonium is removed from a thermal MSR after a burnup of 1.5527 GWd/MTHM (114 full power days).

	Nominal	**Diversion**	**Change**
k_{eff}	1.02253±0.00035	1.01737±0.00032	-505 pcm
β_{eff}	0.00540±0.00005	0.00548±0.00006	1.53%
Λ	5.461e-04±8.1e-07	5.702e-04±7.6e-07	4.41%
I-135 yield	0.0635±0.0000	0.0635±0.0000	-
Xe-135 yield	0.0045±0.0000	0.0042±0.0000	-5.77%
Pm-149 yield	0.0112±0.0000	0.0112±0.0000	-
Xe ρ (pcm)	3.31±0.33	3.62±0.38	9.31%
Sm ρ (pcm)	785±5	825±5	5.15%

Table A6: Change in the six group effective delayed neutron fraction parameters when a SQ of plutonium is removed from a thermal MSR after a burnup of 1.5527 GWd/MTHM (114 full power days).

Group		**Nominal**	**Diversion**	**Change**
1	β_1	0.000159±0.000009	0.000182±0.000009	14.73%
	λ_1	0.0125±0.0000	0.0125±0.0000	-
2	β_2	0.000935±0.000023	0.000971±0.000024	3.82%
	λ_2	0.0315±0.0000	0.0315±0.0000	-
3	β_3	0.000913±0.000023	0.000887±0.000021	-2.86%
	λ_3	0.1093±0.0000	0.1093±0.0000	-
4	β_4	0.002449±0.000035	0.002473±0.000037	-
	λ_4	0.3179±0.0001	0.3179±0.0001	-
5	β_5	0.000708±0.000011	0.000734±0.000019	3.60%
	λ_5	1.3486±0.0011	1.3494±0.0009	-
6	β_6	0.000232±0.000011	0.000232±0.000011	-
	λ_6	8.7746±0.0409	8.7197±0.0333	-0.055%

Diversion of reactor grade plutonium at 366 full powered days

Table A7: Change in reactor parameters when a SQ of plutonium is removed from a thermal MSR after a burnup of 4.9777 GWd/MTHM (366 full power days).

	Nominal	**Diversion**	**Change**
k_{eff}	1.01394±0.00032	1.01365±0.00035	-
β_{eff}	0.00484±0.00005	0.00500±0.00005	3.21%
Λ	4.417e-04±6.4e-07	4.522e-04±6.8e-07	2.36%
I-135 yield	0.0640±0.0000	0.0640±0.0000	-
Xe-135 yield	0.0054±0.0000	0.0042±0.0000	-2.45%
Pm-149 yield	0.0115±0.0000	0.0114±0.0000	-
Xe ρ (pcm)	2.01±0.25	2.31±0.27	15.03%
Sm ρ (pcm)	839±6	866±5	3.16%

Table A8: Change in the six group effective delayed neutron fraction parameters when a SQ of plutonium is removed from a thermal MSR after a burnup of 4.9777 GWd/MTHM (366 full power days).

Group		**Nominal**	**Diversion**	**Change**
1	β_1	0.000147±0.000010	0.000157±0.000010	7.18%
	λ_1	0.0125±0.0000	0.0125±0.0000	-
2	β_2	0.000878±0.000021	0.000939±0.000024	7.01%
	λ_2	0.0312±0.0000	0.0313±0.0000	-
3	β_3	0.000825±0.000020	0.000803±0.000020	-2.77%
	λ_3	0.1093±0.0001	0.1093±0.0001	-
4	β_4	0.002097±0.000036	0.002218±0.000031	5.76%
	λ_4	0.3177±0.0001	0.3177±0.0001	-
5	β_5	0.000673±0.000018	0.000668±0.000016	-
	λ_5	1.3258±0.0032	1.3345±0.0028	-
6	β_6	0.000224±0.000010	0.000215±0.000010	-
	λ_6	8.5862±0.0784	8.6522±0.0671	-

Diversion of steady state plutonium at 2368 full powered days

Table A9: Change in reactor parameters when a SQ of plutonium is removed from a thermal MSR after a burnup of 32.1878 GWd/MTHM (2368 full power days).

	Nominal	Diversion	Change
k_{eff}	1.00407±0.00033	1.00548±0.00035	140 pcm
β_{eff}	0.00486±0.00005	0.00477±0.00005	-2.02%
Λ	2.994e-04±5.9e-07	3.010e-04±6.0e-07	0.55%
I-135 yield	0.0645±0.0000	0.0645±0.0000	-
Xe-135 yield	0.0054±0.0000	0.0054±0.0000	-5.77%
Pm-149 yield	0.0118±0.0000	0.0117±0.0000	-
Xe ρ (pcm)	0.5±0.14	0.7±0.16	40.00%
Sm ρ (pcm)	897±6	928±5	3.37%

Table A10: Change in the six group effective delayed neutron fraction parameters when a SQ of plutonium is removed from a thermal MSR after a burnup of 32.1878 GWd/MTHM (2368 full power days).

Group		Nominal	Diversion	Change
1	β_1	0.000156±0.000009	0.000145±0.000008	-6.64%
	λ_1	0.0126±0.0000	0.0126±0.0000	-
2	β_2	0.000920±0.000022	0.000922±0.000023	-
	λ_2	0.0310±0.0000	0.0310±0.0000	-
3	β_3	0.000798±0.000021	0.000732±0.000020	-8.24%
	λ_3	0.1099±0.0001	0.1098±0.0001	-
4	β_4	0.002078±0.000034	0.002081±0.000036	-
	λ_4	0.3169±0.0001	0.3169±0.0000	-
5	β_5	0.000684±0.000019	0.000663±0.000019	-2.99%
	λ_5	1.2605±0.0059	1.2653±0.0056	-
6	β_6	0.000228±0.000011	0.000221±0.000012	-
	λ_6	7.8618±0.1342	7.4338±0.1484	-0.43%

A.2 Thermal MSR with Pure Pu Diversion and Refuel Uranium to Make Up Reactivity

Diversion of super grade plutonium at 23.2 full powered days

Table A11: Change in reactor parameters when a SQ of plutonium is removed and makeup uranium is added to a thermal MSR after a burnup of 0.316 GWd/MTHM (23.2 full power days).

	Nominal	Diversion	Change
k_{eff}	1.00624±0.00032	1.00516±0.00033	-107 pcm
β_{eff}	0.00618±0.00005	0.00660±0.00006	6.74%
Λ	6.663e-04±8.3e-07	6.847e-04±8.1e-07	2.76%
I-135 yield	0.0631±0.0000	0.0629±0.0000	-0.23%
Xe-135 yield	0.0031±0.0000	0.0027±0.0000	-14.48%
Pm-149 yield	0.0110±0.0000	0.0109±0.0000	-0.69%
Xe ρ (pcm)	3.76±0.38	3.98±0.36	5.96%
Sm ρ (pcm)	728±5	760±5	4.38%

Table A12: Change in the six group effective delayed neutron fraction parameters when a SQ of plutonium is removed and makeup uranium is added to a thermal MSR after a burnup of 0.316 GWd/MTHM (23.2 full power days).

Group		Nominal	Diversion	Change
1	β_1	0.000186±0.000009	0.000194±0.000011	4.42%
	λ_1	0.0125±0.0000	0.0125±0.0000	-
2	β_2	0.001036±0.000024	0.001089±0.000023	5.12%
	λ_2	0.0317±0.0000	0.0318±0.0000	-
3	β_3	0.000974±0.000022	0.001119±0.000025	14.89%
	λ_3	0.1095±0.0000	0.1095±0.0000	-
4	β_4	0.002847±0.000040	0.002987±0.000036	4.92%
	λ_4	0.3177±0.0001	0.3176±0.0001	-
5	β_5	0.000851±0.000019	0.000900±0.000021	5.76%
	λ_5	1.3521±0.0002	1.3524±0.0002	-
6	β_6	0.000285±0.000012	0.000303±0.000013	7.36%
	λ_6	8.7140±0.0164	8.6863±0.0117	-0.03%

Diversion of weapons grade plutonium at 65 full powered days

Table A13: Change in reactor parameters when a SQ of plutonium is removed and makeup uranium is added to a thermal MSR after a burnup of 0.8867 GWd/MTHM (65 full power days).

	Nominal	Diversion	Change
k_{eff}	1.01773±0.00034	1.01571±0.00035	-198 pcm
β_{eff}	0.00576±0.00006	0.00594±0.00006	3.01%
Λ	5.990e-04±7.4e-07	6.160e-04±7.8e-07	2.85%
I-135 yield	0.0633±0.0000	0.0632±0.0000	-0.18%
Xe-135 yield	0.0039±0.0000	0.0036±0.0000	-9.00%
Pm-149 yield	0.0111±0.0000	0.0111±0.0000	-0.54%
Xe ρ (pcm)	3.29±0.34	4.72±0.32	13.34%
Sm ρ (pcm)	763±5	801±5	4.89%

Table A14: Change in the six group effective delayed neutron fraction parameters when a SQ of plutonium is removed and makeup uranium is added to a thermal MSR after a burnup of 0.8867 GWd/MTHM (65 full power days).

Group		Nominal	Diversion	Change
1	β_1	0.000157±0.000010	0.000197±0.000009	25.44%
	λ_1	0.0125±0.0000	0.0125±0.0000	-
2	β_2	0.000956±0.000023	0.001019±0.000023	6.62%
	λ_2	0.0316±0.0000	0.0316±0.0000	-
3	β_3	0.000989±0.000021	0.000925±0.000022	-6.48%
	λ_3	0.1094±0.0000	0.1093±0.0000	-
4	β_4	0.002652±0.000036	0.002668±0.000033	-
	λ_4	0.3177±0.0001	0.3177±0.0001	-
5	β_5	0.000744±0.000019	0.000805±0.000021	8.12%
	λ_5	1.3514±0.0006	1.3521±0.0003	-
6	β_6	0.000264±0.000012	0.000286±0.000014	8.19%
	λ_6	8.6863±0.0239	8.7049±0.0143	0.02%

Diversion of fuel grade plutonium at 114 full powered days

Table A15: Change in reactor parameters when a SQ of plutonium is removed and makeup uranium is added to a thermal MSR after a burnup of 1.5527 GWd/MTHM (114 full power days).

	Nominal	Diversion	Change
k_{eff}	1.02253±0.00035	1.02144±0.00034	-107 pcm
β_{eff}	0.00540±0.00005	0.00561±0.00005	3.93%
Λ	5.461e-04±8.1e-07	5.618e-04±6.7e-07	2.87%
I-135 yield	0.0635±0.0000	0.0634±0.0000	-
Xe-135 yield	0.0045±0.0000	0.0042±0.0000	-6.42%
Pm-149 yield	0.0112±0.0000	0.0112±0.0000	-
Xe ρ (pcm)	3.31±0.33	3.08±0.32	-
Sm ρ (pcm)	785±5	819±6	4.36%

Table A16: Change in the six group effective delayed neutron fraction parameters when a SQ of plutonium is removed and makeup uranium is added to a thermal MSR after a burnup of 1.5527 GWd/MTHM (114 full power days).

Group		Nominal	Diversion	Change
1	β_1	0.000159±0.000009	0.000166±0.000098	4.43%
	λ_1	0.0125±0.0000	0.0125±0.0000	-
2	β_2	0.000935±0.000023	0.000974±0.000024	4.13%
	λ_2	0.0315±0.0000	0.0315±0.0000	-
3	β_3	0.000913±0.000023	0.000887±0.000021	1.23%
	λ_3	0.1093±0.0000	0.1093±0.0000	-
4	β_4	0.002449±0.000035	0.002524±0.000037	3.07%
	λ_4	0.3179±0.0001	0.3177±0.0001	-
5	β_5	0.000708±0.000011	0.000773±0.000019	9.21%
	λ_5	1.3486±0.0011	1.3490±0.0000	-
6	β_6	0.000232±0.000011	0.000247±0.000011	6.43%
	λ_6	8.7746±0.0409	8.7336±0.0232	-

A.3 Fast Spectrum MSR with Increasing Amounts of Plutonium Diverted (2.67 GWd/MTHM - 366 full power days)

Diversion of 0.5% of super grade plutonium around 1 full power year

Table A17: Change in reactor parameters when 0.5% of plutonium (4.8 kg) is removed from an FSMSR after a burnup of 2.67 GWd/MTHM (366 full power days).

	Nominal	Diversion	Change
k_{eff}	1.00460±0.00015	1.00465±0.00015	-
β_{eff}	0.00695±0.00004	0.00699±0.00004	-
Λ	1.261e-06±2.0e-09	1.262e-06±1.8e-09	-
Pm-149 yield	0.0106±0.0000	0.0106±0.0000	-
Sm ρ (pcm)	24±1	24±1	-
Feedback$_{Dop}$ (pcm/°C)	-0.98±0.25	-0.93±0.45	-
Feedback$_{Void}$ (pcm/°C)	-12.68±0.54	-12.26±0.34	-

Table A18: Change in the eight group effective delayed neutron fraction parameters when 0.5% of plutonium (4.8 kg) is removed from an FSMSR after a burnup of 2.67 GWd/MTHM (366 full power days).

Group		Nominal	Diversion	Change
1	β_1	0.000184±0.000007	0.000189±0.00007	-
	λ_1	0.0125±0.0000	0.0125±0.0000	-
2	β_2	0.000960±0.000014	0.000971±0.000014	-
	λ_2	0.0283±0.0000	0.0283±0.0000	-
3	β_3	0.000554±0.000012	0.000564±0.000012	-
	λ_3	0.0425±0.0000	0.0425±0.0000	-
4	β_4	0.001264±0.000016	0.001263±0.000017	-
	λ_4	0.1330±0.0000	0.1330±0.0001	-
5	β_5	0.002121±0.000021	0.002121±0.000021	-
	λ_5	0.2925±0.0000	0.2925±0.0001	-
6	β_6	0.000850±0.000012	0.000848±0.000013	-
	λ_6	0.6665±0.0000	0.6665±0.0001	-
7	β_7	0.000667±0.000016	0.000686±0.000012	2.78%
	λ_7	1.6348±0.0000	1.6348±0.0001	-
8	β_8	0.000316±0.000011	0.000322±0.000008	-
	λ_8	3.5546±0.0000	3.5546±0.0000	-

Diversion of 1% of super grade plutonium around 1 full power year

Table A19: Change in reactor parameters when 1% of plutonium (9.6 kg) is removed from an FSMSR after a burnup of 2.67 GWd/MTHM (366 full power days).

	Nominal	Diversion	Change
k_{eff}	1.00460±0.00015	1.00455±0.00015	-
β_{eff}	0.00695±0.00004	0.00693±0.00004	-
Λ	1.261e-06±2.0e-09	1.256e-06±1.8e-09	-0.40%
Pm-149 yield	0.0106±0.0000	0.0106±0.0000	-
Sm ρ (pcm)	24±1	24±1	-
Feedback$_{Dop}$ (pcm/°C)	-0.98±0.25	-0.91±0.34	-
Feedback$_{Void}$ (pcm/°C)	-12.68±0.54	-12.23±0.30	-

Table A20: Change in the eight group effective delayed neutron fraction parameters when 1% of plutonium (9.6 kg) is removed from an FSMSR after a burnup of 2.67 GWd/MTHM (366 full power days).

Group		Nominal	Diversion	Change
1	β_1	0.000184±0.000007	0.000180±0.00006	-
	λ_1	0.0125±0.0000	0.0125±0.0000	-
2	β_2	0.000960±0.000014	0.000947±0.000015	-
	λ_2	0.0283±0.0000	0.0283±0.0000	-
3	β_3	0.000554±0.000012	0.000556±0.000012	-
	λ_3	0.0425±0.0000	0.0425±0.0000	-
4	β_4	0.001264±0.000016	0.001267±0.000015	-
	λ_4	0.1330±0.0000	0.1330±0.0001	-
5	β_5	0.002121±0.000021	0.002157±0.000021	1.72%
	λ_5	0.2925±0.0000	0.2925±0.0001	-
6	β_6	0.000850±0.000012	0.000857±0.000013	-
	λ_6	0.6665±0.0000	0.6665±0.0000	-
7	β_7	0.000667±0.000016	0.000678±0.000012	-
	λ_7	1.6348±0.0000	1.6348±0.0001	-
8	β_8	0.000316±0.000011	0.000292±0.000008	-7.47%
	λ_8	3.5546±0.0000	3.5546±0.0000	-

Diversion of 5% of super grade plutonium around 1 full power year

Table A21: Change in reactor parameters when 5% of plutonium (48.2 kg) is removed from an FSMSR after a burnup of 2.67 GWd/MTHM (366 full power days).

	Nominal	**Diversion**	**Change**
k_{eff}	1.00460±0.00015	1.00362±0.00015	-98
β_{eff}	0.00695±0.00004	0.00699±0.00004	-
Λ	1.261e-06±2.0e-09	1.256e-06±2.0e-09	-0.32%
Pm-149 yield	0.0106±0.0000	0.0106±0.0000	-
Sm ρ (pcm)	24±1	25±1	2.80%
Feedback$_{Dop}$ (pcm/°C)	-0.98±0.25	-0.94±0.23	-
Feedback$_{Void}$ (pcm/°C)	-12.68±0.54	-12.85±0.25	-

Table A22: Change in the eight group effective delayed neutron fraction parameters when 5% of plutonium (48.2 kg) is removed from an FSMSR after a burnup of 2.67 GWd/MTHM (366 full power days).

Group		**Nominal**	**Diversion**	**Change**
1	β_1	0.000184±0.000007	0.000180±0.00006	-
	λ_1	0.0125±0.0000	0.0125±0.0000	-
2	β_2	0.000960±0.000014	0.000961±0.000015	-
	λ_2	0.0283±0.0000	0.0283±0.0000	-
3	β_3	0.000554±0.000012	0.000550±0.000012	-
	λ_3	0.0425±0.0000	0.0425±0.0000	-
4	β_4	0.001264±0.000016	0.001275±0.000015	-
	λ_4	0.1330±0.0000	0.1330±0.0001	-
5	β_5	0.002121±0.000021	0.002180±0.000021	2.81%
	λ_5	0.2925±0.0000	0.2925±0.0001	-
6	β_6	0.000850±0.000012	0.000855±0.000013	-
	λ_6	0.6665±0.0000	0.6665±0.0000	-
7	β_7	0.000667±0.000016	0.000678±0.000012	-
	λ_7	1.6348±0.0000	1.6348±0.0001	-
8	β_8	0.000316±0.000011	0.000308±0.000008	-
	λ_8	3.5546±0.0000	3.5546±0.0000	-

Diversion of 10% of super grade plutonium around 1 full power year

Table A23: Change in reactor parameters when 10% of plutonium (96.4 kg) is removed from an FSMSR after a burnup of 2.67 GWd/MTHM (366 full power days).

	Nominal	Diversion	Change
k_{eff}	1.00460±0.00015	1.00235±0.00015	-224
β_{eff}	0.00695±0.00004	0.00698±0.00004	-
Λ	1.261e-06±2.0e-09	1.266e-06±2.0e-09	0.42%
Pm-149 yield	0.0106±0.0000	0.0106±0.0000	-
Sm ρ (pcm)	24±1	25±1	-4.31%
Feedback$_{Dop}$ (pcm/°C)	-0.98±0.25	-1.11±0.34	-
Feedback$_{Void}$ (pcm/°C)	-12.68±0.54	-12.23±0.48	-

Table A24: Change in the eight group effective delayed neutron fraction parameters when 10% of plutonium (96.4 kg) is removed from an FSMSR after a burnup of 2.67 GWd/MTHM (366 full power days).

Group		Nominal	Diversion	Change
1	β_1	0.000184±0.000007	0.000184±0.00006	-
	λ_1	0.0125±0.0000	0.0125±0.0000	-
2	β_2	0.000960±0.000014	0.000973±0.000015	-
	λ_2	0.0283±0.0000	0.0283±0.0000	-
3	β_3	0.000554±0.000012	0.000568±0.000012	2.53%
	λ_3	0.0425±0.0000	0.0425±0.0000	-
4	β_4	0.001264±0.000016	0.001268±0.000015	-
	λ_4	0.1330±0.0000	0.1330±0.0001	-
5	β_5	0.002121±0.000021	0.002138±0.000021	-
	λ_5	0.2925±0.0000	0.2925±0.0001	-
6	β_6	0.000850±0.000012	0.000857±0.000013	-
	λ_6	0.6665±0.0000	0.6665±0.0000	-
7	β_7	0.000667±0.000016	0.000692±0.000012	3.75%
	λ_7	1.6348±0.0000	1.6348±0.0001	-
8	β_8	0.000316±0.000011	0.000304±0.000009	-3.89%
	λ_8	3.5546±0.0000	3.5546±0.0000	-

Diversion of 25% of super grade plutonium around 1 full power year

Table A25: Change in reactor parameters when 25% of plutonium (241.0 kg) is removed from an FSMSR after a burnup of 2.67 GWd/MTHM (366 full power days).

	Nominal	Diversion	Change
k_{eff}	1.00460±0.00015	0.99974±0.00017	-484
β_{eff}	0.00695±0.00004	0.00701±0.00004	0.80%
Λ	1.261e-06±2.0e-09	1.274e-06±1.9e-09	0.98%
Pm-149 yield	0.0106±0.0000	0.0105±0.0000	-1.00%
Sm ρ (pcm)	24±1	26±1	5.75%
Feedback$_{Dop}$ (pcm/°C)	-0.98±0.25	-2.13±0.25	117.35%
Feedback$_{Void}$ (pcm/°C)	-12.68±0.54	-12.23±0.24	-

Table A26: Change in the eight group effective delayed neutron fraction parameters when 25% of plutonium (241.0 kg) is removed from an FSMSR after a burnup of 2.67 GWd/MTHM (366 full power days).

Group		Nominal	Diversion	Change
1	β_1	0.000184±0.000007	0.000178±0.00006	-
	λ_1	0.0125±0.0000	0.0125±0.0000	-
2	β_2	0.000960±0.000014	0.000959±0.000015	-
	λ_2	0.0283±0.0000	0.0283±0.0000	-
3	β_3	0.000554±0.000012	0.000552±0.000012	-
	λ_3	0.0425±0.0000	0.0425±0.0000	-
4	β_4	0.001264±0.000016	0.001278±0.000015	-
	λ_4	0.1330±0.0000	0.1330±0.0001	-
5	β_5	0.002121±0.000021	0.002164±0.000023	2.59%
	λ_5	0.2925±0.0000	0.2925±0.0001	-
6	β_6	0.000850±0.000012	0.000845±0.000015	-
	λ_6	0.6665±0.0000	0.6665±0.0000	-
7	β_7	0.000667±0.000016	0.000711±0.000012	6.58%
	λ_7	1.6348±0.0000	1.6348±0.0001	-
8	β_8	0.000316±0.000011	0.000309±0.000009	-
	λ_8	3.5546±0.0000	3.5546±0.0000	-

B Parameters Used in Dynamic models

Table B1: Power production related parameters.

	TMSR	**FSMSR**
Thermal power (MWth)	557	3000
Fraction of heat generated in moderator/reflector	0.06	0.04
Xe gas bubbling decay constant (s^{-1})	0.0347	0.0347

Table B2: Specific heat capacities for materials and heat transfer areas in Simulink model.

	TMSR	**FSMSR**
Fuel salt (MJ/kg-C)	1.967e-3	0.830e-3
Graphite moderator/reflector (MJ/kg-C)	1.773e-3	0.554e-3
Primary coolant salt (MJ/kg-C)	2.386e-3	2.386e-3
Secondary coolant coolant salt (MJ/kg-C)	1.549e-3	1.549e-3
Heat exchanger metal wall (MJ/kg-C)	0.578e-3	0.578e-3
Core heat transfer area (MW/°C)	2.066	1477.4
Fuel salt to primary heat exchanger heat transfer area (MW/°C)	18.528	111.17
Primary coolant to primary heat exchanger heat transfer area (MW/°C)	12.602	75.611
Primary coolant to secondary heat exchanger heat transfer area (MW/°C)	12.602	75.611
Secondary coolant to secondary heat exchanger heat transfer area (MW/°C)	18.000	108.00

Table B3: Initial temperatures for Simulink model

	TMSR	**FSMSR**
Average fuel salt temperature (°C)	645	635
Average graphite/reflector temperature (°C)	661	637
Average primary coolant temperature (°C)	610	573
Average secondary coolant temperature (°C)	514	510

Table B4: Mass and mass flow rates in the primary core system.

	TMSR	**FSMSR**
Total mass of fuel salt (kg)	4.5922e4	4.9327e5
Core time delay (s)	4.7	2
Loop time delay (s)	4.7	2
Mass of core fuel salt node in core (kg)	3444	1.2331e6
Mass of moderator/reflector (kg)	210450	8.8628e8
Fuel salt flow rate (kg/s)	4885	123317
Primary coolant flow rate (kg/s)	3277	11797
Secondary coolant flow rate (kg/s)	3379	12164
Mass of fuel salt in primary heat exchanger (kg)	13777	82695
Mass of metal wall in primary heat exchanger (kg)	14087	84524
Mass of primary coolant in primary heat exchanger (kg)	6940	41641
Mass of primary coolant in secondary heat exchanger (kg)	100	598
Mass of metal wall in primary heat exchanger (kg)	202	1213
Mass of secondary coolant in secondary heat exchanger (kg)	100	598
Time delay for coolant salts between heat exchangers (s)	1.5	1.5

Table B5: Parameters used in the once through stem generator.

	TMSR	**FSMSR**
Heat Capacities		
Inconel wall (MJ/(kg/°C))	456.06e-6	456.06e-6
Feedwater (MJ/(kg/°C))	3200.45e-6	3200.45e-6
Sub-cooled water (MJ/(kg/°C))	4761.39e-6	4761.39e-6
Steam (MJ/(kg/°C))	3588.21e-6	3588.21e-6
Heat Transfer Coeffiencts		
Effective salt to wall heat transfer (MW/m^2-°C)	5674.46e-6	5674.46e-6
Wall to subcooled node (MW/m^2-°C)	8385.01e-6	8385.01e-6
Wall to boil node (MW/m^2-°C)	13349.33e-6	13349.33e-6
Wall to steam node (MW/m^2-°C)	5732.37e-6	5732.37e-6
Steam generator tubes		
number of tubes	5317	27493
Active tub length (m)	6.93	17.07
Starting length of the sub-cooled region (m)	1.18	2.89
Starting length of the boiling region (m)	1.92	4.73
Starting length of the steam region (m)	3.83	9.45
tube inner diameter (m)	1.4148e-3	1.4148e-3
tube outer diameter (m)	1.5875e-3	1.5875e-3
Tube thickness (m)	8.636e-4	8.636e-4
Water Properties		
water cross sectional flow area (m^2)	0.995	5.143
Feedwater flow rate (kg/s)	261.2	1350.5
Water initial pressure (MPa)	12.5	12.5

Vita

Alexander M. Wheeler started his academic career at the University of Tennessee, Knoxville (UTK) in 2011. He received his Bachelors of Science in 2016 with a double major in Nuclear Engineering and Mathematics. He then continued to study at UTK and received a Masters of Science in 2020 in Nuclear Engineering. He is currently pursuing his Doctorate of Philosophy in Nuclear Engineering at UTK.

During his academic career, Alexander has researched and published on several topics relating to Molten Salt Reactors (MSRs). Areas of particular interest are material accountancy and kinetics/dynamics for MSRs. The presented research represents a fusion of those two fields that has not previously been done.